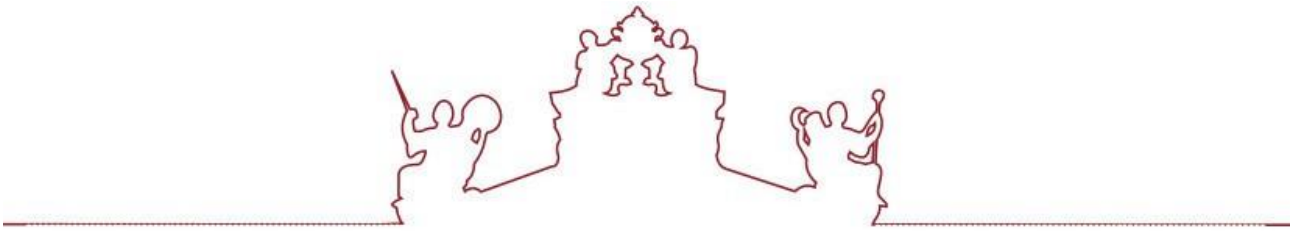

Universidade de Évora – Escola de Ciências e Tecnologia
Universidade Nova de Lisboa – Faculdade de Ciências e Tecnologias

Mestrado em Paleontologia

Dissertação

Changes in the dinoflagellate cyst assemblages along a shallow water (Denmark) – deep water (North Sea) transect during the Burdigalian-Langhian, with focus on the transition to the Miocene Climatic Optimum

Laura Frazão Kellner

Orientador(es) | Lígia Nunes de Sousa Pereira de Castro
Carlos Alexandre Ribeiro
Manuel Carlos Marques Vieira

Évora 2024

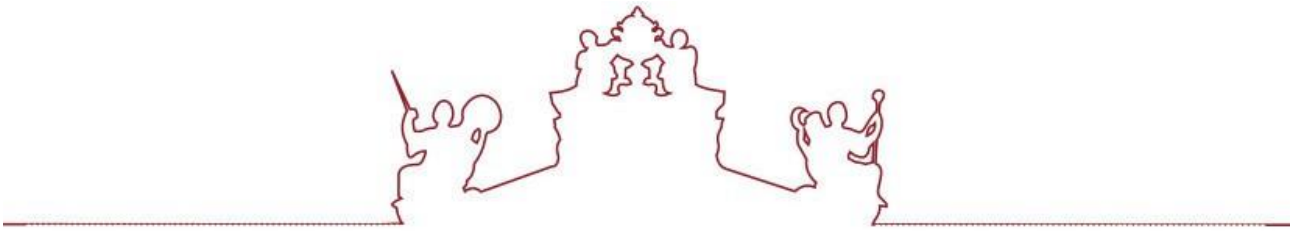

Universidade de Évora – Escola de Ciências e Tecnologia
Universidade Nova de Lisboa – Faculdade de Ciências e Tecnologias

Mestrado em Paleontologia

Dissertação

Changes in the dinoflagellate cyst assemblages along a shallow water (Denmark) – deep water (North Sea) transect during the Burdigalian-Langhian, with focus on the transition to the Miocene Climatic Optimum

Laura Frazão Kellner

Orientador(es) | Lígia Nunes de Sousa Pereira de Castro
Carlos Alexandre Ribeiro
Manuel Carlos Marques Vieira

Évora 2024

A dissertação foi objeto de apreciação e discussão pública pelo seguinte júri nomeado pelo Diretor da Escola de Ciências e Tecnologia:

Presidente | D. Figueiredo (Universidade de Evora)

Vogais | Lígia Nunes de Sousa Pereira de Castro (Universidade Nova de Lisboa - Faculdade de Ciências e Tecnologias) (Orientador)
Zélia Pereira (Laboratório Nacional de Energia e Geologia - Unidade de Geologia, Hidrogeologia e Geologia Costeira) (Arguente)

Évora 2024

To my parents and

grandparents

Acknowledgments

The present dissertation was developed within the scope of the Paleontology Master from Évora University in association with NOVA University of Lisbon. I express my gratitude to both institutions for allowing me to invest in my education and career path and to those of administration and academic services who were involved in this process. Furthermore, I'm grateful to the Department of Geosciences (School of Sciences and Technology, ETC) in Évora and the Department of Earth Sciences (Faculty of Science and Technology, NOVA FCT) in Caparica, for offering me guidance and laboratory space/material for the advancing of my dissertation.

A special thanks to the Geological Survey of Denmark and Greenland (GEUS) and Aker BP for the sample material, for the opportunity to train in palynology and organic geochemistry in the Department of Geoenergy and Storage in Copenhagen, and for travel support when attending the Force congress "Biostratigraphy, conventional and beyond" in Stavanger, Norway.

To my advisor Lígia Castro, thank you for introducing me to the world of palynology and offering me guidance, many opportunities to gain new skills, and for believing in and supporting me during the Master. Your force and resilience regarding student rights in unfair academic situations don't go unseen. Your friendship and motherly care made being far from home not so difficult for all of the master's students. Thank you for all the laughs and moments that we shared.

To my co-advisor Manuel Vieira, a huge thank you for broadening my horizons regarding palynology research/investigation outside Portugal. Without your presence and knowledge, I wouldn't have had many great opportunities and wouldn't have met amazing people that today I hold close to my heart. Thank you for your immediate attention and support in my decisions along the development of my dissertation. Thank you for your availability, honesty, cheerful company, and care.

To my co-advisor Carlos Ribeiro, thank you for the guidance and availability to answer questions/doubts about the dissertation bureaucracy process. Thank you also for your attention and care when hearing the students, and the quick response and solutions to many challenges during the Master.

A special and big thank you to Dra. Karen Dybkjær and Dra. Kasia Śliwińska for their support, immediate availability, dissertation/scientific paper corrections/suggestions,

and all the knowledge transmitted during this journey. Thank you for accepting me with open arms in Copenhagen and for all the lovely time we spent together. I value and appreciate a lot your presence, investment, guidance, and care that was given to me by both of you. Thank you also to Dr. Erick Rasmussen for the geological context corrections and for receiving me, together with Dra. Karen Dybkjær and your beautiful family, for a traditional Danish meal and Christmas activities. Thank you to all the kind workers at GEUS for laboratory help and slide preparation (Dra. Anette Rygge), for the fun time passed in work pauses, and for sharing Christmas activities with delicious hot chocolate.

I dedicate this dissertation to my parents, Maria and Kai. Your immense support and love carried me through many challenges and difficulties during my academic path. I'm eternally grateful for all the emotional and financial support given by both of you. Thank you for helping me cultivate my personal and academic growth. Thank you for believing and reminding me of my capabilities when I was blinded by anxiety and couldn't recognize them. I also dedicate this dissertation to my grandparents (Fernanda, José, Edith, and Werner), since they are important figures of strength to me.

A huge thank you to my boyfriend Francesco for the amazing support, companionship, and words of love/encouragement during my dissertation journey. I'm deeply grateful for you and excited for what's to come, with you by my side.

To my best friend Tatiana, thank you for all the moments of laughter, and for listening and supporting me during the process. Our friendship is precious to me.

To Ana Rita, Ísis, and Ricardo thank you for your support, care, and cheerful friendship.

Thank you to the rest of my big family, for the love and words of encouragement.

The last thanks go to my colleagues and friends: Filipa who chose to share her time and dedication in pair work during the first year of our Master; Mariana, Andreia, Soraya, Victor, Sofia, and Gonçalo for the motivational talks and support; to the researchers (Maria and Vicente) and PhD students (Roberta, Arthur, Fillipo, André, Victor, Alex, Simone, Mark, João, Francisco, and Darío) for the help, laughs and great moments shared; and Professor Paulo Caetano for the amazing company and the many conversations during microscope work.

Laura Kellner,

04/08/2024

Mudanças nas associações de quistos de dinoflagelados ao longo da transição entre águas pouco profundas (Dinamarca) e águas profundas (Mar do norte) durante o Burdigaliano- com foco no Ótimo Climático do Miocénico

Resumo

Um estudo de quistos de dinoflagelados foi realizado em sedimentos do Miocénico Inferior-Médio, com foco na transição para o Ótimo Climático do Miocénico (MCO, ~16,9-14,7 Ma). Comparou-se um transecto proximal (Sønder Vium, onshore Dinamarca) e distal (poço 2/11-12S, offshore Noruega), usando análises de associações de quistos de dinoflagelados, palinofácies e geoquímica orgânica. As variações nos ambientes deposicionais ao longo das sucessões estudadas refletem mudanças na profundidade do mar. As amostras da sondagem 2/11-12S sugerem um ambiente marinho profundo, com dinoquistos oceânicos característicos. Por outro lado, as amostras do Sdr. Vium mostram uma mudança para águas menos profundas com espécies tipicamente neríticas. As temperaturas da superfície do mar obtidas através de membranas lipídicas, revelaram uma fase de aquecimento associado ao MCO. As palinofácies, juntamente com a análise geoquímica orgânica (BIT *index*), oferecerão melhor percepção das mudanças no nível do mar e das variações climáticas, contribuindo para um registo mais completo do Miocénico do Mar do Norte.

Palavras-chave: Quistos de dinoflagelados; Geoquímica orgânica; Mar do Norte; Ótimo Climático do Miocénico**;** Palinofácies**.**

Abstract

A study of dinoflagellate cyst assemblages has been performed on Lower - Middle Miocene sediments, focusing on the transition to the Miocene Climatic Optimum (MCO, ~16,9-14,7 Ma). Here it is compared a proximal (Sønder Vium, onshore Denmark) and distal (2/11-12S well, offshore Norway) transect, using dinocyst assemblages, palynofacies, and organic geochemistry approaches. The variations in depositional environments through the studied successions reflect water depth changes. The samples from the 2/11-12S well suggest a deep marine environment, with characteristic neritic and oceanic dinocyst taxa. On the other hand, samples from the Sdr. Vium indicate a shallowing trend upwards, yielding typical dinocyst neritic species with no oceanic taxa. Sea-surface temperatures were obtained from membrane lipids, revealing a warming phase associated with the MCO. The palynofacies together with the organic geochemistry (BIT index) analysis offer a better perception of water-depth changes and climatic variations, contributing to a more complete Miocene record of the North Sea.

Keywords: Dinoflagellate cysts; Miocene Climatic Optimum; North Sea; Organic geochemistry; Palynofacies.

Table of Contents

Table of Tables

Table of Images

Abbreviations, Siglas e Acronymes

A - Acritarchs

$A_{12}O_3$ – Aluminium oxide

brGDGTs – branched glycerol dialkyl glycerol tetraethers

BS - Bisaccate pollen

CGG Lab. - Compagnie Générale de Géophysique laboratory

CO_2 – Carbonate dioxide

D - Dinoflagellate cysts

DCM – Dichloromethane

Dinocyst - Dinoflagellate cysts

FA - Freshwater algae

FU - Fungal Spores

GDGTs- Glycerol dialkyl glycerol tetraethers

GEUS - Geological Survey of Denmark and Greenland

g - grams

HCL - Hydrochloric acid

HF - Hydrofluoric acid

HNO_3 – Nitric acid

HPLC-MS – Liquid chromatography/mass spectrometry

isoGDGTs – isoprenoid glycerol dialkyl glycerol tetraethers

KOH - Potassium hydroxide

m - meters

Ma – Million years

MCO - Miocene Climatic Optimum

MeOH – Methanol

MMCT - Mid-Miocene Climatic Transition

Na_2SO_4 – Sodium Sulfate

NSP - Non-saccate pollen

NW – Northwest

P/D index - Terrestrial/marine index

PTFE beaker – Polytetrafluoroethylene beaker

PVA - Polyvinyl alcohol adhesive/sealer

S - Spores

Sdr. Vium - Sønder Vium

SST – Sea Surface Temperatures

TLE – Total Lipid Extract

TUP - Thin-walled undifferentiated palynomorphs

UK'_{37} – Alkenone type

UP - Undifferentiated Palynomorph

Introduction

1. Introduction

The Miocene is the first epoch of the Neogene period, spanning from 23.03 Ma to 5.33 Ma. The climate in the Miocene is often defined as a coolhouse (Westerhold et al. 2020), and it is paced by orbitally driven glaciation episodes. However, in relation to the modern type of icehouse climate, the Miocene was warmer than the present. The Miocene epoch has experienced a prominent warming phase known as the Miocene Climatic Optimum (MCO, ~16,9-14,7 Ma) followed by the overall gradual cooling to the culmination transition into the modern type of the icehouse climate (Westerhold et al. 2020; Zachos et al., 2001). The MCO is the last time in Earth's history when the atmospheric CO_2 was higher than today and therefore can be studied as a reference interval for the warmer future. Despite increased interest in the Miocene and the MCO from the paleoclimatological research community, the amount of data and sites penetrating the MCO is limited.

Only a few studies (e.g. Larson et al., 2011; Herbert et al., 2020) have been conducted in the northern countries to understand the Miocene climate variation and its impact on the North Sea region. For the regional paleoenvironmental studies, the central and eastern North Sea basin comprises a rich repository of palynological research data, providing: I) A biostratigraphic framework, composed by Dybkjær & Rasmussen (2000), Dybkjær (2004), Schiøler (2005), Dybkjær & Rasmussen (2007), Dybkjær & Piasecki (2010), Dybkjær et al. (2012), Śliwińska (2019), aiming to refine the North Sea stratigraphic background with the use of dinoflagellate cyst as an efficient tool for stratigraphical framework; II) Palynofacies approaches, as a valuable supplement to sedimentological and seismic studies, for better interpretation of depositional environments (e.g. Dybkjær, 2004b; Dybkjær et al., 2019); III) Relative sea-level variation studies, to reveal the dynamic between climatic, eustatic sea-level changes, and regional/local tectonics in the development of sedimentary sequences (e.g. Dybkjær, 2004a; Śliwińska, 2014; Śliwińska et al., 2019; Śliwińska et al. 2024).

In this study, the palynofacies analysis was applied to better understand how sediment succession of the Miocene age under various depositional settings (proximal/distal), can reflect changes in depositional environments and reflect relative water-depth changes. Factors such as distance to shoreline, freshwater influx into marine settings, depositional energy level, and degradation have a strong sorting effect and a distinct impact on the distribution of the different organic particles (e.g. Tyson 1995, De Vernal 2009). Thus, the comparison of relative abundances between different organic particles

assemblages (e.g. dinoflagellate cyst, non-saccate pollen, bisaccate pollen, spores, fungal spores, freshwater algae, and acritarchs) allows a perception of the deepening or shallowing trends when looking at a geologic succession (Tyson, 1995; De Vernal, 2009; Dybkjær et al., 2019). Marine palynomorph assemblages (dinoflagellate cysts or dinocysts) can also provide insight into past surface water conditions due to their sensitivity to temperature, salinity, nutrient supply, and light availability changes (e.g. Dale, 1996; Pross & Brinkhuis, 2005). This characteristic makes dinocysts good indicators of environmental changes in the past (see Dale, 1996; Sluijs et al., 2005; De Vernal, 2009; Quaijtaal et al., 2014). With this, an identification of dinocyst taxa was also performed, aiming for further knowledge on dinocyst paleoenvironment distribution and paleoclimate preference.

Along with palynological studies, organic proxies have been explored to gain knowledge of climate variation and sea surface temperatures (SST) during the Miocene in the North Sea Basin. Using long-chain alkenones (UK'_{37}), Herbert et al., (2020) reconstructed past sea surface temperature evolution in the eastern North Sea basin from the Sdr. Vium core, covering the onset of the MCO and the following cooling. The sea surface temperature showed an increase to 28ºC in the Early-Middle Miocene, followed by a gradual decrease to 24ºC in the late Miocene. Śliwińska et al., (2024), gathered temperature records from land and sea, suggest that the onset of the MCO in the eastern North Sea Basin seems to be related to a sequence of warming steps or pulses in both the marine and terrestrial realms and that some of these steps are synchronous, some are not. As part of this project, it was performed an organic geochemistry pilot analysis (long chain alkenones and glycerol dialkyl glycerol tetraether, GDGT) lipids to obtain SST from the Central North Sea.

The analyses of this project were carried out on sediment cores retrieved from the Lower to Middle Miocene succession in the North Sea Basin:

1) The Sønder Vium well (DGUnr 102. 948) located in the eastern North Sea, onshore Denmark (in the western part of Jutland, Figure 3.2). The Sønder Vium well was drilled in 2002 and has been studied for many sedimentological, palynological, and geochemical approaches (e.g. Rasmussen et al., 2010; Dybkjær & Piasecki 2010; Larsson et al., 2011; Śliwińska et al., 2024).
2) The 2/11-12S well located in the central North Sea, in the southernmost part of the Norwegian sector (Figure 3.2). The 2/11-12S well was drilled in 2019 by Aker BP and publicly available data are currently limited to the integrated stratigraphic framework (Sheldon et al. submitted), including the dinocyst stratigraphy.

The Miocene succession in the Sdr. Vium core was deposited relatively close to the coastline and the water depth oscillated between 0 and 200 m (e.g. Sliwinska et al., 2024), while the 2/11-12S well is located closer to the central part of the North Sea Basin, further away from the coastline. Environmental analysis of the 2/11-12S core are missing.

In this work, it was applied the existing stratigraphic framework for both wells (Dybkjær & Piasecki 2010, Sliwinska et al. 2024 for Sdr Vium, and Sheldon et al. submitted for 2/11-12S). The correlation between these cores is based on detailed dinoflagellate cyst events (Dybkjær & Piasecki 2010).

The purpose of this study is:

- Investigate the diversity and distribution of dinocyst assemblages and other organic particle assemblages from proximal (Sønder Vium) and distal (2/11-12S) sites, to better understand changes in depositional environments and water-depth.
- Obtain SST signals on the distal 2/11-12S well through organic proxies to recognize and compare climatic variations in the central and eastern North Sea during the Miocene.

Literature review

2. Literature review

Before starting a research project it is important to understand what literature is available and relevant to create a rich background on the research topic. In this literature review, a brief state of the art is presented. The literature selected for the present study helped refine initial research questions, provided geologic backgrounds, and was significant in the interpretation of results and further discussion. For an efficient review, key points were selected regarding the research topic: Miocene climate, geological history/evolution, stratigraphy, dinocysts (paleoclimate indicators), water-depth changes, literature challenges, and current research contributions.

Miocene climate

To acquire knowledge on the Cenozoic climate, Zachos et al. (2001) and Westerhold et al. (2020) were selected. Zachos et al. (2001) reviewed the progress in defining the evolution of global climate over the Cenozoic Era. This research covers Neogene complex climate evolution, mentioning the climate variation during the middle Miocene and its influence on the eustatic sea level changes. Westerhold et al. (2020), share a new high resolution astronomically dated, continuous composite of benthic foraminifer isotope records, and the identification of four climate states (Hothouse, Warmhouse, Coolhouse, and Icehouse) over the last 66 million years. With this new method, Westerhold et al. (2020) support the idea that the Miocene is wrongly viewed as a coolhouse since it covered a prominent warming phase, the MCO.

Steinthorsdottir et al. (2021) offers a review of the state-of-the-art for the Miocene climate. Focusing on key subjects such as ocean circulation, biogeochemical cycling, ice sheet dynamics, and biotic adaptation research, Steinthorsdottir et al. (2021) suggests that the Miocene epoch (23.04 Ma – 5.33 Ma), as a time of global warmth, can be used as an analogy for future warming scenarios. Analysing past climate changes and their biotic responses can give the possibility to better predict current and future global changes. The rich knowledge shared by Steinthorsdottir et al. (2021) was useful for gaining a clearer view of the Miocene history and its importance for nowadays climate studies.

The paleoenvironmental studies in the North Sea basin often resort to organic proxies (Alkenones or GDGTs) for obtaining sea surface temperatures (SST). Alkenones (UK'_{37}) were used by Herbert et al. (2020) to estimate SST during the interval of the MCO in the eastern part of the North Sea (onshore, Denmark). The estimation of SSTs values reached up

to 28ºC, during the Late Burdigalian, with a following decrease to 24ºC in the Middle/Late Langhian. The SST values given by Herbert et al. (2020), were used for comparison with the results of the current study.

Pollen and spore analysis by Larsson et al. (2011), provided background knowledge of the current project. Larsson et al. (2011) conducted a palynological investigation on Lower and Upper Miocene sediment samples from Jylland (Denmark, including the Sdr. Vium core) offering a detailed insight into the rich and diverse pollen assemblages and allocating them into standardized climatic groups. Despite Larsson et al. (2011) not mentioning dinoflagellate cyst assemblages, it shows a Miocene flora reconstruction that coincided with the arrival of the Miocene Climatic Optimum creating an open window to the past.

Geologic history and evolution of the North Sea

The geological history and evolution of the North Sea basin are described by many authors. From its development in the Carboniferous to Early Cretaceous due to rift systems, by McClay et al. (1986) and Ziegler (1990), to internal basin structural changes and systems mentioned by Vejbæk et al. (2006), the literature that composes the online repository of the North Sea geological background is rich. Episodes of big basinal configurations are discussed by Liboriusen et al. (1987), Mogensen & Jensen (1994), Rasmussen (2009; 2013), and Knox et al. (2010). Changes in sediment routing systems in the basin, from the end of the Eocene to the beginning of the Oligocene, are presented by Rundberg & Eidvin (2005), Jarsve et al. (2014), and Sømme et al. (2019). The Miocene period is covered by Ziegler (1990) and Rasmussen et al. (2010; submitted), sharing about delta systems strongly influenced by the eustatic sea-level changes.

For the chosen study locations, Schiøler et al. (2007), Rasmussen (2010; submitted), and Sheldon et al. (2018) helped to define the geologic evolution of each site. For the distal setting, Schiøler et al. (2007) was used as guidance to characterize the correspondent geologic formation (Lark Formation). Despite the work of Schiøler et al. (2007) being made from drill core samples from the Danish sector of the North Sea, some of the formations are also spread across to the Norwegian sector. Thus, the previous characterization is valid for the Norwegian sector. Schiøler et al. (2007), combined the pioneering work of Rhys (1974) and Deegan and Scull (1977) on central and northern North Sea lithostratigraphic schemes with previous revised lithostratigraphic studies restricted to the Paleogene (66 Ma – 23.04 Ma) and Neogene (23.04 Ma – 2.58 Ma) (e.g. Hardt et al., 1989; Knox & Holloway, 1992)

to present the complete lithostratigraphy of the Palaeogene-Lower Neogene succession of the Danish sector of central North Sea. This study contains a detailed description of the central North Sea formations that cross the Danish Sector, mentioning lithology, depositional environments, biostratigraphy with age-diagnostic dinocysts, geological age, and subdivision of the formation. To complement the previous geologic description, Sheldon et al. (2018) shared further knowledge on the Norwegian sector lithology, focusing on diatom ooze. This type of sediment is present in the current project materials.

Based on the initial research of Denmark's geology done by J.G. Forchhammer (1794–1865), P.J. Ravn (1866–1951), N.E.K. Hartz (1867–1937), and geological insight offered by the drilling campaigns of the Geologic Survey of Denmark (GEUS), between 1917 and 1963, Rasmussen (2010) combined all the geological, seismic and stratigraphic knowledge to create and revised lithostratigraphy of the Upper Oligocene-Miocene succession of Denmark. This work yields a detailed description of each formation in the Miocene geologic succession of Denmark, also mentioning lithology, depositional environment, biostratigraphy with age-diagnostic dinocysts, geological age, subdivision of the formations, adding a final chapter of paleogeography reconstruction. Rasmussen et al. (subbmitted) was consulted for more up-to-date knowledge on the eastern and central North Sea lithostratigraphy. This work also provided important information to reconstruct the geologic background of the proximal setting.

Stratigraphy

Dybkjær and Rasmussen (2000; 2007; 2010), Dybkjær (2004), and Schiøler (2005) offered a distinct approach to biostratigraphy studies. This biostratigraphic-rich knowledge served as guidance for the methods and results interpretation of the current project. Dinocysts revealed to be an efficient tool of geological dating and age correlation to refine sequence stratigraphic models. With palynological dating, onshore (Denmark) and offshore (Danish North Sea sector) Miocene assemblages of dinocysts were recorded. Posteriorly, Dybkjær and Piasecki (2010), published the Neogene dinoflagellate cyst zonation for the eastern North Sea basin. The Sdr. Vium core studied here was used as a backbone for the dinocyst zonation by Dybkjaer & Piasecki (2010). The very recent study by Sheldon et al (submitted) provided the multidisciplinary stratigraphical framework of the 2/11-12S well (one of the sites of this project), drilled by Aker BP.

Dinocysts (paleoclimate indicators)

Apart from being an efficient tool for geological dating, previous studies such as Dale (1996) and Pross & Brinkhuis (2005) firmly support dinocysts as paleoenvironmental indicators, due to their great sensitivity to changes in the environment. Sluijs et al. (2005), Zonneveld et al. (2013), and Quaijtaal et al. (2014) also used dinocysts for reconstructing environmental changes in the past, showing diverse dinocyst taxa environment distribution (inner neritic to oceanic zones) and response to different climate regimes (warmer or colder climates). Recent studies also use dinocysts to study variations in depositional environments, like deep-marine turbidites, and the application supporting sequence stratigraphic interpretations (Vieira & Jolley, 2020; Jolley et al., 2022). The dinocyst taxa with a preference for warm waters mentioned in previous studies were used as a reference to identify possible warm-water indicators in the current project samples, as the time interval covered coincides with MCO.

Water depth changes

Tyson (1995) offers insight into the various physicochemical and biological processes that determine the production, distribution, deposition, and diagenesis of organic matter in the natural environment. Furthermore, Tyson (1995) supports that different depositional environments yield different organic particle assemblages and that the change in these environments and assemblages can be linked with water depth variation.

Following the same view as Tyson (1995), Dybkjær et al. (2019) suggest that palynofacies approaches can offer new perceptions of deepening and shallowing trends, positions of sequence boundaries and flooding surfaces, and regression and transgressive system tracts. With the support of the past distribution of sedimentary particle studies (e.g. Tyson, 1995; Muller, 1959; Mudie, 1982; Roncaglia & Kuijpers, 2006), Dybkjær et al. (2019) outlined a palynofacies reference dataset that can be used as a tool for a correct interpretation of depositional environments. Grouping distinct categories for palynomorph assemblages and data on relative abundances and distribution creates a clear signal of similarities and differentiation in depositional environments.

The knowledge shared by Tyson (1995) and Dybkjær et al. (2019), helped with the interpretation of results and understanding of the shallowing and deepening trends.

Śliwińska et al. (2024) gathered existing proxy records, such as pollen, spores, leaves, plant fragments, and the organic biomarkers alkenones and membrane lipids, with previous knowledge of precipitation trends and water depths to compare the Miocene climate with the present in the eastern North Sea Basin. Śliwińska et al. (2024) further provided an overview of water depth changes in the Sdr. Vium core, which are based on biofacies studies (foraminifera). These changes were similar to modern-day water depths in the eastern North Sea, predominantly shallow (0–50 m water depth) and occasionally up to 150 m deep. The previous knowledge helped with the interpretation and discussion of results from the present study.

Challenges of literature

During the literature search, two challenges surfaced. The amount of data on the 2/11-12S is limited due to the 2/11-12S being a recent well and part of the data is confidential. Furthermore, there is a limited amount of data about the MCO in the northern high latitudes due to few sites penetrating this interval.

Contribution of this study

The current research project offers a deeper look into the palynomorphs (dinocysts and other organic particle assemblages) diversity and distribution of proximal (Sønder Vium well) to distal (2/11-12S well) transect, together with the first paleotemperature signals obtained from the marine sediment samples of the 2/11-12S well. The different depositional environments reflected in the relative abundance and diversity variation in these assemblages can give us a better perception of water-depth changes and climatic variations. Focusing on the MCO (Burdigalian-Langhian), the understanding of the water depth and climatic changes will contribute to a more complete Miocene record.

Geologic context

3. Geologic Context

3.1. Geology of the North Sea

The development of the North Sea Basin is the result of late Carboniferous to Early Cretaceous rift tectonism and the following collapse of the Caledonian Mountain chain (McClay et al., 1986; Ziegler, 1990). The numerous rift phases formed different graben systems that successively subsided, associated with the succeeding thermal relaxation. All this resulted in a complex mosaic of horsts and grabens (Vejbæk et al. 2007) that later controlled the subsidence pattern in the North Sea realm. However, the reactivation of fault systems and inversion of former graben complexes during the Cretaceous and Cenozoic periods resulted in the uplift of former graben segments and reactivation of salt structures (Liboriusen et al., 1987, Mogensen & Jensen, 1994; Rasmussen 2009, 2013) strongly influencing the sediment routing systems during the Cenozoic. The development of the hinterland, Fennoscandia (present day, the nordic countries peninsula), also influenced the filling of the Eastern North Sea during the Cenozoic. At the beginning of the Cenozoic, the relief of the Scandinavian Mountain Chain was reduced, probably less than 500 m (Gabrielsen et al., 2010; Jarsve et al., 2014; Sømme et al., 2019). As a consequence of the opening of the North Atlantic oceans in the late Paleocene and Early Eocene, the westernmost part of the Fennoscandian Shield (present-day West Norway) was uplifted, and a new source area was created in the northernmost part of the North Sea (e.g. Knox et al., 2010). This resulted in sediment influx and deposition of deep marine fans in the northmost part of the North Sea and the North Atlantic basin. However, the eastern part of the North Sea Basin remained sediment starved with only deposition of hemipelagic clay (Rasmussen et al., 2008; Nielsen et al., 2015). Resumed uplift of Fennoscandia by the end of the Eocene and beginning of the Oligocene resulted in a change in sediment routing systems in the North Sea Basin (Rundberg & Eidvin, 2005; Jarsve et al., 2014; Sømme et al., 2019). A huge amount of sediments was directed into the central and eastern part of the North Sea Basin, and for the first time sediment sourced from Scandinavian was directed southward into the central part of the Cenozoic North Sea Basin. This resulted in the progradation of delta–slope systems south of present-day west Norway (Michelsen et al., 1998; Schiøler et al., 2007; Jarsve et al., 2014). In the Miocene, these delta systems prograded further south across present-day Denmark (Rasmussen et al., 2010). The Lower Miocene – lower Middle Miocene delta systems that occupied the eastern North Sea were strongly controlled by

eustatic sea-level changes and in total, three regressive-transgressive phases occurred. During the Middle Miocene, major flooding of these deltas took place due to the reorganization of the tectonic regime in NW Europe (Ziegler 1990; Rasmussen 2004). Delta progradation from Fennoscandia resumed in the Late Miocene and continued into the Pliocene (Rasmussen et al., submitted).

3.2. Paleoenvironment

During the Cenozoic, the climate was warm and humid (e.g., Zachos et al. 2001, Lyle et al., 2008). An extremely warm period existed in the early Eocene (Zachos et al. 2001, Westerhold et al. 2020) followed by a gradual cooling. The Eocene Oligocene Transition at ca. 34 Ma marks the most pronounced global climatic shift when Earth entered a coolhouse state, characterised by lower atmospheric CO_2 and permanent ice cover in Antarctica (e.g. Hutchinson et al., 2021). The Oligocene in Northern Europe was humid, and a warm temperate climate prevailed in Northern Europe (e.g. Utescher et al., 2009). The warm temperate climate continued into the Miocene. The Oligocene and Miocene witnessed some brief orbitally driven cooling episodes (Westerhold et al., 2020). In the Early to Middle Miocene, present-day Denmark was covered by vegetation typical for warm temperate but also humid/semi-humid character, such as broadleaved deciduous forests and swamp forest associations (Larsson et al., 2011). *Taxodium* was the most dominant plant in the swamp forest, while in the hardwood forest that bordered the swamp *Alnus, Ulmus,* and *Acer* prevailed (Larsson et al., 2011). In the more well-drained areas *Magnolia, Castanea,* and *Juglans* thrived (Larsson et al., 2011).

This climatic pattern of the coolhouse condition was interrupted by a brief period of greenhouse conditions between 16.9 and 14.7 Ma, the MCO (Zachos et al., 2001). MCO was the last time in Earth's history where CO2 was as high or higher than modern values (i.e. above 420 ppm; Hönish et al., 2023).

The MCO was followed by a global climatic deterioration, the Mid-Miocene Climatic Transition, which led to the development of bipolar glaciation and the development of the modern icehouse climate type.

3.3. Miocene sedimentary succession in the eastern North Sea (Sønder Vium Well, onshore Denmark)

The Miocene succession onshore Denmark consists of sedimentary rocks and is subdivided into 11 lithostratigraphic units (Rasmussen et al., 2010; Rasmussen et al., submitted). In the Lower Miocene, three sand-rich formations were deposited in fluvio-deltaic depositional environments. These are known as the Billund, Bastrup, and Odderup Formations (Figure 3.1). The marine interfingering units are referred to as the Vejle Fjord, Klintinghoved, and Arnum Formations. In the westernmost part of the Danish sector, the marine mud-rich units of the Klintinghoved and Arnum Formations interfinger with clay and diatomite-rich sediments of the Dany and Nora Formations (Rasmussen et al., submitted). The deposition of the Odderup, Arnum, and Nora Formations continued into the early part of the Middle Miocene where the deposition of fluvial-deltaic systems was overtaken by mud-rich marine sediments referred to as the Hodde and Ørnhøj Formations (Rasmussen et al. 2010, submitted). The Upper Miocene was characterised by the deposition of the marine Gram Formation which in turn was succeeded by resumed sand-rich fluvio-delta deposits of the Marbæk and Luna Formations (Rasmussen et al. 2010, submitted).

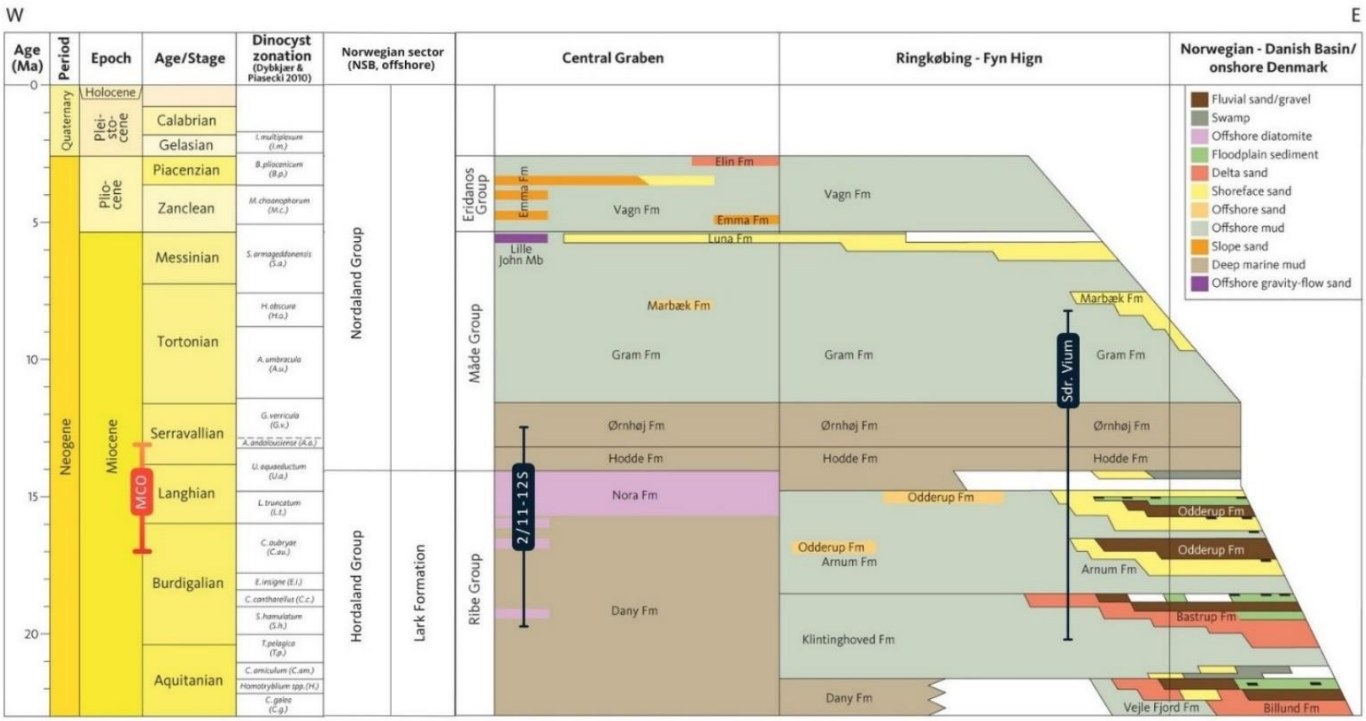

Figure 3.1. Location of the Sønder Vium, 2/11-12S well, and the time interval of the MCO plotted against the new Danish lithostratigraphic framework for the Neogene (**Source**: modified from Rasmussen et al., submitted).

The stratigraphic framework of the Danish Miocene succession is based on sequence stratigraphy (e.g. Michelsen et al. 1995, 1998; Rasmussen, 2004a; Sørensen et al., 1997; Gregersen et al., 1998; Clausen et al., 1999; Dybkjær, 2004a; Rasmussen & Dybkjær, 2005; Rasmussen et al., 2006), strontium isotope stratigraphy (e.g., Howarth & McArthur, 1998; McArthur et al., 2001; Eidvin & Rundberg 2001, 2007) and biostratigraphy (see more in Dybkjær & Piasecki, 2010 and Sliwinska et al., 2024) and can be extended into the Central North Sea. Dybkjær and Piasecki (2010) provided a dinoflagellate cyst zonation for the Danish onshore/offshore Neogene, based on an extensive analysis of onshore wells, outcrops, and offshore wells. The Sønder Vium well, which is penetrating the most stratigraphically complete Miocene succession onshore Denmark, has been used as the backbone of the zonation, yielding 10 of the 19 of these biozones.

The Sønder Vium well is located in Jylland (Denmark) (Figure 3.2) and covers an age interval from the Burdigalian to the Tortonian (Rasmussen, 2010) (Figure 3.1).

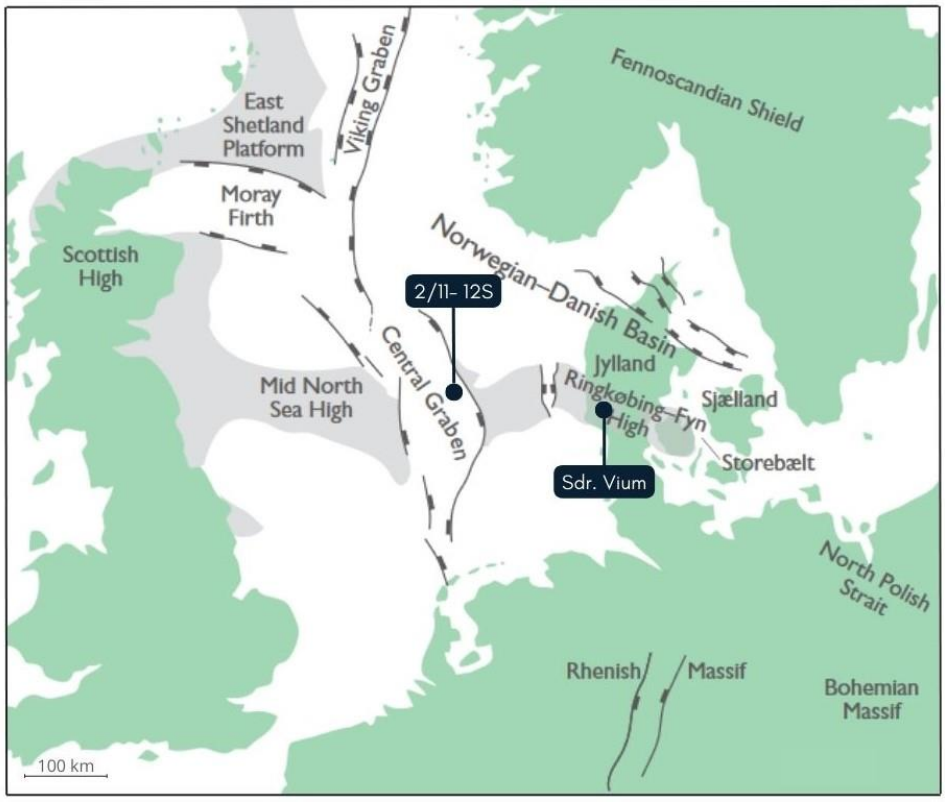

Figure 3.2. Location of the Sdr. Vium and 2/11-12S wells and major structural elements in the greater North Sea area (**Source**: adapted from Schiøler et al., 2007).

3.4. The 2/11-12S well (central North Sea)

The 2/11-12S well is located in the Norwegian part of the central North Sea (Figure 3.2). The well penetrates the upper part of the Lark Formation, the offshore equivalent of which is the lithostratigraphy of the Norwegian section of the North Sea as shown in Figure 3.1. This part of the upper Lark Fm was deposited at the termination of a shoreline progradation from the southern Scandes (Scandinavian Mountain range) and is time equivalent to the Odderup Fm from the onshore Denmark (Sheldon et al., 2018).

The Lark Formation is part of the Hordaland Group and extends itself through the Central part of the North Sea Basin and is mainly composed of different mudstone intervals (Schiøler et al., 2007). The Lower to Middle Miocene succession of the Lark Formation in the Central Graben area layers of abundant biogenic silica composed of diatoms, radiolarians, and sponge spicules were recognised (Sulsbrück & Toft, 2018; Sheldon et al., 2018; Rasmussen et al., submitted; Sheldon et al. submitted). Recently, two new lithological units have been identified in the Central Graben (Norwegian sector) of the North Sea: the Lower Miocene Dany Formation (muddy and silty deposits) and the Middle Miocene Nora Formation (high content of silica/diatomite), see Rasmussen et al. (submitted) (Figure 3.1). The new study by Sheldon et al. (submitted) provides a multidisciplinary biostratigraphic framework for the Miocene succession in the southern part of the Norwegian sector of the North Sea based on dinocyst, microfossil, nannofossil, diatom, and silicoflagellate events. Well 2/11-12S is one of the two fully cored wells that were used by Sheldon et al. (submitted) to provide the stratigraphic framework.

Material & Methods

4. Material and Methods

4.1. Sampling and laboratory preparation

4.1.1. Sønder Vium well, Denmark

Ten samples were collected from the Danish Sdr. Vium core covering an interval from 146.67 m to 43.12 m, spanning the Lower Miocene to Middle Miocene (Figure 4.3). For the purpose of this study, the 10 samples were retrieved from three Miocene formations: Klintinghoved Formation (at 146.67 m); Arnum Formation (at 133.32 m, 119.07 m, 112.67 m, 95.42 m, 88.02 m, 74.02 m, 53.42 m, and 51.42 m); and Ørnhøj Formation (at 43.12 m). These samples supplement the existing sample set (see Sliwinska et al. 2024 for details). The studied interval covers the following dinocysts zones: *Sumatradinium hamulatum*, *Cordosphaeridium cantharellus*, *Exochosphaeridium insigne*, *Cousteaudinium aubrye*, *Labyrinthodinium truncatum*, *Unipontodinium aquaeductum, and Achomosphaera andalousiense* zones sensu Dybkjær and Piasecki (2010). In this study, we applied the stratigraphic framework of the Sdr. Vium well following Dybkjær and Piasecki (2010) and Sliwinska et al., 2024.

All samples were processed at the Palynological Laboratory at the Geological Survey of Denmark and Greenland (GEUS) in Copenhagen, following the internal preparation methods (Poulsen, 1996): Sediment samples were dried and manually crushed. Approximately 20 g of sediment (<2 mm particles) from each sample was used for the preparation of palynological slides. Applied treatment included HCl, HF, neutralization, brief oxidation with HNO_3 and KOH, heavy liquid separation, and filtering with 11 µm nylon nets. Glass slides were mounted with glycerin jelly and acid-resistant organic particles larger than 11 µm for the palynofacies analysis. An extra set of slides was produced for the dinoflagellate cyst analysis, after filtering the acid-resistant organic particles on a 20 µm nylon net.

The slides were firstly examined with a Leica DM 2000 normal light microscope with a Leica DFC295 camera attached, at GEUS in Copenhagen, and secondly with a Leica DM 2500 LED normal light microscope with a Leica Flexacam C3 camera attached at NOVA FCT in Campus of Caparica.

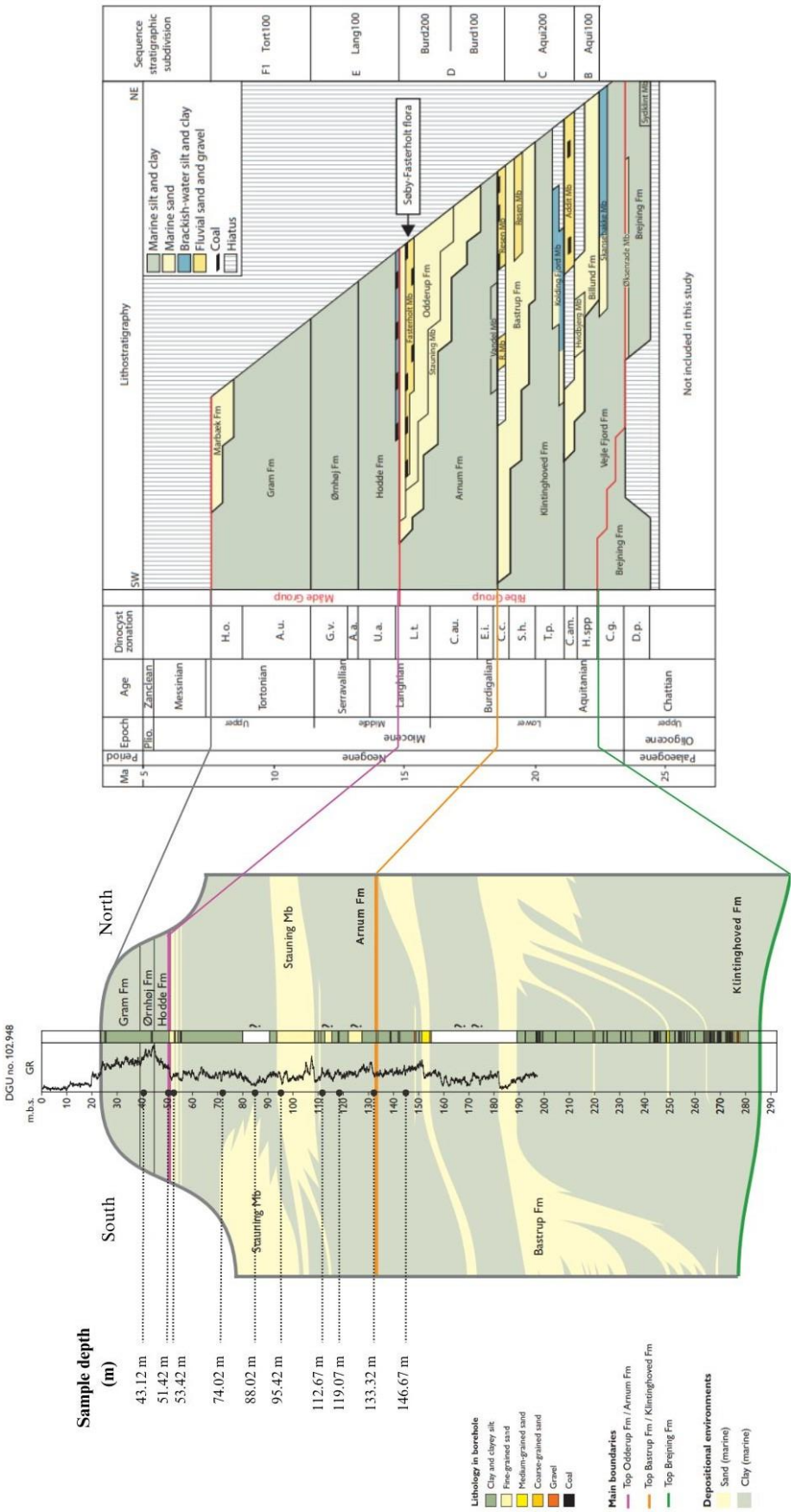

Figure 4.3. Distribution of samples retrieved, and correlation between the stratigraphic column of the Sønder Vium well and the lithostratigraphic framework of the uppermost Oligocene – Miocene of onshore Denmark (**Source**: adapted from Rasmussen et al., 2010).

4.1.2. 2/11-12S, Southern Norwegian North Sea

Eleven sediment samples were collected from sediment cores spanning from a depth of 1670 m to 1611 m (Fig. 4.4).

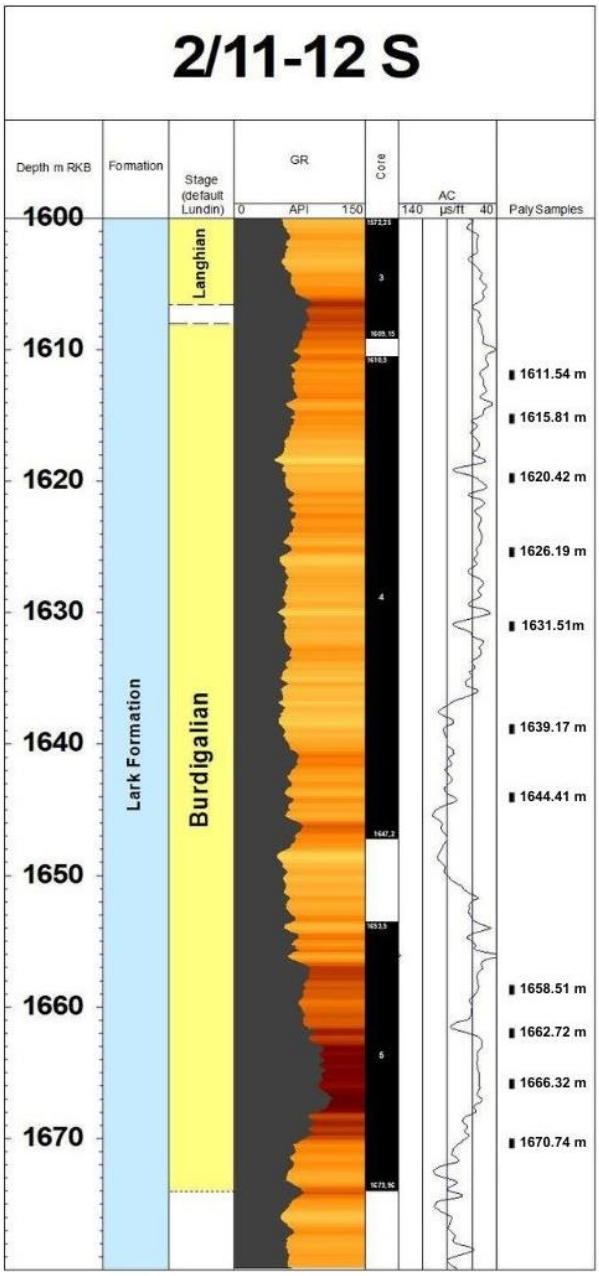

Figure 4.4. Distribution of retrieved samples from the 2/11-12S well, against the south Norwegian North Sea Lithostratigraphy. The figure was drafted by Manuel Vieira (dissertation advisor) and modified by Laura Kellner (dissertation author).

All samples were processed at the CGG Laboratories in the United Kingdom, following the next procedure:

Washing on a 63 μm sieve as per the initial sample processing. Samples are then placed into a Soxhlet for oil extraction. For the dissolution of the carbonates, about 40 to 50 g of the extracted sample is placed in a 500 ml PTFE beaker, followed by concentrated HCl until effervescence ceases. Silicates are removed with 60% HF and the sample is passed through a 10 μm sieve. For all the following sieving steps a 10 μm sieve was used. The remaining sample is placed in approximately 50 ml HCL once more to remove silica gels/precipitates. The samples were sieved again and posteriorly oxidized with Nitric Acid (HNO_3). The samples are then sieved out of HNO. Humic acids in the samples are broken down by the addition of Cleanall (strong industrial alkali detergent solution) and then sieved. The samples are then stained with a mixture of potassium hydroxide (KOH), water, and Gram's safranine solution depending on age and amount of oxidation, to improve the visibility of palynomorphs. The samples are then swirled to sink the heavier organic particles and mineral material, and the lighter material is sieved. The residue retained on the sieve is transferred to a labeled kerogen tube with PVA added. The residue is then spread over a coverslip, which is in turn mounted onto a microscope slide.

The slides were examined with a Leica DM 2500 LED microscope and a Leica Flexacam C3 camera attached, at the Department of Earth Sciences at the NOVA FCT in Campus of Caparica.

4.2. Palynomorphs counting method

Palynomorphs from both wells were assigned to one of the nine categories: 1) Non-saccate pollen (NSP); 2) Bisaccate pollen (BS); 3) Spores (S); 4) Fungal Spores (FU); 5) Freshwater algae (FA); 6) Acritarchs (A); 7) Dinocysts (D); 8) Undifferentiated Palynomorphs (UP); and 9) Thin-walled undifferentiated palynomorphs (TUP). A minimum of 300 particles per sample were identified and counted, making a total of 6300 particles counted in both cores. Fragments of particles that can be identified were counted as one particle. The categories comprising undifferentiated palynomorphs and thin-walled undifferentiated palynomorphs contain all degraded particles and particles that it is not possible to categorize.

For the dinocyst analysis, a minimum of 200 specimens per sample were identified, when possible, down to the species taxonomic level, making a total of 4420 specimens counted in both cores. Archeopyles or fragmented plates were counted as one specimen, only

when the morphology (e.g. processes and other minor elements) permitted taxonomic identification. Fragmented elements or dinocysts with no possible identification were counted as unidentified dinocysts. The dinocyst nomenclature follows Williams et al. (2017).

Raw data from both wells is shown in Appendix A (categories) and D (dinocyst taxa). The relative abundances of the non-saccate pollen and the dinocysts is shown in Appendix B (categories) and E (dinocyst taxa).

4.3. Relative Abundances of palynomorphs

After obtaining the raw data for the counting, the program Excel was used to calculate the relative abundances of each category and taxa, per sample, through the following equation:

$$\text{Rel. Abun. of selected category (\%)} = \frac{\text{category raw counting value} * 100}{\text{Total particles}} \quad \text{(I)}$$

The relative abundances of the categories were used for comparison purposes between wells. The values are shown in Appendix B (categories) and E (dinocyst taxa).

4.4. P/D Index

The P/D index expresses the ratio between terrestrial (including non-saccate pollen, spores, fungal spores, and freshwater algae) vs. marine (dinocysts) palynomorphs and can be used to determine the relative to proximity to the coastline (e.g., Dybkjær et al., 2019). A low P/D index value reveals a low terrestrial signal, meaning that there's less proximity to the coastline, in contrast, a high P/D index value reflects proximity to the coastline (McCarthy et al., 2003). The P/D index calculated follows:

$$\frac{\mathrm{P}}{(\mathrm{D}+\mathrm{P})} * 100\% \quad \text{(II)}$$

where P = (NSP+S+FU+FA).

Bisaccate pollens and acritarchs were not included in the index estimates. Due to the combination of wind transport and their floating abilities ("Neves effect" in Traverse, 1994), bisaccate pollen has its presence in marine, terrestrial, and brackish water environments. Thus, bisaccate pollens are not good indicators of marine or terrestrial environments. Acritharcs were also not included due to the lack of environmental information about this group. The P/D index values are shown in Appendix C.

4.5. Dinocysts and other palynomorphs as environmental indicators

Several studies (e.g. Dale, 1996, Pross & Brinkhuis, 2005) affirm that organic-walled dinocysts can be found in all the main aquatic environments, such as marine and brackish, being sensitive to environmental changes in the surface water (e.g. light availability, salinity, variation in sea-surface temperature and nutrient supply). Thus, dinocysts can be used for reconstructing environmental changes in the past (Dale, 1996; Sluijs et al., 2005; Zonneveld et al., 2013; Quaijtaal et al., 2014; Castro, 2016).

The taxa found in this study are used as an indicator of climate and environmental changes (Table 4.1 and Table 4.2). Other categories of palynomorphs, like freshwater algae, can also be indicators of depositional environments since diverse organic particles have different distributions in diverse depositional environments, see e.g. Tyson 1995 and Dybkjær et al. (2019).

Table 4.1. Dinoflagellate cyst taxa and their climate preferences.

Environment	Dinocyst	References
Warm water	*Impagidinium paradoxum*	Dale, 1996; Head, 1997; Zonneveld et al., 2013
	Lingulodinium machaerophorum	Quaijtaal et al., 2014
	Melitasphaeridium choanophorum	
	Polysphaeridium zoharyi	

Table 4.2. Dinoflagellate cyst taxa and their distribution preferences.

Environment	Dinocyst	References
Inner neritic	*Homotryblium* spp.	Dybkjær, 2004; Sluijs et al., 2005
Neritic	*Operculodinium* spp.	Pross & Brinkhuis, 2005
	Spiniferites spp.	Sluijs et al., 2005; Quaijtaal et al., 2014
	Cleistosphaeridium placacanthum	
	Dapsilidinium pseudocolligerum	
	Lingulodinium machaerophorum	
	Polysphaeridium zoharyi	
Oceanic	*Impagidinium* spp.	Dale, 1996; Dybkjær, 2004;
	Nematosphaeropsis spp.	Pross & Brinkhuis, 2005

4.6. Organic Geochemistry

The Sdr.Vium has previously been analysed for paleotemperatures based on the long-chain alkenones (UK'37 index; Herbert et al., 2020). In this project, it was tested the possibility of obtaining the paleotemperature record from the 2/11-12S well. During a research visit at GEUS (December 2023) selected samples were extracted and separated, to test for the presence and analyse both long-chain alkenones and membrane lipids (GDGTs). For this purpose, seven sediment samples were taken from the interval, 1672.00 m to 1491.61 m. The sample distribution is shown in Figure 4.5.

Between 10 and 20 g of sediment from each sample was freeze-dried (in order to remove the moisture from the sediment) and mechanically powdered. Then, a mixture of DCM and MeOH was added to the sediments (9:1). The volume of solvent was twice the amount of sediment. Each sample was mixed for 10 seconds on the sample shaker and placed in the Ethos X (Advanced microwave extraction system). The method used consists of a 10 mn ramp to 70ºC (1000W), a 10-minute hold at 70ºC (1000W), and a 20-minute cooling phase.

When finished, time was given for all the particles to settle. After waiting, decantation occurred. It is added more solvent and shaken, to rinse one more time the sample making sure it gets all the components that are needed out. The sample is put aside for the particles to settle.

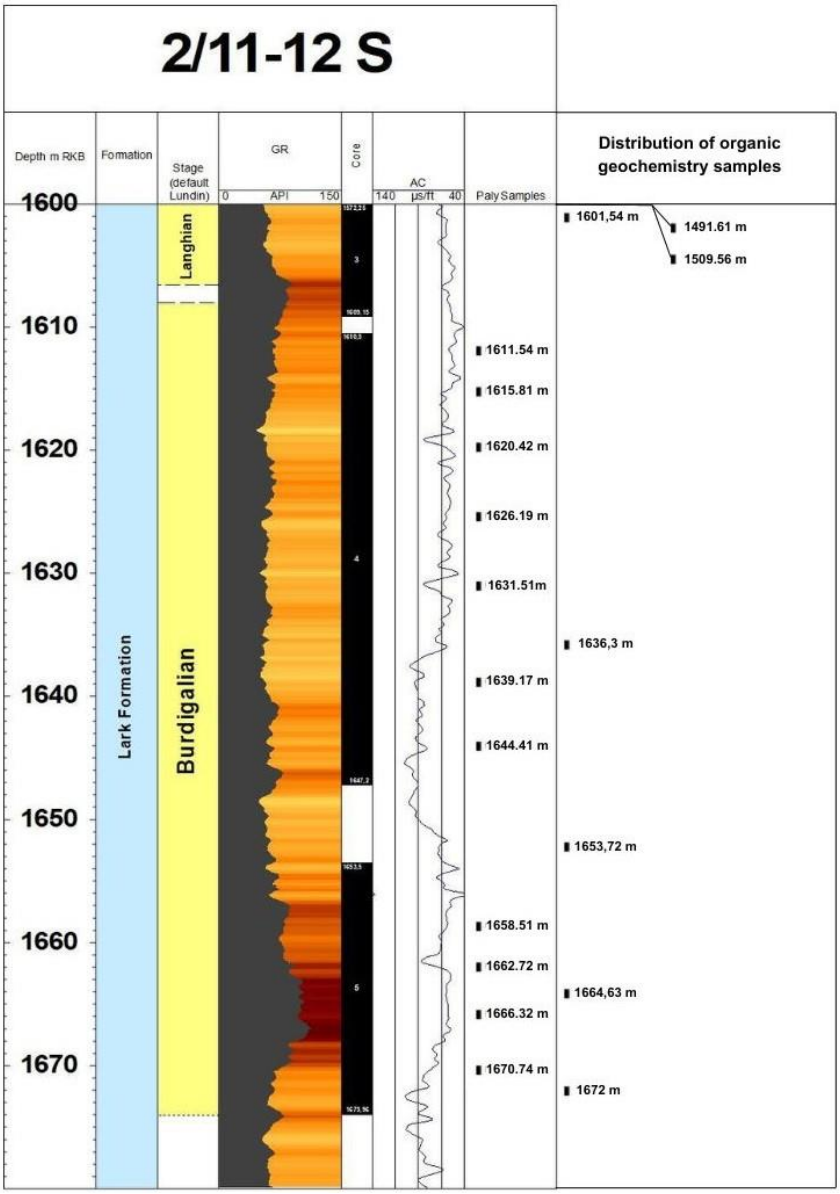

Figure 4.5. Distribution of retrieved samples from the 2/11-12S well, for the organic geochemistry analysis. The figure was drafted by Manuel Vieira (dissertation advisor) and modified by Laura Kellner (dissertation author).

The TLE was transferred to 60 ml vials and placed in the TurboVap LV, at a water temperature of 26ºC temperature with a Nitrogen flow of 1 L/ml. The vials are once removed when the solvent evaporates totally.

For the filtering/elimination of the small fraction, particles in the samples are used in a small glass pipette with extracted glass cotton and Na_2SO_4. Once passes through the collumn, the extract is transferred to a pre-weighted 8ml vial and placed under Nitrogen flow again. After evaporation, the vial is weighed to obtain the Total Lipid Extract weight.
The extract is passed through a column with activated Aluminium oxide ($A_{l2}O_3$) (activated in an oven for a constant 150ªC and cooled down for 2 hours). Hex/DCM (9:1), DCM/MeOH (1/1), and DCM/MeOH (9:1) solvents were used to separate the TLE into the apolar, ketone, and polar fractions of the sample. The vials containing these fractions were put under the Nitrogen flow. After evaporation, the vials are weighted.

Some samples revealed the presence of hydrocarbons in the apolar fraction. The Ketone and polar fractions were sent and analysed for possible Alkenones and GDGTs at Utrecht University (Netherlands).

Alkenones were shown to be absent. Only glycerol dialkyl glycerol tetraethers (GDGT), from the polar fraction, were detected through high-pressure liquid chromatography/mass spectrometry (HPLC-MS). Thus, the GDGTs were selected as proxies to obtain sea surface temperature (SST) estimations. Before attaining the SST estimations, it is important to identify the GDGTs distribution and possible anomalous sources. For a better understanding of these factors, the following organic proxies were calculated: the BIT index (Hopmans et al., 2004), the %GDGT-0 index (Sinninghe Damsté et al., 2012), the MI Index or Methane index (Zhang et al., 2011), the RI index (Zhang et al., 2016), and the $f_{Cren':Cren'+Cren}$ index (O'Brien et al., 2017).

The TEX_{86} is considered a proxy of SST and is defined by the distribution of isoprenoid glycerol dialkyl glycerol tetraethers (isoGDGT, e.g., crenarchaeol) (Schouten et al., 2002). The crenarchaeol is a compound associated with marine archaea, while other types of GDGT, such as branched GDGT (e.g., brGDGT-Ia, IIa, and IIIa) are synthesized by soil and river bacteria (Schouten et al., 2013) (See Appendix G, for the different structures of GDGTs). The isoGDGT values (e.g. GDGT-0, 1, 2, 3; crenarchaeol and crenarchaeol') and the branched GDGT were obtained by mass spectrometry and used to calculate the following indices:

$$TEX_{86} = \frac{(GDGT-2+GDGT-3+GDGT-crenarchaeol)}{(GDGT-1+GDGT-2+GDGT-3+GDGT-crenarchaeol)} \quad (III)$$

To understand the ratio between the branched GDGT (synthesized by soil and river bacteria) and the crenarchaeol (synthesized by marine archaea), the BIT index described in Hopmans et al. (2004) was used:

$$\mathrm{BIT} = \frac{(\mathrm{GDGT-Ia} + \mathrm{GDGT-IIa} + \mathrm{GDGT-IIIa})}{(\mathrm{GDGT-Ia} + \mathrm{GDGT-IIa} + \mathrm{GDGT-IIIa} + \mathrm{crenarchaeol})} \quad \text{(IV)}$$

When obtained, BIT values close to 0 mean the absence of branched GDGTs. On the other hand, values close to 1 mean the absence of crenarchaeol.

Regarding finding the source of potential constraining inputs and encountering anomalous GDGT's distribution, the %GDGT-0, MI, RI, and $f_{Cren':Cren' + Cren}$ indices were calculated.

For the %GDGT-0 Index, the equation is proposed by Sinninghe Damsté et al. (2012):

$$\%\mathrm{GDGT-0} = \left(\frac{\mathrm{GDGT-0}}{\mathrm{GDGT-0} + \mathrm{crenarcheaol}}\right) \times 100 \quad \text{(V)}$$

When the values of %GDGT-0 >67%, the samples may be affected by an additional source.

The MI Index, proposed by Zhang et al. (2011):

$$MI = \frac{(GDGT-1 + GDGT-2 + GDGT-3)}{(\mathrm{GDGT-1} + \mathrm{GDGT-2} + \mathrm{GDGT-3} + \mathrm{crenarchaeol} + \mathrm{crenarchaeol'})} \quad \text{(VI)}$$

The MI Index is calculated to identify methanotrophic archaea. Obtained values above 0,5, must be excluded.

The Ring Index, defined by Zhang et al. (2016):

$$\mathrm{RI} = 0 \times \left(\frac{\mathrm{GDGT-0}}{\sum \mathrm{GDGT}}\right) + 1 \times \left(\frac{\mathrm{GDGT-1}}{\sum \mathrm{GDGT}}\right) + 2 \times \left(\frac{\mathrm{GDGT-2}}{\sum \mathrm{GDGT}}\right) + 3 \times \left(\frac{\mathrm{GDGT-3}}{\sum \mathrm{GDGT}}\right)$$

$$+4 \times \left(\frac{\mathrm{crenarcheaol}}{\sum \mathrm{GDGT}}\right) + 4 \times \left(\frac{\mathrm{crenarcheaol'}}{\sum \mathrm{GDGT}}\right) \quad \text{(VII)}$$

Where,

$$\sum GDGT = \text{GDGT} - 1 + \text{GDGT} - 2 + \text{GDGT} - 3 + \text{crenarchaeol} + \text{crenarchaeol}' \quad \text{(VIII)}$$

$$\text{RI}_{\text{TEX}} = -0.77(\pm 0.38) \times \text{TEX}_{86} + 3.32(\pm 0.34) \times (\text{TEX}_{86})^2 + 1.59(\pm 0.10) \quad \text{(IX)}$$

$$\Delta\text{RI} = \text{RI}_{\text{TEX}} - \text{RI}_{\text{sample}} \quad \text{(X)}$$

The ring index values can reflect samples influenced by non-thermal factors, and if the TEX_{86} follows modern-day behaviour. Zhang et al. (2016) suggest that TEX_{86}-SST values deviating by more than |0.3| from the modern TEX_{86}-RI relationship should be excluded, as they may be impacted by non-thermal sources.

And for the relative abundance of crenarchaeol isomer (O'Brien et al., 2017), $f_{Cren':Cren' + Cren}$:

$$\text{f}_{\text{Cren}':\text{Cren}'+\text{Cren}} = \left(\frac{\text{crenarcheaol}'}{\text{crenarcheaol} + \text{crenarcheaol}'}\right) \quad \text{(XI)}$$

The values given by this equation can help to identify anomalous GDGT distributions, and those that vary between 0.00–0.16 are close to the lower values of the modern core-top sediments.

The ratio between GDGT-2 and GDGT-3 was also calculated, following the simple equation:

$$\frac{\text{GDGT} - 2}{\text{GDGT} - 3} \quad \text{(XII)}$$

Before calculating the Temperature in ºC (degrees), a calibration of the TEX_{86} must occur. The calibration is influenced by the latitude from where the samples are. Since the 2/11-12S is considered to be mid-latitude, TEX_{86}^{H} was chosen (Kim et al., 2010):

$$\text{TEX}_{86}^{\text{H}} = \log\left(\frac{GDGT - 2 + GDGT - 3 + crenarchaeol}{GDGT - 1 + GDGT - 2 + GDGT - 3 + crenarchaeol}\right) \quad \text{(XIII)}$$

After obtaining values from the previous indices and confirming if any constraints are present, it is possible to obtain the SST.

For obtaining values of SST, the following equations of TEX_{86}^{H} and Temp [ºC] were used:

$$\text{Temp } [^{\circ}\text{C}] = 68.4 \times (\text{TEX}_{86}^{\text{H}}) + 38.6 \quad \text{(XIV)}$$

The raw values obtained from the chromatography/mass spectrometry and indexes are shown in Appendix F.

Results

5. Results

5.1. The Sønder Vium core (Denmark)

In the Sdr. Vium well, was identified 6 genera, 24 species, and 2 subspecies of dinocysts (Fig. 5.6). The preservation of the dinocysts is moderate to good. The most abundant dinoflagellate cyst species are *Cleistophaeridium placacanthum* (3% - 27%), *Dapsilidinium pseudocolligerum* (2% - 9%), *Lingulodinium machaerophorum* (1% - 11%), *Operculodinium centrocarpum* (1% - 8%), and *Spiniferites* spp. (27% - 54%). The genus *Spiniferites, Cleistophaeridium placacanthum,* and the "mini-dinos" (3% - 18%) dominate throughout the entire studied succession (see chapter 6 for more information on "mini-dinos").

The age-diagnostic dinocysts events recognised in our dataset include the first occurrence (FO) of *Cousteaudinium aubrye* at 112.67 m, and the FO of *Labyrinthodinium truncatum* at 53.42 m (Fig. 5.6). *Exochosphaeridium insigne* was found only in one sample, at 112.67 m. These occurrences support the previously published dinocyst zonation and datings of the Miocene succession in the Sdr. Vium well (Sliwinska et al. 2024).

A single appearance of *Chiropteridium galea* (Late Oligocene – earliest Miocene age) is observed in the top sample (43.12 m) of the Sønder Vium well, dated as Langhian, suggesting only minor reworking.

The palynofacies data varied up through the succession (Fig. 5.6). The lower part of the studied succession (146.67 m to 112.67 m) reveals an abrupt change: the relative abundance of non-saccate pollen decreased from 51% to 19%, while the abundance of dinocysts increased from 21% to 47%. Before the middle section (119.07 m to 112.67 m), both groups are equally frequent: the non-saccate increases to 41% and the dinocysts decrease to 41%. At 112.67 m a small increase in dinocysts relative abundance up to 46%, coincides with a decrease of non-saccate pollen to 37%. Between 110 m and 98 m there is a core gap, because of the presence of the loose/unconsolidated character of the sandy sediments of the Odderup Formation. The interval from 95.42 m to 51.42 m is characterised by a higher terrestrial input than the interval below the core gap (146.67 m to 112.67 m), where the relative abundances of the non-saccate pollen ranges between 39% and 54%, and the dinoflagellate cyst abundances range between 7% and 32%. The topmost sample at 43.12 m, representing the basal part of the Ørnhøj Formation, is characterised by the highest relative abundance of dinocysts (54%) recognised in any of the analysed samples.

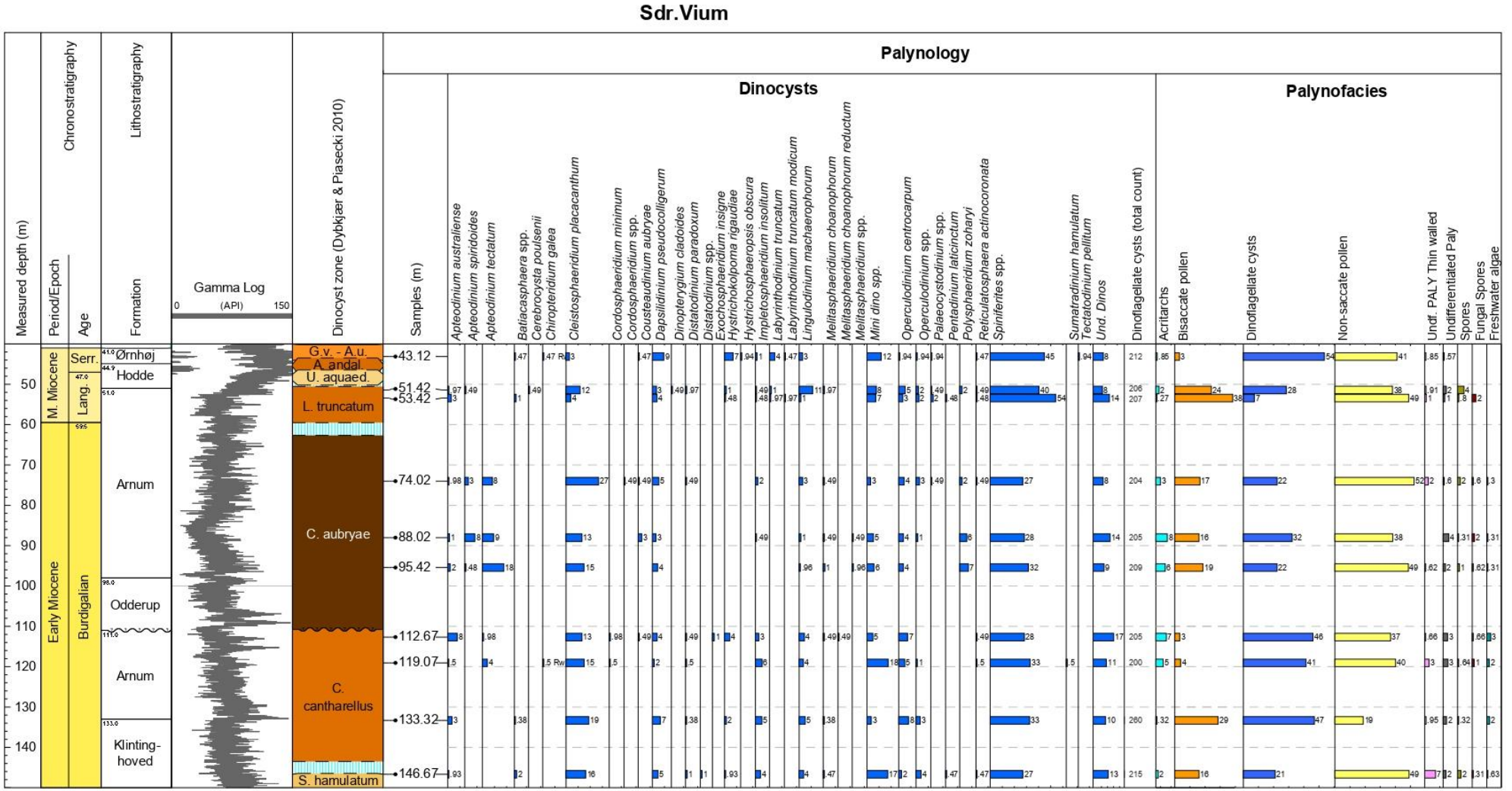

Figure 5.6. Sønder Vium well range chart, with the relative abundances (%) of the established categories of palynomorphs and dinocyst taxa against the dinocyst zones defined by Dybkjær and Piasecki (2010) and the onshore Danish lithostratigraphy of the Middle Miocene. The figure was created by Manuel Vieira (dissertation advisor) and modified by Laura Kellner (dissertation author)

Overall, the basal part (146.67 m) of the studied succession is dominated by non-saccate pollen. At 133.32 m, a change to a dinocyst-dominant environment is observed. From 119.07 m to 51.42 m, a period of gradual increase of non-saccate pollen initiates, reaching a pick between 74.02 m and 53.42 m. At the top (43.12 m), a return to a dinocyst-dominant environment is seen.

The relative abundance of bisaccate pollen varies between 3% and 38% throughout the studied succession. Spores and fungal spores vary from 0.32% to 4%, and 0.31% to 2%, respectively. Acritarchs are present in every sample with an abundance variation between 0.27% and 8%, with the highest relative abundance in the middle part of the succession (119.07 to 88.02 m). Freshwater algae only appear in the lower and middle part of the succession (146.57 m to 74.2 m), varying from 0.30% to 3% (Fig. 5.6).

The P/D index decreases in the lowest part of the studied succession (146.67 m - 133.3 m), from 71% to 31%. From 133 m to 53 m, we observe an increase in the P/D index, from 31% to 88%. In the uppermost part of the succession (53 m to 43 m), the P/D index decreases significantly from 88% to 43% (see appendix C, for P/D index values).

The neritic (see Table 4.2) are commonly present in the Sdr. Vium well including e.g. *Operculodinium* spp., *Cleistophaeridium placacanthum,* and *Dapsilidinium pseudocolligerum.* No oceanic taxa are present in this succession.

Warm-water species (Table 4.1) such as *Lingulodinium machaerophorum, Melitasphaeridium choanophorum,* and *Polysphaeridium zoharyi* are observed throughout the succession. While *Lingulodinium machaerophorum* and *Melitasphaeridium choanophorum* are present in almost/every sample, *Polysphaeridium zoharyi* starts to occur at 92.42 m.

5.2. 2/11-12S (central North Sea)

In the 2/11-12S well, was identified 6 genera, 20 species, and 1 subspecies of dinocysts (Fig. 5.7). The preservation of dinocysts was also moderate to good. The most commonly occurring dinoflagellate cyst taxa are *Cleistophaeridium placacanthum* (2% - 13%), *Impletosphaeridium insolitum* (1% - 22%), *Lingulodinium machaerophorum* (2% - 6%), *Operculodinium* spp. (2% - 11%), *Nematosphaeropsis* spp. (1% - 8%), *Spiniferites* spp. (21% - 47%) and the "mini-dinos" (9% - 24%). The genus *Spiniferites* is abundant throughout the studied interval, but more dominant towards the top. The species *Impletosphaeridium insolitum* is very abundant in the lower part, but the relative abundance decreases above 1643.61 m, and the "mini-dinos" dominate the upper part of the succession.

The age-diagnostic dinoflagellate cyst events recognized in the dataset include the FO *Cousteaudinium aubrye* at 1639.17 m with the LO at 1611.54 m, and *Cordosphaeridium cantharellus* was only found in one sample at 1662.72 m.

No reworked taxa were found in the 2/11-12S well samples.

The palynofacies data (Fig. 5.7) showed an overall trend with increasing dinocyst abundances and decreasing non-saccate pollen upwards. Throughout the succession, the dinocysts abundance ranges between 35% and 76%, increasing gradually upwards the studied succession. The non-saccate pollen varies between 12% and 44%. The lower part of the succession (1670.70 m to 1639.17 m) is characterized by the highest relative abundance of non-saccate pollen (between 22% to 44%). In the upper part of the studied succession (1639.17 m to 1611.54 m), non-saccate pollen is present, but less common (12% - 37%).

Bissacate pollen is present throughout the entire succession and varies from 5% to 22%, showing a pattern similar to the non-saccate pollen with the highest relative abundances in the lower part of the succession (1670.70 m to 1639.17 m). Spores and fungal spores occur in very low numbers (<1%) and are present in most of the samples. Freshwater algae were recorded in fewer samples than spores and fungal spores but ranged within the same percentage (<1%). Acritarchs are present in every sample, with a relative abundance value between 1% and 4% (Fig. 5.7).

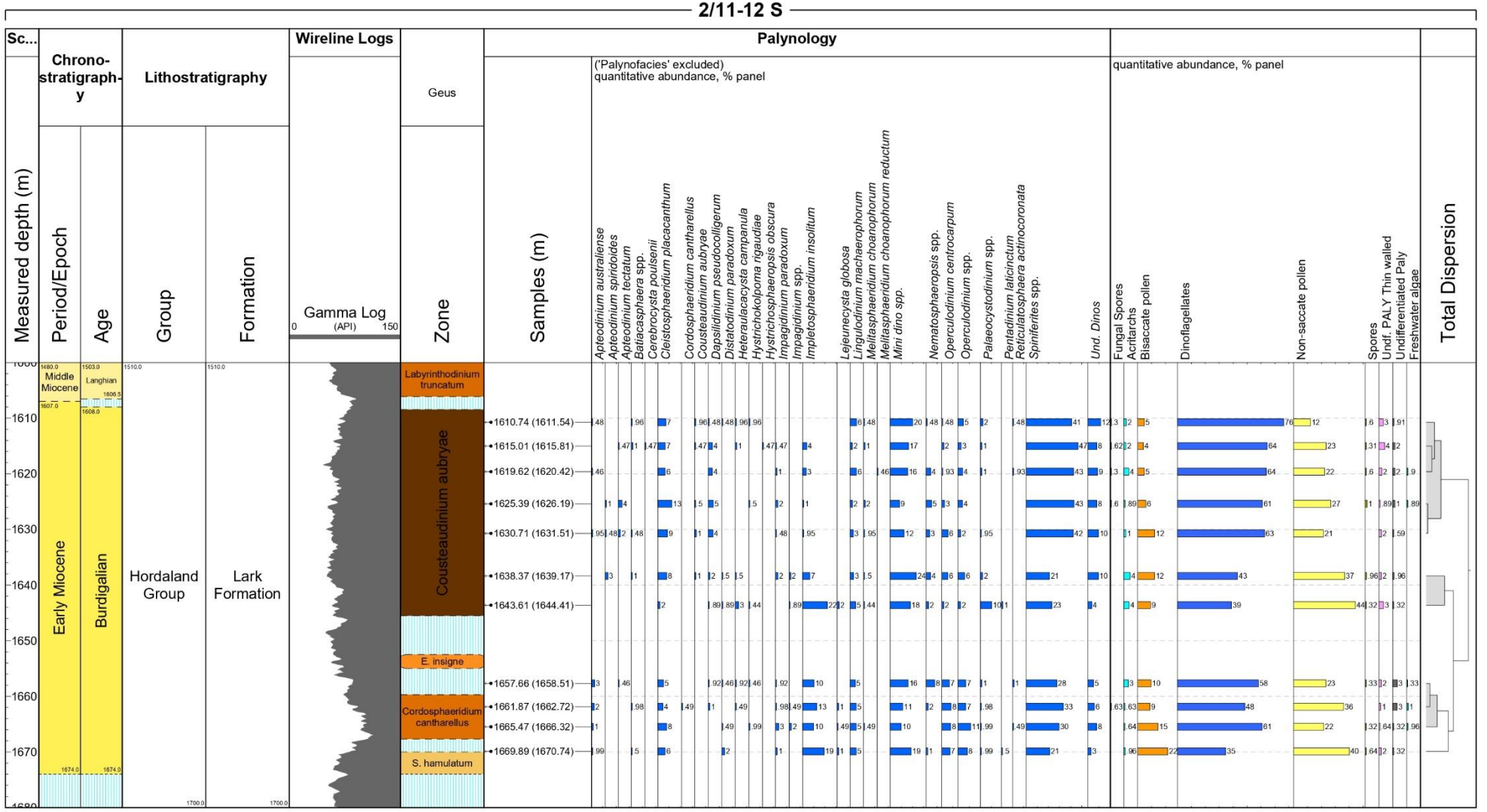

Figure 5.7. The 2/11-12S well range chart, with the relative abundances (%) of the established categories of palynomorphs and dinocyst taxa against the dinocyst zones defined by Dybkjær and Piasecki (2010) and the offshore Central North Sea lithostratigraphy of the Middle Miocene.

The P/D index shows the highest values (between 44% and 54%) in the lower part of the succession (1670.70 m to 1639.17 m). In the upper part of the succession, 1639.17 m to 1611.54 m, the P/D index only ranges between 15 to 47% (see appendix C, for P/D index values).

Regarding environment distribution, some neritic and oceanic taxa (see Table 4.2) are present in the 2/11-12S (e.g. *Cleistophaeridium placacanthum*, *Impagidinium* spp., and *Nematosphaeropsis* spp.). No inner neritic taxa are present.

Warm-water species (Table 4.1) such as *Lingulodinium machaerophorum*, and *Melitasphaeridium choanophorum* were found present throughout the succession. *Lingulodinium machaerophorum* is present in all of the samples, with higher percentages in the upper part of the succession (1639.17 m to 1611.54 m). *Melitasphaeridium choanophorum* occurs more frequently from 1644.41 to 1611.54 m.

5.3. Geochemistry

The BIT values (Figure 5.8) ranged between 0 and 0.09, meaning the absence of branched GDGTs.

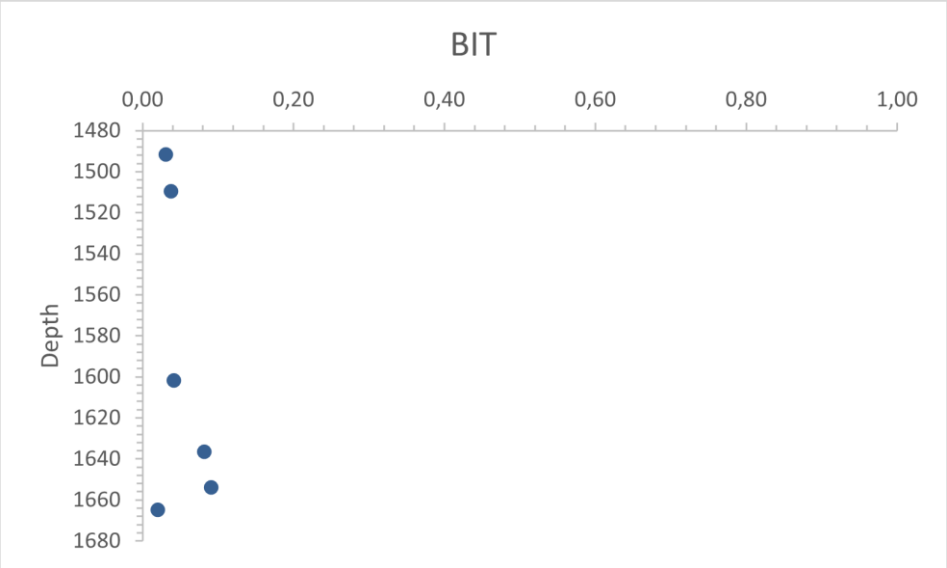

Figure 5.8. BIT values from the pilot analysis done on the 2/11-12S well sediments.

The %GDGT-0 (Figure 5.9) varies between 43.98% and 57.05%, being lower than the standard percentage for additional methanogenic sources (67%) as suggested by Damsté et al. (2012).

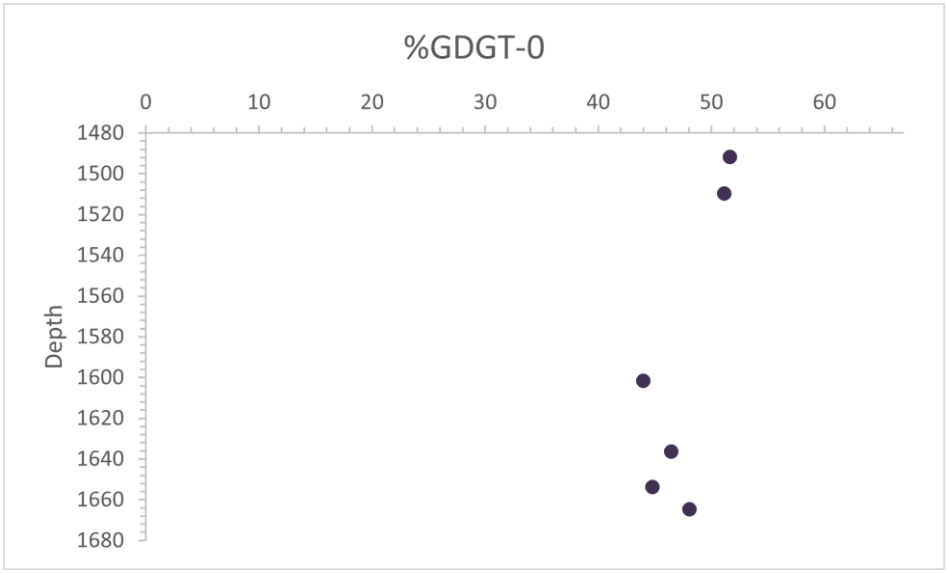

Figure 5.9. (%) GDGT-0 values from the pilot analysis done on the 2/11-12S well sediments.

The MI values (Figure 5.10) are between 0.18 and 0.28. Since the values were lower than 0.5, no samples were excluded.

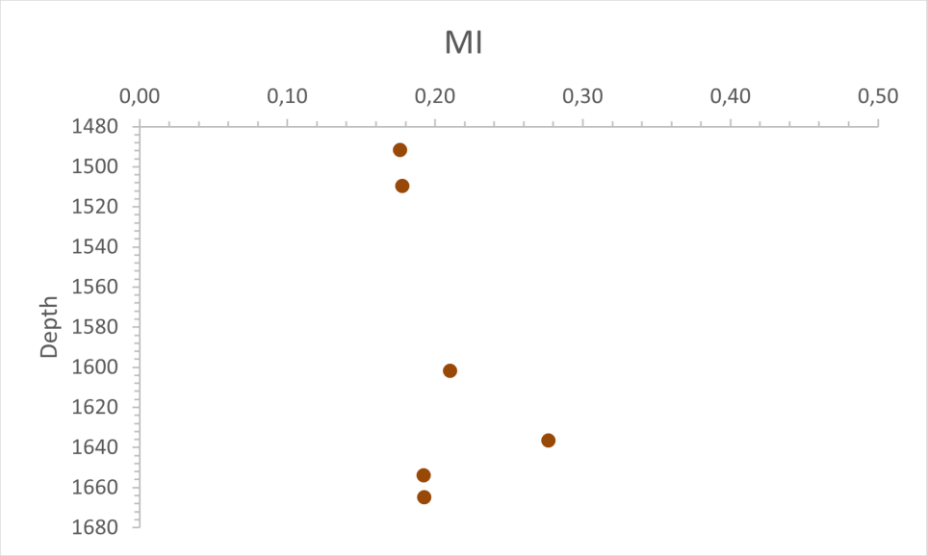

Figure 5.10. MI values from the pilot analysis done on the 2/11-12S well sediments.

The RI index (Figure 5.11) and the RI_{TEX} pursue (Figure 5. 12) values between 1.67 to 2.19 and 1.67 to 2.31, having small variations between them. Thus, the ΔRI is between -0.01 and 0.15 not deviating more the |0.3|. No samples were excluded.

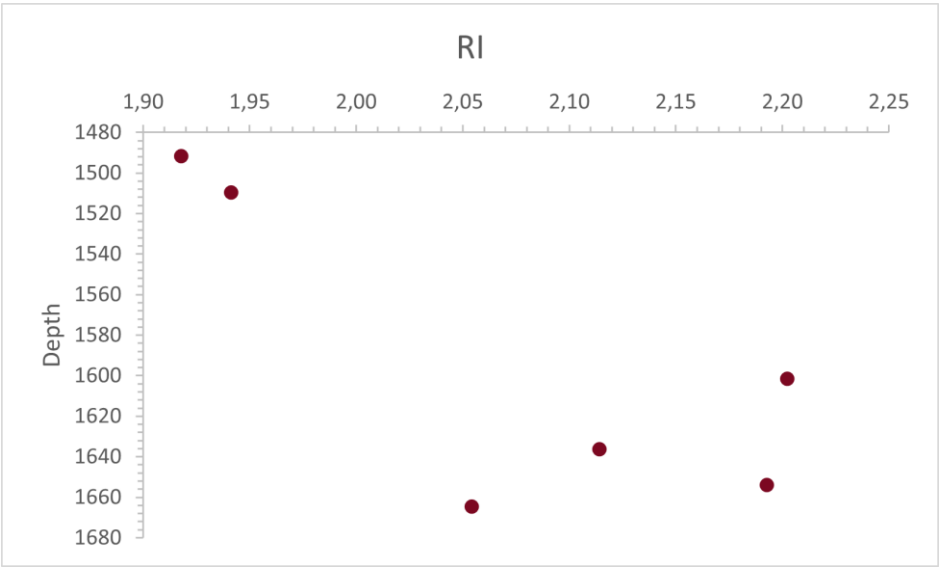

Figure 5.11. RI values from the pilot analysis done on the 2/11-12S well sediments.

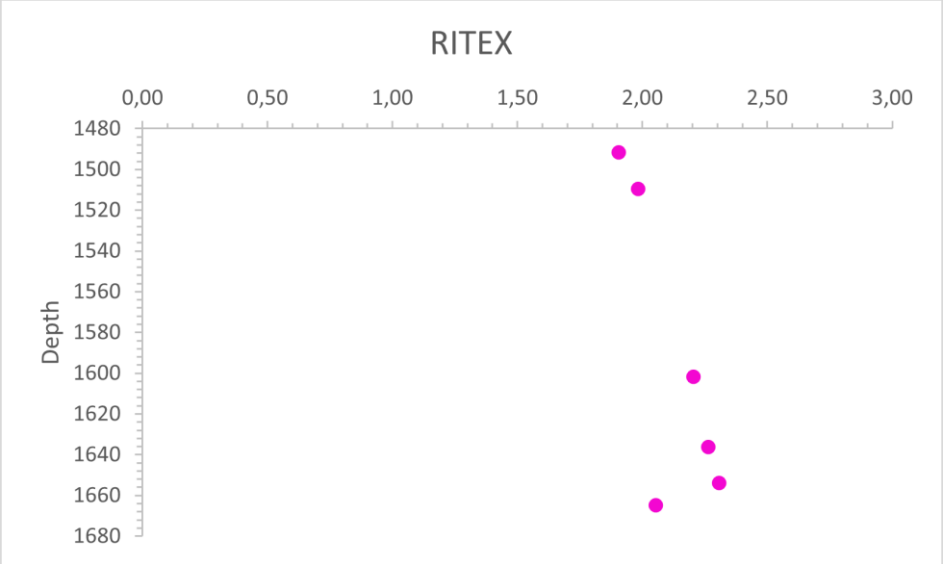

Figure 5.12. RI_{TEX} values from the pilot analysis done the 2/11-12S well sediments.

The $f_{Cren':Cren' + Cren}$ values (Figure 5.13) are between 0.00 and 0.06, being close to the lower values of the modern (0.00–0.16) core-top sediments (O'Brien et al., 2017).

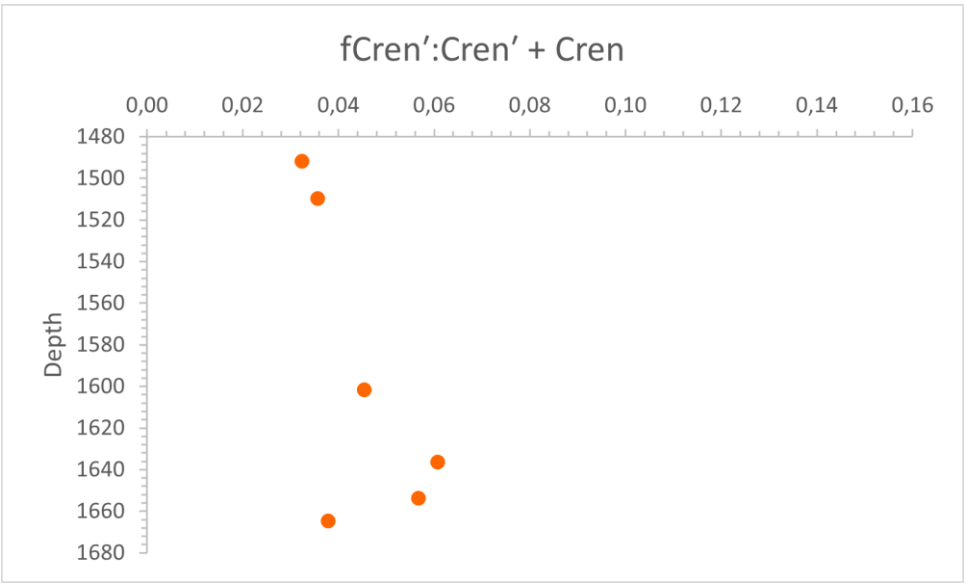

Figure 5.13. $f_{Cren':Cren' + Cren}$ values from the pilot analysis done on the 2/11-12S well sediments.

The ratio between GDGT-2 and GDGT-3 (Figure 5.14) varies between 1.98 and 3.55. The sample with a depth of 1672.07 m has no concentration value since GDGT-3 mass is null. Thus, the sample is excluded.

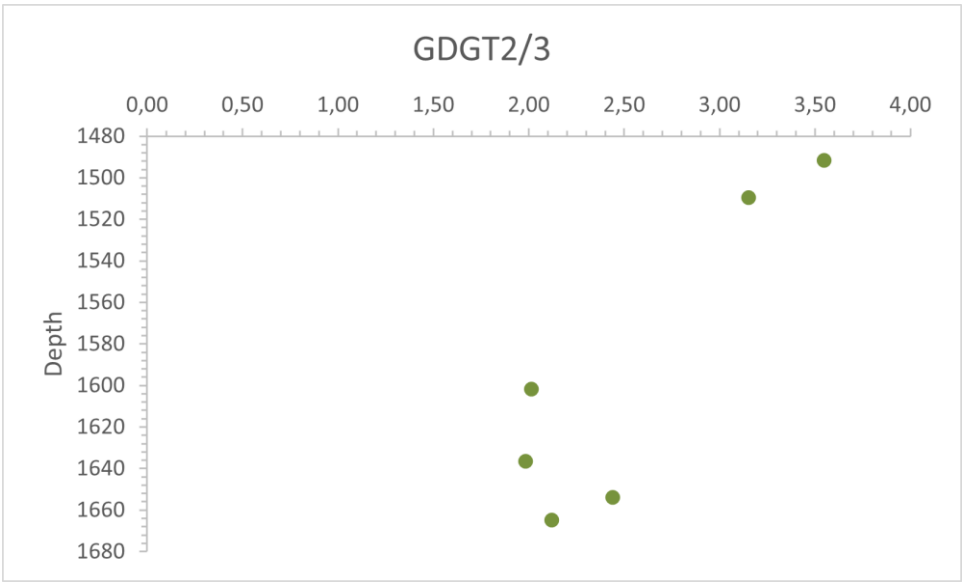

Figure 5.14. GDGT-2/GDGT-3 values from the pilot analysis done on the 2/11-12S well sediments.

The raw TEX_{86}^{H} calibration values are between -0.50 and -0.23. The absolute SST (Figure 5.15) obtained from the seven samples ranges between 14ºC and 23ºC. It is visible an increase in temperature (18ºC to 23ºC) from a depth of 1672,07 m to 1664,69 m. At the depth of 1653,80 m, the temperature reaches a maximum of 23ºC. A gradual decrease, from 23ºC to 14ºC, is observed in the depths of 1653,80 m to 1491,74 m.

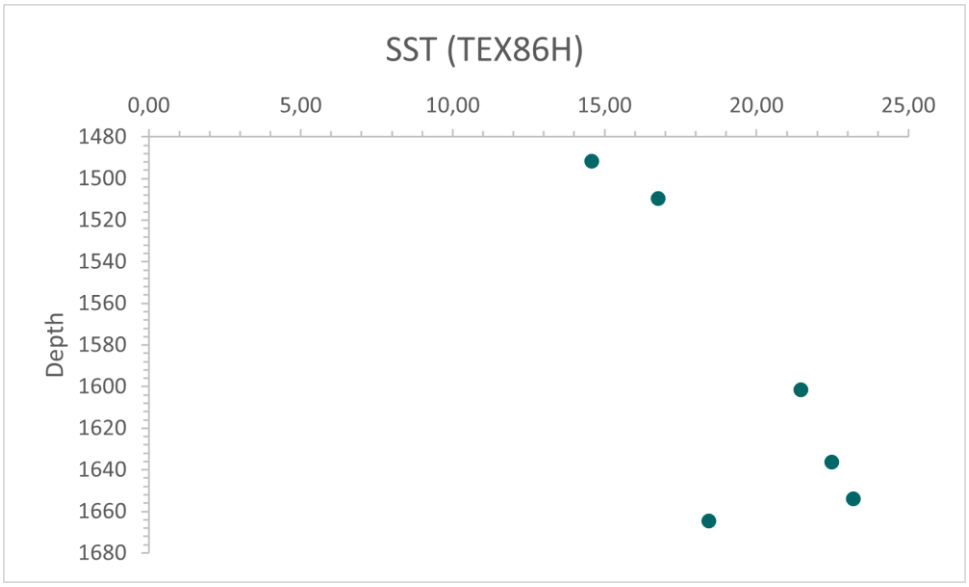

Figure 5.15. Sea Surface temperatures (ºC) from the 2/11-12S well.

6. Systematics

In both settings, 39 taxa were identified: 8 genera, 29 species, and 2 subspecies of dinocysts.

Palsys and Dinoflaj3 were used for the dinocyst taxa's taxonomy and descriptions (https://palsys.org/genus; http://dinoflaj.smu.ca/dinoflaj3/index.php/Main_Page).

6.1. Taxonomy

Apteodinium australiense (Deflandre and Cookson, 1955), Williams, 1978

Originally: *Gymnodinium australiense*

Taxonomic junior synonym: *Emslandia crassimurata*, according to Lucas-Clark (1987)

Holotype: Deflandre and Cookson, 1955, pl. 5, fig. 1

Age: Middle Miocene

Subchapter 6.2, Plate 1, A

Diagnosis:

Ovoidal cyst, divided into two approximately equal parts by a narrow, shallow, strongly helicoid girdle. The cyst has a short and broad apical horn connected to the girdle. The longitudinal furrow appears visible on the hypotheca. The cingulum is well developed. The wall is finely granulated and has a slight appearance of suggestive lines of plates. The archaeopyle is trapezoidal, precingular, and the posterior margin of the archeopyle is in contact with the paracingulum. The size is intermediate.

Apteodinium spiridoides Benedek, 1972

Emendation by: Benedek and Sarjeant, 1981, p. 319 as *Emslandia spiridoides*

Taxonomic junior synonym: *Apteodinium tectatum*, according to Lucas-Clark (1987)

Holotype: Benedek, 1972, pl. 2, fig. 1; Benedek and Sarjeant, 1981, fig.2, no. 1-3; Jan du Chêne et al., 1986, pl. 11, fig. 6-9.

Age: Middle Oligocene

Diagnosis:

Ovoidal cyst with a short and broad apical horn. The wall consists of three units: the ectophragm and autophragm connected by a middle unit with "processes" merged with a small and round channel in between. A bulge is present in the endophragma below the horn. No parasutural structures are present. The paracingulum and the parasulcus are grooved with the absence of short "processes" separating the ectophragm and autophragm. The paracingulum is narrow. The archeopyle is trapezoidal and the posterior margin is in contact with the paracingulum. The archeopyle is precingular and formed by the loss of paraplate 3"". The size is intermediate.

Apteodinium tectatum Piasecki, 1980

Taxonomic senior synonym: *Apteodinium spiridoides*, according to Lucas-Clark (1987)

Holotype: Piasecki, 1980, pl. 2, fig. 4-6; Jan du Chêne et al., 1986, pl. 10, figs. 5-8

Subchapter 6.2, Plate 1, B

Age: Middle Miocene

Diagnosis:

Ovoidal cyst with a short and broad apical horn. The wall also consists of three units, like *Apteodinium spiridoides* but has short "processes" separated independently by round channels. A bulge is present in the endophragma below the horn. No parasutural structures are present. The paracingulum and the parasulcus are grooved with the absence of short "processes" separating the ectophragm and autophragm. The paracingulum is narrow. The archaeopyle is trapezoidal and the posterior margin is in contact with the paracingulum. The archeopyle is precingular and formed by the loss of paraplate 3"".

Comments:

In this study, *Apteodinium tectatum* differs from other identified species of the genus mainly for the features of the wall. Regarding the wall pattern, *Apteodinium spiridoides* has a soft granulate with small white stains, while the *Apteodinium tectatum* has wider white

stains. The *Apteodinium australiense* is granulated but doesn't present any stains. Between the ectophragm and autophragm, *Apteodinium tectatum* has short "processes" separated by channels and the *Apteodinium spiridoides* has the "processes" merged with a small and round channel in between. The *Apteodinium australiense* has an absence of the "processes", having a hollow middle unit between the ectophragm and autophragm.

Genus *Batiacasphaera* Drugg, 1970b

Emendation by: Morgan, 1975; Dörhöfer and Davies, 1980

Taxonomic junior synonyms: *Sentusidinium*, according to Dörhöfer and Davies (1980)

Type species: *Batiacasphaera compta*, Drugg, 1970b (figs. 6A–B)

Subchapter 6.2, Plate 1, E

Diagnosis:

Subspherical cyst without septa, spines, or processes. Only composed by the autophragm. No parasutural features are present, although isolated surface features of low relief appear. The paratabulation is only indicated by the archeopyle. The archeopyle is apical. The suture of the archeopyle is in a zigzag shape. The size is small to intermediate.

Cerebrocysta poulsenii de Verteuil and Norris, 1996

Holotype: de Verteuil and Norris, 1996, Plate 12, figs. 9-14

Subchapter 6.2, Plate 1, C

Age: Early to Late Miocene

Diagnosis:

Ovoid and proximochorate cyst. The wall is simple with septa, in a fence-like pattern where some septa are connected, and others show little connectivity. The septa do not delimit tabulation but are suggestive of it. The archeopyle is mid-dorsal and precingular being quite large and suggestive of standard gonyaulacalean 3". The angles of the margin are rounded.

There are no depressions on the cyst to indicate a cingulum or sulcus and no apical pore structure. The size is small.

Cleistosphaeridium placacanthum (Deflandre and Cookson, 1955), Eaton et al., 2001

Originally: *Hystrichosphaeridium*

Emendation by: May (1980) as *Systematophora placacantha*

Taxonomic junior synonyms: *Baltisphaeridium panniforme*, according to Sarjeant (1984b)

Holotype: Deflandre and Cookson, 1955, pl. 9, figs. 1-2; Fauconnier and Masure, 2004, pl. 76, figs. 14-16.

Subchapter 6.2, Plate 2, B

Age: Miocene

Diagnosis:

Globular cyst, circular or asymmetrical in outline, with a large number of processes that are aligned to divide the whole surface into more or less polygonal plate-like areas or fields. Each field is separated from its neighbours by an area devoid of appendages. Processes solid, of variable form, somewhat flexuous, simple, or branched with pointed or hammer-shaped extremities, widening at the base. Sometimes the bases of 2 or more processes are connected by bridge-like strands (Deflandre and Cookson, 1955). Size is intermediate to big.

Genus *Cordosphaeridium* Eisenack, 1963

Taxonomic junior synonym: *Tityrosphaeridium*, according to Lentin and Williams (1985)

Emendation by: Morgenroth (1968); Davey (1969c); Sarjeant (1981); He Chengquan (1991)

Type species: originally as *Hystrichosphaeridium inodes*, Klumpp, 1953 (pl.18, figs. 1–2); *Cordosphaeridium inodes*, Eisenack, 1963

Diagnosis:

The central body can be spherical to ellipsoidal. Endophragm and periphragm are appressed between processes and are rarely clearly differentiated. It has 22 to 30 fibrous, solid, or hollow intratabular processes. The processes are commonly branched and expanded distally. The periphragm between the processes is faintly coarsely ornamented to commonly fibrous. No parasutural features. The paratabulation is gonyaulacacean, indicated by processes. The archeopyle is formed from the 3" plate, precingular, and operculum free. The position of the paracingulum is marked by six intratabular processes. The parasulcus is not clearly indicated, but the position may be suggested by a few to several small slender processes. The size is intermediate to large.

Cordosphaeridium Cantharellus (Brosius, 1963), Gocht, 1969

Originally: *Hystrichosphaeridium*

Holotype: Brosius, 1963, pl. 6, fig. 1; Fensome et al., 1993a, fig.1 - p. 1021.

Subchapter 6.2, Plate 2, C

Age: Late Oligocene

Diagnosis:

Spherical/ovoid cyst with delicate and smooth inner body. The inner body has a diameter of 50 µm. It can bear between 15 to 20 processes. The processes are big and hollow tree-like processes with bundled fibers that can already be discerned near the process bases. The processes have also a cylindrical shape, are slightly narrow in the middle, and broaden weakly distally. In the distal membrane of the funnel, they become evenly fibrous or split into single bundles. The archeopyle is precingular and apical. Formed by the loss of plate 3".

Cordosphaeridium minimum (Morgenroth, 1966) Benedek, 1972

Originally: *Cordosphaeridium inodes minimum*

Taxonomic senior synonym: *Hystrichosphaeridium latirictum* according to Fensome et al. (2009)

Holotype: Morgenroth, 1966, pl. 5, fig. 6-7

Age: Early Eocene

Diagnosis:

The central body is ellipsoidal with an uneven membrane surface. The processes are trumpet-shaped with a hollow structure. The acheopyle is small compared to other species from the genus. The size is small. The central body can measure in diameter 20 µm and the processes are between 8 to 11 µm.

Cousteaudinium aubryae de Verteuil and Norris, 1996a

Holotype: de Verteuil and Norris, 1996a, pl. 1, figs. 1-3, 6, 9

Subchapter 6.2, Plate 1, I

Age: Lower to Middle Miocene

Diagnosis:

Cousteaudinium aubryae is morphologically variable concerning the degree of separation between the endoblast and periblast, which ranges from fully inflated with no process shafts to closely appressed at the limbi. The endoblast and periblast are in contact only at the margins of the apical archeopyle. The endoblast can be subspherical to spherical, and the periblast subspherical and variably chorate. When the endoblast and periblast are closely appressed at the limbi, the tegillum can form hollow, tubular, open or distally perforate, intratabular processes that in width and shape approximate the geometry of the tabulation elements. These processes can be distally slightly flared and irregularly denticulate. The tabulation as indicated by the processes is gonyaulacalean The archeopyle margin is rounded with a low, geniculate ventral protuberance. Cousteaudinium aubryae are an intermediate to large cribroperidinioidean cysts.

Comments:

The specimens of *Cousteaudinium aubryae*, in this study, did not present a resemblance to the species *Hystrichokolpoma rigaudiae*, as mentioned in de Verteuil and Norris (1996). However, it showed a slight resemblance to the *Pentadinium laticinctum*.

Despite being similar, the *Pentadinium laticinctum* has processes that are gonal rather than intratabular, differentiating from *Cousteaudinium aubryae*.

Dapsilidinium pseudocolligerum (Stover, 1977) Bujak et al., 1980

Originally: *Polysphaeridium*

Taxonomic senior synonym*: Polysphaeridium pastielsii* according to Mertens et al. (2014)

Holotype: Stover, 1977, pl. 1, fig. 14-16

Age: Early Oligocene to Early Miocene

Diagnosis:

The cyst is chorate with a spherical body. Generally, the cyst has 40 or more nontabular processes. The endophragm is typically thicker than the periphragm, and the wall layers are appressed between processes. The processes are uniform in size and shape. They are hollow, slightly wider proximally than distally, and the surface of processes is smooth. The archeopyle is apical and the archeopyle suture is only slightly angular. The operculum is free and constituent apical paraplates are not delineated on its surface. Except for the archeopyle, indicators of paratabulation and parasulcus are absent. The operculum is free and the constituent apical paraplates are not delineated on its surface. Except for the archeopyle, indicators of paratabulation and parasulcus are lacking. The size of the central body can be 36 to 45 µm, and the processes can arrive at a length of 15 to 23 µm.

Dinopterygium cladoides Deflandre, 1935

Taxonomic junior synonym: *Toolongia medusoides*, according to Yun Hyesu (1981)

Holotype: Deflandre, 1935, pl. 8, fig. 6; Deflandre, 1936b, pl. 8, figs. 1-2.

Age: Senonian

Diagnosis:

In the frontal view, the outline of the theca is hexagonal. The furrow is transversely straight and separates the cyst into approximately two equal parts. It is bordered on both sides by large membranous expansions, which run around the theca. The large and flexible membrane appears to be supported by thin, straight, or curved horns. The upper part has the shape of a truncate pyramid. The ribs are lined with aliform crests, which, at their vertical angles, form a kind of membranous horns. The lower part is rounded with similar crests. The wall has punctation marks that are also found within the transverse furrow. The diameter of the cyst can reach 85 µm.

Genus *Distatodinium* Eaton, 1976

Taxonomic junior synonym: *Bipolaribucina*, according to Chen et al. (1988)

Emendation by: Zevenboom and Santarelli in Zevenboom (1995); Fensome et al. (2009)

Type species: *Distatodinium craterum*, Eaton, 1976 (pl. 9, fig. 1)

Diagnosis:

The central body is an elongated ellipsoidal. The processes can be simple or branched, variable in breadth, flattened and blade-like in cross-section, proximally expanded and ramified. Ramifications are typically complex. Occasionally, slender tubular processes are present. The number of processes varies from about 14 (in some species without an operculum) to about 60 or more. Processes are aligned into rows that are parallel to the long axis of the cyst body and situated on or close to reflected plate boundaries. Many are also arranged in a more or less circular way around the central body. Adjacent processes can also be connected by a membrane. Paratabulation is not clearly indicated. The archeopyle is apical, and the suture has a zigzag cut, but is commonly difficult to discern. It is operculum free. The Paracingulum is not indicated or expressed as an equatorial and does not yield processes. The Parasulucus is also not indicated. The size can be intermediate to large.

Distatodinium paradoxum (Brosius, 1963) Eaton, 1976

Originally: *Hystrichosphaeridium*

Taxonomic junior synonym: *Distatodinium craterum*, according to Fensome et al. (2009)

Holotype: Brosius, 1963, pl. 4, fig. 6; Fensome et al., 1995, fig. 2 - p. 1639

Subchapter 6.2, Plate 1, D

Diagnosis:

The central body is an elongated outline with a smooth surface. The processes are typically slender, simple or branched, distally and proximally expanded, usually flattened and blade-like in cross-section, occasionally tubular. Distally they are bifurcate or trifurcate with some secondary and tertiary branchlets at the extremities. The number of processes can reach 20. In addition to the alignment of the processes into rings around the cyst body, there is also some alignment into rows parallel to the long axis. A membrane may proximally unite adjacent longitudinally aligned processes. The archeopyle is apical. The operculum bears four processes, two of which are proximally united by a membrane. The size of the central body can be up to 46 µm and the length of the processes up to 24 µm.

Exochosphaeridium insigne de Verteuil and Norris, 1996

Holotype: de Verteuil and Norris, 1996 pl. 3, figs. 5, 6, 8- 10

Age: Lower Miocene

Diagnosis:

Proximochorate and spherical cyst. The autophragm is homogenous and dense, with a pattern of fibers with intervening spaces. The processes are evenly distributed, nontabular, fibrous, and distally truncated. The archeopyle is precingular and operculum free. The sulcus can be indicated by a mid-ventral group of less robust processes.

Comments:

Exochosphaeridium insigne was identified due to some processes having a “cut-shape” distally. *Operculodinium centrocarpum* can be misidentified as *E. insigne* however, *O. centrocarpum* is generally bigger and has longer processes relative to its central body. The processes are also thinner compared to E. insigne.

Heteraulacacysta campanula Drugg and Loeblich, 1967

Holotype: Drugg and Loeblich, 1967, pl. 1, fig. 8a-c

Subchapter 6.2, Plate 2, D

Age: Middle Eocene

Diagnosis:

The cyst is proximate with a cingular archeopyle. The epitract is bell-shaped and the hypotract is cup-shaped. Both endophragm and periphragm are thin. The endophragm is smooth but the periphragm is ornamented with grana and irregular spines. The sutural ledges arise from the periphragm and are radially striated. The cingular flanges are radially striate. They fit closely together with no cingular furrow between them. The cyst can be 55 to 72 μm in length and have a width of 63 to 97 μm.

Hystrichokolpoma rigaudiae Deflandre and Cookson, 1955

Taxonomic junior synonyms: *Galea xiphea* and *Hystrichosphaeridium stellatum*, both according to Sarjeant (1983)

Holotype: Deflandre and Cookson, 1955, pl. 6, fig. 6

Subchapter 6.2, Plate 1, F

Age: Eocene to Miocene

Diagnosis:

Globular cyst with axial symmetry and a smooth wall. The processes present two types of shape and are disposed of parallel series starting from apical pole. The bases of the large processes are marked by lines forming quadrangular areas that give the impression of plates. The large processes are generally widened and provided with more or less numerous and sometimes relatively long horns distally. The large process situated at the apical pole is often longer than the others and is sometimes prolonged into a hollow horn. The narrow tubular processes are slightly widened or divided at their extremities. The narrow processes forming the equatorial series are about 10 in number, of which some may be paired. The

diameter of the central body can be between 35 to 45 µm, the length of the larger processes can be 20 to 30 µm and the smaller processes 18 to 25 µm.

Hystrichosphaeropsis obscura Habib, 1972

Holotype: Habib, 1972, pl. 21, fig. 1

Subchapter 6.2, Plate 1, G

Age: Late Miocene

Diagnosis:

Bicavate cyst with a rectangular hypotract. The internal capsule is oval and commonly closely appressed to the outer membrane in the area of the cingulum. The surface of the internal capsule is densely granular, and the outer membrane is smooth. Despite the difficulty regarding general cyst tabulation, tabulation of the cingulum is usually best expressed. The archeopyle (3") is precingular, large, and rectangular. The cyst size ranges between 70 to 95 µm.

Genus *Impagidinium* Stover and Evitt, 1978

Type species: originally as *Leptodinium dispertitum*, Cookson and Eisenack, 1965a (pl. 12, figs. 5–6); *Impagidinium disperitum*, Stover and Evitt, 1978

Diagnosis:

The shape of the cyst is ellipsoidal. The wall is composed of the authophragm only. The parasutural septa are smooth with uniform height. The archeopyle is precingular and it is formed from the 3” plate, and operculum free. The paracingulum is indicated by four to six rectangular to elongate-hexagonal paraplates. The parasulcus is clearly delimited by parasutural features, except where bordering septa are absent. The size can be small to large.

Impagidinium paradoxum (Wall, 1967) Stover and Evitt, 1978

Originally: *Leptodinium*

Holotype: Wall, 1967, pl. 15, fig. 5

Subchapter 6.2, Plate 2, G

Age: Middle Miocene to Holocene

Diagnosis:

The cyst is ovoid. The most clearly visible diagnostic characteristic is the parasutural septa. The septa have a low height and a smooth surface. The cyst is also divided equatorially into epithecal and hypothecal regions by a relatively wide, descending girdle displaced by its width ventrally. The longitudinal furrow broadens onto the hypotheca and is weakly inclined. The archeopyle is formed by the 3".

Impletosphaeridium insolitum Eaton, 1976

Holotype: Eaton, 1976, pl. 21, fig. 5; Bujak et al., 1980, pl. 5, fig. 5

Subchapter 6.2, Plate 2, E

Age: Early to Middle Eocene

Diagnosis:

The cyst has a spherical body with a smooth or finely granular surface. The processes are numerous and slender. They are simple with small distal bulbous spherical termination and may be thickened by the development of the proximal membrane. The diameter of the central body can range from 15 to 24 μm, and the length of the processes can go up to 9 μm.

Labyrinthodinium truncatum Piasecki, 1980

Emendation by: de Verteuil and Norris, 1996a, p. 150

Holotype: Piasecki, 1980, pl. 2, figs. 9-11; Fensome et al., 1995, figs. 1-3 - p. 1855; Fauconnier and Masure, 2004, pl. 51, figs. 5-6

Subchapter 6.2, Plate 1, H

Age: Middle Miocene

Diagnosis:

Small chorate cyst with a spherical central body, composed of two wall layers. Endophragma is hyalin and structureless, periphragma is smooth to spongeous at the surface of the main body, and smooth with scattered microgranulaes when forming crests and processes. Periphragma forms an open reticulum of adjoining crests from which membraneous processes arise. All the processes are equal in length and slightly expanded distally into small platforms. No structures reflect paratabulation, paracingulum, or parasulcus, except for the archeopyle sutures. The archaeopyle is large and polygonal. The diameter of the central body can reach 23 to 40 µm and the process length can be from 4 to 10 µm.

Labyrinthodinium truncatum modicum De Verteuil and Norris, 1996

Holotype: Plate 14, figs. 7- 12

Age: Lower to Middle Miocene

Diagnosis:

Proximate and spherical cyst. The morphology of the wall and processes are similar to Labyrinthodinium truncatum but the cyst size is small. The processes are nontubular and numerous, having a length of 1 to 3 µm. Low septa may be present or absent at the bases of the processes. Distally, the processes can be without well-developed platforms. Some specimens lack recognizable processes, having only low, evenly distributed blade-like septa. The size of the central body can reach from 17 to 36 µm.

Lejeunecysta globosa Biffi and Grignani, 1983

Holotype: Biffi and Grignani, 1983, pl. 2, fig. 6

Age: Oligocene

Diagnosis:

Peridinioid cyst. The cyst is compressed dorsoventrally, with a rounded pentagonal ambitus. The epicyst is conical, with convex sides and rounded apex. The hypocyst is

trapezoidal. The antapical horns are represented by two rounded protrusions with an almost absent antapical depression. The paracingulum is continuous, marked by transverse folds. The autophragm is smooth and slightly punctate. Regarding process development, the cyst is proximate. The archeopyle is formed by the loss of intercalary 2a, symmetrically situated on the middorsal line and extending almost to the paracingulum. The size of the cyst can reach 68 to 90 µm.

Lingulodinium machaerophorum (Deflandre and Cookson, 1955) Wall, 1967

Originally: *Hystrichosphaeridium*

Taxonomic junior synonym: *Cleistosphaeridium disjunctum*, according to Reid (1974)

Holotype: Deflandre and Cookson, 1955, pl. 9, fig. 4

Subchapter 6.2, Plate 1, J

Age: Miocene

Diagnosis:

The central body can be subspherical, or ellipsoidal. The membrane is thick, punctated, and covered by numerous (15 to 20) long, stiff, conical, pointed processes resembling the blade of a dagger. Their bases are circular and minutely striated, and their distal extremities are flexuous, closed, and bear spinules. The size of the central body can range between 41 to 54 µm and the processes can vary in length, 13 to 18 µm. The archeopyle is precingular and can be formed by the loss of five plate areas (1" to 5"), four plates (2" to 5") or very rarely, only the dorsal precingular plate 3".

Genus *Melitasphaeridium* Harland and Hill, 1979

Type species: Deflandre and Cookson, 1955 (text-figs. 23–26) as *Hystrichosphaeridium choanophorum*

Diagnosis:

Skolochorate cyst with subspherical body. Regarding the wall layers, the periphragm is smooth or faintly ornamented. The processes are hollow, intratabular processes with strongly aculeate or slightly expanded distally to funnel-shaped tips with smooth or denticulate margins. Generally, the number of processes varies between 19 and 25 µm. The archeopyle is precingular and formed by the loss of a 3" plate. Is operculum free.

Melitasphaeridium choanophorum (Deflandre and Cookson, 1955) Harland and Hill, 1979

Taxonomic junior synonym: *Melitasphaeridium aequabile*, according to Head and Wrenn (1992)

Emendation by: Harland and Hill, 1979 as *Melitasphaeridium choanophorum*

Holotype: Deflandre and Cookson, 1955, text-figs. 23–26; Fensome et al., 1993a, figs. 1–4, p. 1055)

Subchapter 6.2, Plate 1, K

Age: Pliocene

Diagnosis:

Spherical or subspherical chorate cyst. It is composed of two wall layers that are continuous, conspícuos, and smooth to microreticulate. Has hollow, tubular processes that are formed completely from the periphagm. They have flared, stellate distal tips of variable morphology. The processes are approximately half the diameter of the central body in length and are rigid to slightly flexuous. The archeopyle is precingular and is formed by the loss of the 3" plate. The diameter of the central body can reach between 30 to 34 µm and the processes 15 to 17 µm.

Melitasphaeridium choanophorum var. reductum Strauss and Lund, 1992

Holotype: Strauss and Lund, 1992, pl. 2, figs. 13-14

Age: Middle Miocene

Diagnosis:

Similar morphology of *Melitasphaeridium choanophorum*, but with completely reduced distal processes, or with very narrow distal process terminations. These can be with smooth or short-spined margins.

Mini dinos spp., Piasecki

Subchapter 6.2, Plate 2, F

Diagnosis:

The group “mini-dinos” was created for dinocysts that are too small (<30 um) for genera/species identification, but visually distinct from other types of palynomorphs (e.g. acritarchs). Their appearance varies, but most of them are chorate.

Genus *Nematosphaeropsis* Deflandre and Cookson, 1955

Taxonomic junior synonym: *Trabeculidium*, according to Stover and Williams (1987)

Emendation by: Williams and Downie, 1966c

Type species: Deflandre & Cookson 1955, p. 258 (pl. 8, fig. 5) as *Nematosphaeropsis balcombiana*

Subchapter 6.2, Plate 2, H

Diagnosis:

Chorate to proximochorate cyst with a spherical and smooth central body. It bears processes that are gonal or intergonal, connected distally by penitabular trabeculae. The gonal processes are distally trifurcate and intergonal processes are bifurcate. It bears six from each trifurcate process and four from each bifurcate process. Pairs of penitabular trabeculae may be partially joined to each other. This connection can be by short, transverse strands or by direct fusing of the trabeculae in the span between the process terminations that they are joining. These structures can vary from solid subcylindrical rods to ribbon-like membranes of various widths. The archeopyle is precingular and is formed by the loss of the 3” plate. Is operculum free. The size can be small to intermediate.

Comments:

Species of this genus can be differentiated by the type of penitabular trabeculae. These structures can be singular to each species.

Genus *Operculodinium* Wall, 1967

Emendation by: Matsuoka et al., 1997, p. 22

Type species: Deflandre and Cookson, 1955 (pl. 8, figs. 3–4), as *Hystrichosphaeridium centrocarpum*

Diagnosis:

Spherical to ovoid cysts with simple, dorsal precingular archeopyles (reflecting plate 3``), and with the absence of polar structures. A ventral sulcal depression is often present. The cyst wall is double-layered, where the periphragm can be microgranulated. The central body is covered by nontabular processes, cones, or spines. The processes are typically capitate, hollow, and closed distally. The size can be small to big.

Operculodinium centrocarpum (Deflandre and Cookson, 1955) Wall, 1967

Originally: *Hystrichosphaeridium centrocarpum*

Taxonomic junior synonyms: *Operculodinium? echigoense*, according to Matsuoka et al. (1997)

Holotype: Deflandre and Cookson, 1955, pl. 8, figs. 3-4

Subchapter 6.2, Plate 2, J

Age: Miocene

Diagnosis:

Ellipsoidal cyst, covered with numerous straight, slender processes placed irregularly or with a certain alignment. The processes are solid, showing radiating fibrils at their point of insertion on the cyst which is ornamented with a fine reticulum. The slightly widened apices of the processes are fringed with 10 or more small, curved spines. The surface of the

periphragm has a granular pattern. The diameter of the central body can be between 54 to 80 µm and the length of the processes is 13 to 18 µm.

Comments:

The *Operculodinium centrocarpum* can be distinguished from other *Operculodinium* species through the granular wall pattern and process morphology. The diagnostic characteristics in the processes are proximally a triangular-shaped process base due to radiating fibrils, and distally the small spines.

Genus *Palaeocystodinium* Alberti, 1961

Taxonomic senior synonym: *Svalbardella*, according to Lindgren (1984)

Taxonomic junior synonym: *Cystodiniopsis* in Vozzhennikova (1967)

Emendation by: Fensome et al., 2009

Type species: *Palaeocystodinium golzowense*, Alberti, 1961 (pl.7, fig. 12)

Subchapter 6.2, Plate 2, I

Diagnosis:

Proximate and elongated ellipsoidal cyst with single slender apical and antapical horns at both poles. The wall has no parasutural features and the periphragm can be smooth or faintly ornamented. The antapical horn may have a short lateral spur. The archeopyle is formed by the loss of the 2a plate. Is operculum free. The paracingulum and parasulcus are not normally indicated. The size is large.

Pentadinium laticinctum Gerlach, 1961

Emendation by: Benedek et al., 1982, p. 268–272.

Holotype: Gerlach, 1961, pl.26, fig. 5-6, text-figs. 6-7

Subchapter 6.2, Plate 2, A

Age: Middle Oligocene to Middle Miocene

Diagnosis:

This cyst consists of a strong, granulated dark-colored capsule enveloped by a clear, soft outer layer. This layer has sutural cavations between one-sixth and one-eighth of the diameter of the central body. The boundaries between some paraplates are incompletely expressed by sutural outgrowths, and the mid-ventral region is occupied by a greatly widened sulcus. The archeopyle is a single precingular plate, formed by a loss of 3".

Comments:

In this study, *Pentadinium laticinctum* was identified through the different morphology of the inner and outer layers. No greatly widened sulcus was seen.

Polysphaeridium zoharyi (Rossignol, 1962) Bujak et al., 1980

Taxonomic junior synonym: *Polysphaeridium subtile*, according to Islam (1983b)

Taxonomic senior synonym: *Hystrichosphaera intermedia*, according to Matsuoka (1983a)

Holotype: Rossignol, 1962, pl. 2, fig. 10

Subchapter 6.2, Plate 1, L

Age: Pleistocene

Diagnosis:

Ellipsoidal cyst with a micro granular wall surface. The processes are proximally striated, numerous, and have bifurcated termination. The length of the processes is small compared to the central body. The size of the central body can reach 45 μm and the length of the processes can be variable but not much longer than 10 μm.

Reticulatosphaera actinocoronata (Benedek, 1972) Bujak and Matsuoka, 1986

Taxonomic junior synonym: *Reticulatosphaera stellata*, according to Bujak and Matsuoka (1986)

Emendation by: Bujak and Matsuoka, 1986

Holotype: Benedek, 1972, pl. 12, fig.13; Benedek and Sarjeant, 1981, fig.10/5; text-fig.11

Subchapter 6.2, Plate 2, L

Age: Middle/ Late Oligocene

Diagnosis:

Chorate and subspherical cyst with a finely granular wall surface. The processes are intratabular and tubiform with ramifying distal extremities. The bilateral ramifications can further branch widely, and an irregular network can be formed by distal trabeculae connecting adjacent processes. A trapezoidal and precingular archeopyle is formed by the loss of the 3" plate and is free of operculum. The size of the central cyst can be between 13 to 15 µm. The length of the processes to the branching point can be 12 to 17 µm.

Genus *Spiniferites* Mantell, 1850

Taxonomic junior synonym: *Hafniasphaera*, according to Stover and Williams (1987, p. 117)

Emendation by: Sarjeant, 1970, p. 75; Sarjeant, 1981, p. 108

Type species: *Spiniferites ramosus* (Ehrenberg, 1838) Loeblich and Loeblich, 1966

Subchapter 6.2, Plate 2, K

Diagnosis:

Subspherical cyst with parasutural ridges connecting the processes bases. The wall between the processes can be smooth to very ornamented. The processes can be solid or hollow, and their tips are normally trifurcated or bifurcated. Closely spaced processes can be fused from bases upwards. Paratabulation can be indicated by the ridges of the processes. The archeopyle is precingular, 3'', and operculum free. The paracingulum and the parasulcus are indicated by the parasutural features. The size of the cyst can be bigger than 40 µm.

Sumatradinium hamulatum De Verteuil and Norris, 1996

Holotype: de Verteuil and Norris, 1996, Plate 16, figs. 2-5

Age: Early Miocene

Diagnosis:

The cyst is proximate and typically dorsoventrally compressed. The hipocyst sides are straight to convex with two short, symmetric, moderately pointed to rounded antapical lobes. The epicyst is the widest at the cingulum but converges two flanks into an apical compression. The wall has a maze-like pattern created by very small curvilinear structural elements. The archeopyle is formed by the loss of the 2a plate. It is operculum free. The size of the cyst can vary between 69 and 95 µm.

Tectatodinium pellitum Wall, 1967

Taxonomic junior synonym: *Tectatodinium grande*, according to Head (1994a)

Emendation by: Head, 1994a, p. 308, 310

Holotype: Wall, 1967, pl. 16, fig. 12

Age: Miocene to Holocene

Diagnosis:

The cyst is proximate and ovoid shaped with usually a slight apical protuberance. The wall appears to have a spongy texture. The archeopyle is precingular and formed by the loss of the third precingular paraplate. The operculum monoplacoid and free. There are no indications of paratabulation. The size of the cyst can range from 38 and 53 µm.

6.2. Plates

The selected dinocyst taxa and palynofacies organic particles are presented in Plate 1, Plate 2, and Plate 3. The scales in the photos provide the correspondent measures. The images in Plate 2 were taken by Dr. Karen Dybkjaer, in GEUS (Copenhagen), with the same microscope and camera mentioned in the Material & Methods, chapter 4.

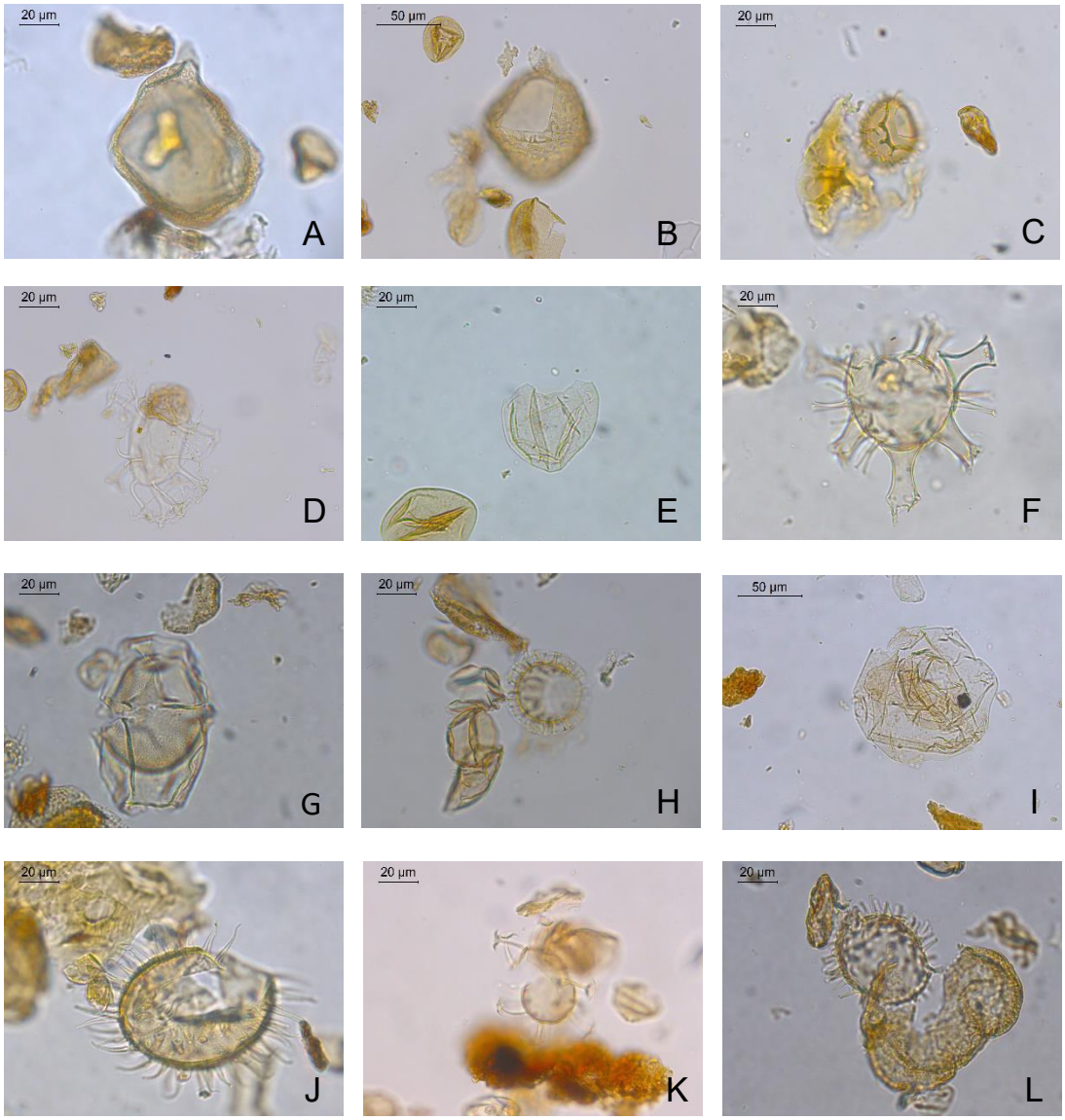

Plate 1

Specimens of dinocysts taxa found in Sønder Vium well (onshore Denmark). For other palynofacies palynomorphs and phytoclasts see Plate 3. During microscope work, coordinates were taken with an England Finder (EF).

A. *Apteodinium cf. australiense*, Sdr. Vium, depth 51.42 m, EF: H17 2-4, 2

B. *Apteodinium Tectatum*, Sdr. Vium, depth 74.02 m, EF: K56-4, 1

C. *Cerebrocysta poulsenii*, Sdr. Vium, depth 51.42 m, EF: L50-3, 1

D. *Distatodinium paradoxum*, Sdr. Vium, depth 74.02 m, EF: Q32, 1

E. *Batiacasphaera* spp., Sdr. Vium, depth 133.32 m, EF: F25-3,1

F. *Hystrichokolpoma rigaudiae*, Sdr. Vium, 51.42 m, EF: C43 2-4, 1

G. *Hystrichosphaeropsis obscura*, Sdr. Vium, depth 51.42 m, EF: D41-1, 1

H. *Labyrinthodinium truncatum*, Sdr. Vium, depth 51.42 m, EF: M41-3, 2

I. *Cousteaudinium aubryae*, Sdr. Vium, depth 95.42 m, EF: N51-3, 2

J. *Lingulodinium machaeophorum*, Sdr. Vium, depth 51.42 m, EF: G19-1, 1

K. *Melitasphaeridium choanophorum*, Sdr. Vium, depth 51.42 m, EF: H19 1, 4

L. *Polysphaeridium zoharyi*, Sdr. Vium, depth 51.42 m, EF: C46, 1

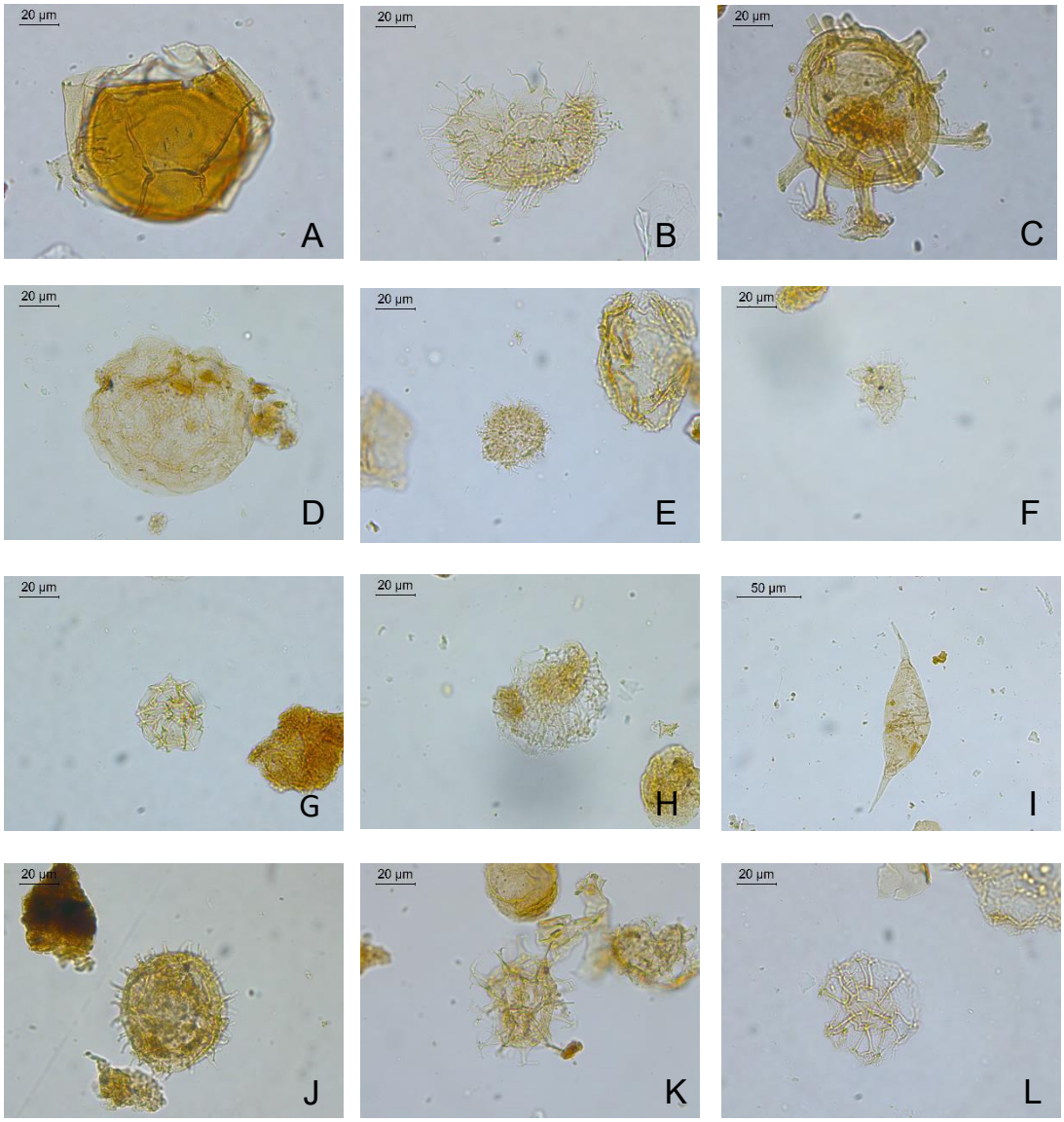

Plate 2

Specimens of dinocysts taxa found in the 2/11-12S well. For other palynofacies palynomorphs and phytoclasts see Plate 3. During microscope work, coordinates were taken with an England Finder (EF).

A. *Pentadinium laticinctum,* 2-11-12S well, depth 1602.42 m, EF: P46, 1

B. *Cleistosphaeridium placacanthum*, 2/11-12S well, depth 1506.91 m, EF: K52-2, 1

C. *Cordosphaeridium cantharellus*, 2/11-12S well, depth 1660.54 m, EF: Q32 1-2, 2

D. *Heteraulacacysta campanula,* 2-11-12S well, depth 1622.46 m, EF: V41, 1

E. *Impletosphaeridium insolitum*, 2/11-12S well, depth 1655.57 m, EF: H42-2, 2

F. Mini dinos spp., 2/11-12S well, depth 1506.91 m, EF: H49, 1

G. *Impagidinium paradoxum*, 2-11-12S well, depth 1549.83 m, EF: D50, 1

H. *Nematosphaeropsis* spp., 2/11-12S well, depth 1514.15 m, EF: Q20-2, 1

I. *Palaeocystodinium* spp., 2/11-12S well, depth 1622.46 m, EF: M33-2, 1

J. *Operculodinium centrocarpum,* 2-11-12S well, depth 1491.74 m, EF: K41 1-2, 1

K. *Spiniferites* spp., 2/11-12S well, depth 1504.6 m, EF: R49, 1

L. *Reticulatosphaera actinocoronata*, 2/11-12S well, depth 1602.42 m, EF: O54, 1

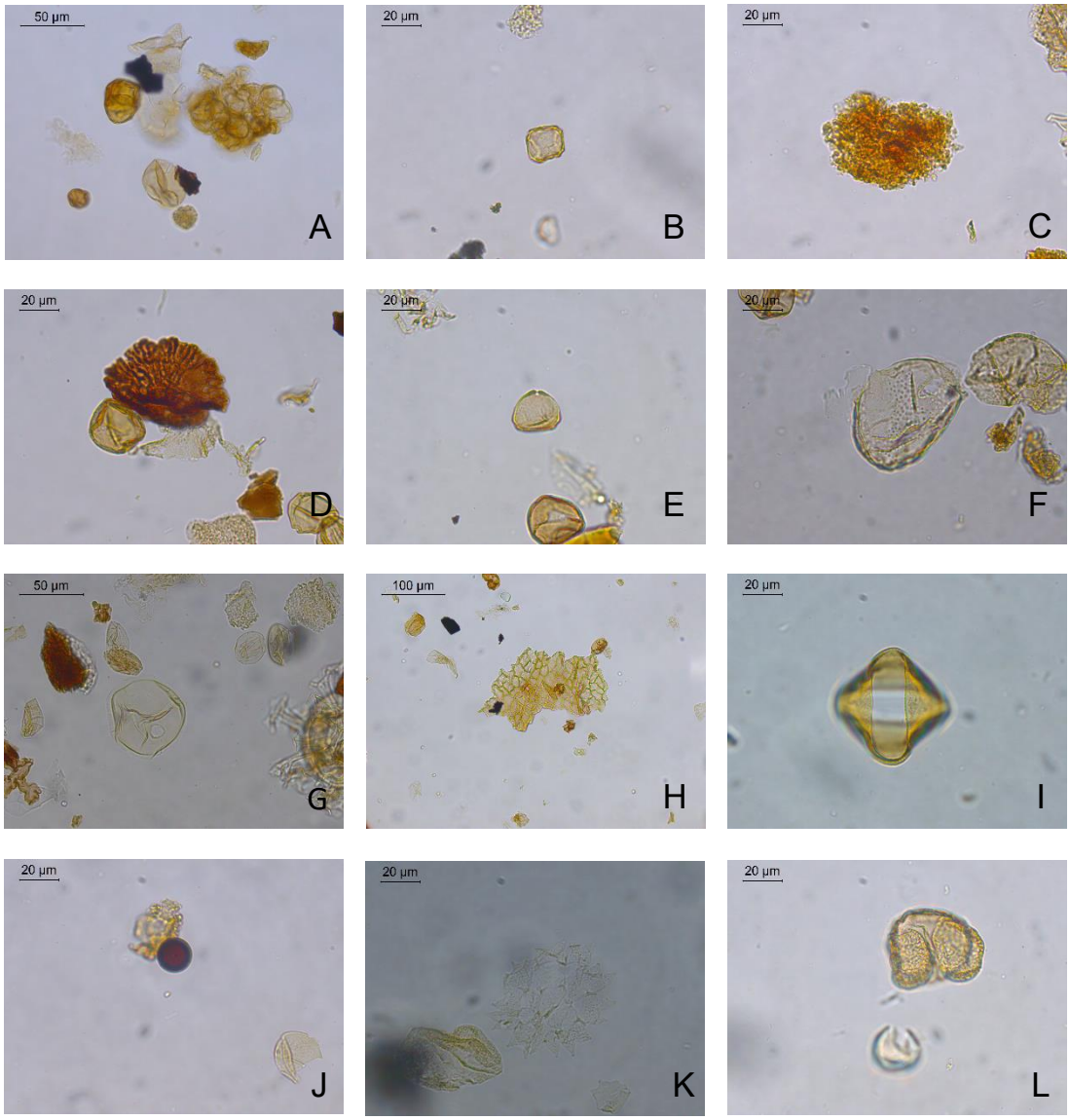

Plate 3

Specimens of the different categories of palynomorphs assemblages. For dinoflagellates see Plate 1 and Plate 2. During microscope work, coordinates were taken with an England Finder (F).

A. Aggregated pollen, Sdr. Vium well, depth 51.42 m, EF: F25

B. Four-porate pollen, Sdr. Vium well, depth 51.42 m, EF: O26 3

C. AOM, Sdr. Vium well, depth 51.42 m, EF: O25

D. Fungal fruiting body, Sdr. Vium well, depth 53.52 m, EF: O25

E. *Corylus* tri-porate pollen, Sdr. Vium well, depth 51.42 m, EF: P26

F. Freshwater algae (*Cyclopsiella granosa/lusatica),* Sdr. Vium well, depth 51.42 m, EF: G38-2

G. Freshwater algae (*Cyclopsiella elliptica)*, Sdr. Vium well, depth 88.02 m, EF: R35-4

H. Cuticle, Sdr. Vium well, depth 88.02 m, EF: E37-1

I. Freshwater algae (*Mougeotia lactevirans),* Sdr. Vium well, depth 133.32 m, EF: X50 2-4

J. Fungal spore, Sdr. Vium well, depth 51.42 m, EF: O24 3

K. Freshwater algae (*Pediastrum* spp.*)*, Sdr. Vium well, depth 88.02 m, EF: C57-2

L. Bissacte pollen, Sdr. Vium well, depth 51.42 m, EF: P26

Discussion

7. Discussion

7.1. Importance of equal laboratory procedures

After interpreting and comparing results between both wells, the distal well revealed slightly different values from what was expected. In Kellner et al. (submitted), 40 samples from 5 cored intervals of the 2/11-12S well spanning from a depth of 1671.22 m to 1489.04 m, including the sample interval (1670.74 m to 1611.54 m) of this study, were analysed. The distal values in Kellner et al. (submitted) revealed that the 2/11-12S well (offshore Norway) presents dominance of dinocysts with a low P/D index throughout the succession, reflecting a fully marine environment with long distance to shoreline/freshwater influx. Minor variations in the relative abundances of the palynomorphs groups e.g., dinocysts, non-saccate, and bisaccate pollen occur up through the studied succession.

Comparing the distal P/D index between this study and Kellner et al. (submitted), this study's P/D index presents higher values, reflecting more proximity to the coastline. Looking at the relative abundance of terrestrial palynomorphs, this study's values are higher than those of Kellner et al. (submitted). The diversity of dinocyst taxa also appears much lower in this study.

After spotting the differences, laboratory methods were compared. The comparison of slide laboratory procedures showed that the CGG Laboratories (see subchapter 4.1.2) had as an initial step the washing of the extracted samples with a 63 μm mesh, different from the GEUS Laborathoy procedure (see subchapter 4.1.1). This means that particles above 63 μm were removed from the samples processed for this study. Large taxa are less frequent, while smaller palynomorphs like pollen are more frequent. This difference can be explained by filtering on a 63 μm mesh.

As a consequence of this step, the ratio of terrestrial and marine palynomorphs is altered. Removing a big part of the dinocysts explains the higher value of non-saccate pollen compared to Kellner et al. (submitted) results.

7.2. Dinocyst events

Even with the loss of dinocyst taxa diversity, both sites yielded well-preserved dinocyst assemblages. Despite differences in the relative abundance and composition of dinocyst assemblages (see below), key dinocyst events for the Burdigalian-Langhian succession have been identified in both wells (See Appendix H, for correlation figure image between both

wells). Based on these events, the studied successions could be subdivided into the dinocyst zones *C. cantharellus, E. insigne, C. aubryae,* and *L. truncatum* defined by Dybkjær & Piasecki (2010).

7.3. Water depth changes and proximity to land areas

The samples from the Sdr. Vium well reflected that this site was located in a marine setting but very close to the land area in the Early - early Middle Miocene. The palynomorph assemblages are dominated by non-saccate pollen (19% to 52%), contrasting with dinocysts that are less common (7% to 47%, only reaching 54% in the uppermost sample due to regional flooding). Spores and fungal spores make up 0.31% to 4% of the assemblages, while acritarchs make up 0.27% to 8% and freshwater algae 0.31% to 3%.

Distinct variations in the abundance of terrestrial and marine palynomorphs reflect changes in depositional environments through time. Palynomorph assemblages from the Sdr. Vium core indicates that the lower part of the Arnum Formation (133,32 m to 112,67 m) was deposited under less terrestrial influence than the upper part of the Arnum Fm (95.42-53.42 m). A gradual change from a more marine (P/D index minimum, 27, at 133,32 m) to a more terrestrial-influenced environment (P/D index maximum, 88, at 53,42 m) is observed, suggesting a shallowing water depth. The topmost sample, shows a P/D index of 43, suggesting a more marine-influenced environment when the Ørnhøj Formation was deposited, possibly reflecting the regional flooding which ended the overall shallowing trend. These interpretations agree with those of Rasmussen et al. (2010) and Śliwińska et al. (2024) who present data on the water depths and episodes of progradation and flooding in the eastern part of the North Sea, during the Miocene. During the Late Burdigalian, the water depth at the site represented by the Sdr. Vium well, was predominantly shallow, varying between 0 and 50 m. At the base of Arnum Fm (130 m - 120 m) (see Fig. 4 in Śliwińska et al., 2024), the water depth is recorded near 50 m. Towards the upper part (80 m – 70 m), a shallowing occurred and the water depth decreased almost to half of the depth. In contrast, during the Serravallian (Ørnhøj Fm) the water depth increased to more than 150 m deep. These variations in water depth can be related to the fall in relative sea level and increased sediment input to the southeast (present-day Jylland, Denmark) from the Southern Scandes (Scandinavian Mountain Range) resulting in a prograding coastline during the Burdigalian

and early Langhian, and the flooding of the same area as a consequence of the accelerating subsidence of the basin during the Serravallian, suggested by Rasmussen et al. (2004, 2010). On the other hand, the 2/11-12S well represents a site far from land, where dinocysts dominate the palynomorph assemblage (34% to 76%), and the non-saccate pollens are significantly less common (12% to 44%) along with acritarchs (0.63% to 5%). Fungal spores and spores make up less than 2% of the palynomorphs. Freshwater algae (<2%) were recorded sporadically.

Furthermore, the BIT index values in the 2/11-12S are below 0.5 suggesting only a very low abundance of branched GDGTs (synthesized by soil and river bacteria). These values corroborate the dominance of dinocysts and the low terrestrial input, supporting that a fully marine environment persisted in the 2/11-12S site.

In the 2/11-12S well, the lower part of the Dany Formation (1670.74 m to 1639.17 m) was deposited with higher terrestrial influence than the upper part of the Dany Fm (1639.17 m to 1611.54 m). A small gradual decrease in the relative abundance of terrestrial palynomorphs (P/D index variation of 47 to 15) is observed from 1639.17 m to 1611.54 m.

The terrestrial input in the Dany Formation (1671.22 m to 1602.0 m) can probably be related to the previously mentioned increased sediment input from the Southern Scandes resulting from delta systems, during the late Burdigalian to Langhian.

7.4. Proximal-distal trend

Our results suggest that the Sdr. Vium site, as a proximal setting, was a shallow marine environment since it is characterized by a high abundance of terrestrial (non-saccate pollen and spores) palynomorphs, as well as high values of the P/D index. In contrast, the 2/11-12S site, as a distal setting, is shown to be a fully marine environment with a high abundance of marine (dinocysts) palynomorphs and low values of the P/D index. Our results confirm that the ratio between the terrestrial and marine palynomorphs is an excellent indicator of proximity to the coastline.

Regarding the other palynomorph categories, fungal spores and spores have very low percentages in the 2/11-12S site. This can be explained by the easy degradation and short-distance transport of these particles. Thus, they are associated with nearshore marine environments (Ingold, 1971; Rees, 1980; Tyson, 1995). Acritarchs are common in both sites. However, in the Sdr. Vium, acritarchs have a higher relative abundance compared to the

2/11-12S site, especially where the shallowing trend is observed (133,32 m to 53,42 m). Since acritarchs are characteristic of marine environments with terrestrial influence, they are associated with coastal environments (Tyson, 1995; De Vernal, 2009). Freshwater algae appear very sporadically in the 2/11-12S site, contrary to the Sdr. Vium site where freshwater algae are present in almost every sample. Since freshwater algae do not tolerate brackish or saline waters, they indicate freshwater influx into the marine environment (Tyson, 1995). Our results show that fungal spores, acritarchs, and freshwater algae can also be good indicators of the proximity of the coastline, even if less abundant.

Due to the loss of dinocyst diversity (explained in the subchapter 7.1), the 2/11-12S site shows lesser diversity than the Sdr. Vium site. Despite that, there are still some similarities and differences between the proximal and distal assemblages. For example, *Nematosphaeropsis* spp. are only present in the 2/11-12S site. This is due to the preference of this genus for outer neritic to oceanic waters (see Dale, 1996; Dybkjær et al., 2004; Pross & Brinkhuis, 2005). The absence of this genus in the Sdr. Vium well supports that in this site a shallow marine environment dominated. The shared taxa between the sites includes cosmopolitan taxa, such as *Spiniferites* spp. and *Operculodinium centrocarpum*, or age-diagnostic taxa that occur exclusively in the Burdigalian-Langhian ages, such as *Cousteaudinium aubryae* and *Labyrinthodinium truncatum*.

Regarding synchronicities between both sites, it is difficult to evaluate since the terrestrial and marine ratio in the 2/11-12S site is altered due to the loss of dinocyst abundance. However, samples analysed by Kellner et al. (submitted) (See Appendix H, for correlation figure image between both wells), show that the Dany Fm (Middle/Late Burdigalian) was deposited with higher terrestrial influence than the overlying Nora Formation (1586.21 m to 1602.0 m), Hodde Formation (1510.0 m to 1501.0 m), and the Ørnhøj Formation (1501.0 m to 1480.0 m). This result still corroborates with the terrestrial influence found in this study's 2/11-12S samples.

The interval Middle to Late Burdigalian coincides with a period of increased sediment input from the Southern Scandes (due to the delta systems) in the direction of the North Sea, resulting in a prograding coastline (see Rasmussen et al., 2010).

7.5. Temperature trends

Warm-water dinocyst taxa were identified in both settings (Table 4.1). The warm-water species *Lingulodinium machaerophorum* is distributed throughout the successions, with some small fluctuations in its abundance. In the Sdr. Vium site *Melitasphaeridium choanophorum* is also distributed throughout the succession, contrasting with the 2/11-12S site where *Melitasphaeridium choanophorum* appears more frequently in the *C. aubryae* Zone (1645.53 m to 1608.44 m). The species *Polysphaeridium zoharyi* only appears in the Sdr. Vium site, from the *C. aubryae* Zone (95.42 m) to the beginning of the *L. truncatum* Zone (53.42 m). The absence of *P. zoharyi* in the 2/11-12S site may be due to the loss of dinocyst taxa diversity through the methods misstep, since in Kellner et al. (submitted) samples *P. zoharyi* is present. The stratigraphic interval of the *C. aubryae* Zone to the beginning/middle of the *L. truncatum* Zone coincides with the MCO period (Late Burdigalian-Early Langhian, ~16.9 to 14.7 Ma), suggested by Zachos et al (2001). The occurrence of the warm-water species *P. zoharyi* in the Sdr. Vium site and *M. choanophorum* in the 2/11-12S site corroborate timewise with the warmer period of MCO.

Additionally, the organic geochemistry analysis of the 2/11-12S samples revealed SSTs between 14ºC to 23ªC during the Middle/Late Burdigalian to the Serravallian ages. An increase in temperature is seen in Middle to Late Burdigalian (1664.63 m to 1653.72 m), passing from 18ºC to a maximum of 23ºC. From the Middle Burdigalian (1653.72 m) to Early Langhian (1601.54) a gradual decrease was recorded, 23ºC to 21ºC. By the Late Langhian (1509.56 m), the SST shows a big drop in temperature, passing from 21ºC to 16ºC. In the early Serravallian, the SST drops to a minimum of 14ºC. This trend supports Zachos et al. (2001) when affirming that the MCO peaked in the late Middle Miocene and was followed by a gradual cooling.

Herbert et al. (2020) estimated SSTs from the Sdr. Vium core are based on alkenones (UK37). Higher temperatures were recorded (up to 28ºC) compared to this study's values. The onset of warmer SSTs in Herbert et al. (2020) was approximately at a depth of 90 m in the Sdr. Vium core (Middle/Late Burdigalian*, C. aubryae* zone). The maximum value of SST (23ºC, at 1653.72 m) from the 2/11-12S site occurs before the *C. aubryae* zone (1645.53 m to 1608.44 m). By biozone correlation, the values from the 2/11-12S site suggest that the warm phase started earlier.

Looking at the warm water dinocyst, in this study's Sdr. Vium samples, *P. zoharyi* starts occurring (95.42 m) a little before then Herbert et al. (2020) onset of warmer temperatures. Śliwińska et al. (2024), also presents data from the Sdr. Vium on MCO. Their results also reveal an earlier flux of warm water dinocyst taxa.

Conclusion

8. Conclusion

The results clearly show how palynomorph assemblages are influenced by – and reflect - changes in the depositional environments. A palynofacies analysis was used to calculate marine and terrestrial ratios in the Lower to Middle Miocene succession of the proximally located Sønder Vium well (Denmark) and the distally located 2/11-12S well (Southern Norwegian North Sea), aiming to reveal water depth changes and climatic variations. Regarding the terrestrial/marine ratio, the data revealed a marine environment far from the coastline with a deepening trend in the 2/11-12S site (dominance of marine palynomorphs, lower P/D index) and a marine environment near the coastline with a shallowing trend (higher abundance of terrestrial palynomorphs, higher P/D index) in the Sønder Vium site. The proximal to distal dinocyst assemblages showed similarities and differences. The genus *Nematosphaeropsis* spp. was only present in the 2/11-12S site, due to their preference for outer neritic to oceanic waters. The absence of this genus in the Sdr. Vium site supports a dominant shallow marine environment. The shared taxa between the sites include cosmopolitan taxa, such as *Spiniferites* spp. and *Operculodinium centrocarpum*, or age-diagnostic taxa that occur exclusively in the Burdigalian-Langhian ages, such as *Cousteaudinium aubryae* and *Labyrinthodinium truncatum*. The interval where these trends occurred coincides with the MCO. To obtain SSTs from the 2/11-12S site, a geochemistry analysis was used to understand the distribution of glycerol dialkyl glycerol tetraethers (GDGT), through liquid chromatography/mass spectrometry. The analysis revealed an increase in SSTs from 18ºC to a maximum of 23ªC during the Middle/Late Burdigalian, hinting at a warming phase. However, by the Late Langhian and Early Serravallian temperatures drop to 16ºC and 14ºC, suggesting a cooling phase. Warm-water dinocyst taxa were found in both sites. The warm-water species *P. zoharyi* and *M. choanophorum* start to occur more frequently during the Middle/Late Burdigalian, agreeing with the onset of warmer SSTs of the 2/11-12S well.

In essence, this study shares a deeper look into the diversity of proximal to distal Miocene dinocyst assemblages and how the distribution of organic particles can reveal shallowing and deepening trends. Together with organic geochemistry analysis on membrane lipids (GDGTs) for obtaining SSTs, it aims for a better perception of water-depth changes and climate variation. By supporting previous literature and sharing additional knowledge for the 2/11-12S well on the MCO, the data herein is hoped to contribute to the

North Sea Miocene record. Any contribution is valuable since the amount of data and sites penetrating the MCO is limited.

Bibliography

9. Bibliography

Castro, L. (2016). Dinoflagelados e outros palinomorfos do Miocénico do sector distal da Bacia do Baixo-Tejo. *PhD,* Faculdade de Ciências e Tecnologia da Univ. Nova Lisboa: 380 pp., 241 figs.

Clausen, O. R., Gregersen, U., Michelsen, O., & Sørensen, J. C. (1999). Factors controlling the Cenozoic sequence development in the eastern parts of the North Sea. *Journal of the Geological Society*, *156*(4), 809–816. https://doi.org/10.1144/gsjgs.156.4.0809

Dale, B. (1996). Dinoflagellate cyst ecology: Modeling and geological applications. *Palynology: Principles and Applications*. https://sci-hub.ru/https://cir.nii.ac.jp/crid/1571698600127201664

De Vernal, A. (2009). Marine palynology and its use for studying nearshore environments. *IOP Conference Series: Earth and Environmental Science*, *5*(1), 012002. https://sci-hub.ru/https://iopscience.iop.org/article/10.1088/1755-1307/5/1/012002/meta

Deegan, C.E. & Scull, B.J. (compilers) (1977): A standard lithostratigraphic nomenclature for the central and northern North Sea. Institute of Geological Sciences Report 77/25, 36 pp. London: Her Majesty's Stationery Office.

Dybkjær, K. (2004a). Dinocyst stratigraphy and palynofacies studies used for refining a sequence stratigraphic model—Uppermost Oligocene to lower Miocene, Jylland, Denmark. *Review of Palaeobotany and Palynology*, *131*(3–4), 201–249.

Dybkjær, K. (2004b). Morphological and abundance variations in Homotryblium-cyst assemblages related to depositional environments; uppermost Oligocene–Lower Miocene, Jylland, Denmark. *Palaeogeography, Palaeoclimatology, Palaeoecology*, *206*(1–2), 41–58.

Dybkjær, K., & Rasmussen, E. S.. (2007). 'Organic-Walled Dinoflagellate Cyst Stratigraphy in an Expanded Oligocene–Miocene Boundary Section in the Eastern North Sea Basin (Frida-1 Well, Denmark) and Correlation from Basinal to Marginal Areas'. *Journal of Micropalaeontology 26*(1):1–17. doi: 10.1144/jm.26.1.1.

Dybkjær, K., King, C., & Sheldon, E. (2012). Identification and characterisation of the Oligocene–Miocene boundary (base Neogene) in the eastern North Sea Basin—Based

on dinocyst stratigraphy, micropalaeontology and $\delta^{13}C$-isotope data. *Palaeogeography, Palaeoclimatology, Palaeoecology*, *363*, 11–22.

Dybkjær, K., & Piasecki, S. (2010). Neogene dinocyst zonation for the eastern North Sea Basin, Denmark. *Review of Palaeobotany and Palynology*, *161*(1–2), 1–29.

Dybkjaer, K., & Rasmussen, E. S. (2000). Palynological dating of the Oligocene–Miocene successions in the Lille Bælt area, Denmark. *Bulletin of the Geological Society of Denmark*, *47*(87), 103.

Dybkjær, K., Rasmussen, E. S., Śliwińska, K. K., Esbensen, K. H., & Mathiesen, A. (2019). A palynofacies study of past fluvio-deltaic and shelf environments, the Oligocene-Miocene succession, North Sea Basin: A reference data set for similar Cenozoic systems. *Marine and Petroleum Geology*, *100*, 111–147.

Eidvin, T., & Rundberg, Y.. (2001). 'Late Cainozoic Stratigraphy of the Tampen Area (Snorre and Visund Fields) in the Northern North Sea, with Emphasis on the Chronology of Early Neogene Sands.' *Norwegian Journal of Geology/Norsk Geologisk Forening, 81*(2), 119-160.

Eidvin, T., and Rundberg,Y.. (2007). 'Post-Eocene Strata of the Southern Viking Graben, Northern North Sea; Integrated Biostratigraphic, Strontium Isotopic and Lithostratigraphic Study.' *Norwegian Journal of Geology/Norsk Geologisk Forening, 87*(4), 391-450.

Gabrielsen, R. H., Faleide, J. I., Pascal, C., Braathen, A., Nystuen, J. P., Etzelmuller, B., & O'Donnell, S. (2010). Latest Caledonian to Present tectonomorphological development of southern Norway. *Marine and Petroleum Geology*, *27*(3), 709–723.

Gregersen, U. (1998). Upper Cenozoic channels and fans on 3D seismic data in the northern Norwegian North Sea. *Petroleum Geoscience*, *4*(1), 67–80. https://doi.org/10.1144/petgeo.4.1.67

Hardt, T., Holtar, E., Isaksen, D., Kyllingstad, G., Lervik, K.S., Lycke, A.S. & Tonstad, K. (1989): Revised Tertiary lithostratigraphic nomenclature for the Norwegian North Sea. In: Isaksen, D. & Tonstad, K. (eds): A revised Cretaceous and Tertiary lithostratigraphic nomenclature for the Norwegian North Sea. Norwegian Petroleum Directorate (NPD) Bulletin, *5*, 35–55.

Head, M. (1996). Modern dinoflagellate cysts and their biological affnities. In *American Association of Stratigraphic Palynologists Foundation* (Vol. 3, pp. 1197–1248).

Herbert, T. D., Rose, R., Dybkjær, K., Rasmussen, E. S., & Śliwińska, K. K. (2020). Bihemispheric Warming in the Miocene Climatic Optimum as Seen from the Danish North Sea. *Paleoceanography and Paleoclimatology*, *35*(10), e2020PA003935. https://doi.org/10.1029/2020PA003935

Hönisch, B., Royer, D. L., Breecker, D. O., Polissar, P. J., Bowen, G. J., Henehan, M. J., Cui, Y., Steinthorsdottir, M., McElwain, J. C., Kohn, M. J., Pearson, A., Phelps, S. R., Uno, K. T., Ridgwell, A., Anagnostou, E., Austermann, J., Badger, M. P. S., Barclay, R. S., & Zhang, L. (2023). Toward a Cenozoic history of atmospheric CO_2. *Science (New York, N.Y.)*, *382*(6675), eadi5177. Cenozoic CO_2 Proxy Integration Project (CenCO2PIP) Consortium*†. https://doi.org/10.1126/science.adi5177

Hopmans, E. C., Weijers, J. W. H., Schefuß, E., Herfort, L., Sinninghe Damsté, J. S., & Schouten, S. (2004). A novel proxy for terrestrial organic matter in sediments based on branched and isoprenoid tetraether lipids. *Earth and Planetary Science Letters*, *224*(1–2), 107–116. https://doi.org/10.1016/j.epsl.2004.05.012

Hutchinson, D. K., Coxall, H. K., Lunt, D. J., Steinthorsdottir, M., de Boer, A. M., Baatsen, M., von der Heydt, A., Huber, M., Kennedy-Asser, A. T., Kunzmann, L., Ladant, J.-B., Lear, C. H., Moraweck, K., Pearson, P. N., Piga, E., Pound, M. J., Salzmann, U., Scher, H. D., Sijp, W. P., & Zhang, Z. (2021). The Eocene–Oligocene transition: A review of marine and terrestrial proxy data, models and model–data comparisons. *Climate of the Past*, *17*(1), 269–315. https://doi.org/10.5194/cp-17-269-2021

Ingold, C. T. (1971). *Fungal spores: Their liberation and dispersal*. Clarendon Press.

Jarsve, E. M., Faleide, J. I., Gabrielsen, R. H., & Nystuen, J. P. (2014). Mesozoic and cenozoic basin configurations in the North Sea. In A. W. Martinius, R. Ravnås, J. A. Howell, R. J. Steel, & J. P. Wonham (Eds.), *From Depositional Systems to Sedimentary Successions on the Norwegian Continental Margin* (1st ed., pp. 417–452). Wiley. https://doi.org/10.1002/9781118920435.ch15

Jolley, David, Manuel Vieira, Simin Jin, and David B. Kemp. (2022). 'Palynofloras, Palaeoenvironmental Change and the Inception of the Paleocene Eocene Thermal

Maximum; the Record of the Forties Fan, Sele Formation, North Sea Basin'. *Journal of the Geological Society 180*(1): jgs 2021-131. doi: 10.1144/jgs2021-131.

Kellner, L., Dybkjær, K., Sliwinska, K., Rasmussen, E. S., Vieira, M., & Castro, L. (Submitted). Lower-Middle Miocene dinoflagellate cysts assemblages and palynofacies along a shallow water–deep water transect, eastern to central North Sea. *Climate of the Past*.

Kim, J.H., Van Der Meer, J., Schouten, S., Helmke, P., Willmott, V., Sangiorgi, F., Koç, N., Hopmans, E. C., & Damsté, J. S. S. (2010). New indices and calibrations derived from the distribution of crenarchaeal isoprenoid tetraether lipids: Implications for past sea surface temperature reconstructions. *Geochimica et Cosmochimica Acta*, *74*(16), 4639–4654. https://doi.org/10.1016/j.gca.2010.05.027

Knox, R., Bosch, A., Rasmussen, E. S., Heilmann-Clausen, C., Hiss, M., Lugt, I. de, Kasiński, J., King, C., Köthe, A., Słodkowska, B., Standke, G., & Vandenberghe, N. (2010). Cenozoic. In *Petroleum Geological Atlas of the Southern Permian Basin Area* (pp. 211–223). European Association of Geoscientists & Engineers (EAGE). https://pub.geus.dk/en/publications/cenozoic

Knox, R. W. O., Holloway, S., & Cordey, W. G. (1992). *Paleogene of the central and northern North Sea*. British Geological Survey, 133.

Larsson, L. M., Dybkjær, K., Rasmussen, E. S., Piasecki, S., Utescher, T., & Vajda, V. (2011). Miocene climate evolution of northern Europe: A palynological investigation from Denmark. *Palaeogeography, Palaeoclimatology, Palaeoecology*, *309*(3–4), 161–175.

Liboriussen, J., Ashton, P., & Tygesen, T. (1987). The tectonic evolution of the Fennoscandian Border Zone in Denmark. *Tectonophysics*, *137*(1–4), 21–29.

Lyle, M., Barron, J., Bralower, T. J., Huber, M., Olivarez Lyle, A., Ravelo, A. C., Rea, D. K., & Wilson, P. A. (2008). Pacific Ocean and Cenozoic evolution of climate. *Reviews of Geophysics*, *46*(2), 2005RG000190. https://doi.org/10.1029/2005RG000190

McArthur, J. M., & Howarth, R. J. (1998). Strontium isotope stratigraphy: LOWESS version 2. A revised best-fit to the marine Sr-isotope curve for 0 to 206 Ma, with a revised look-up table for derivation of numeric age. *Abstracts AAPG Annual Meeting, May 17–20, 1998, Salt Lake City, Utah*,

2.https://scihub.ru/https://discovery.ucl.ac.uk/id/eprint/10095885/1/Sr_isotope_stratigraphy_LOWESS_%28v2_1998%29.pdf

McArthur, J. M., Howarth, R. J., & Bailey, T. R. (2001). Strontium Isotope Stratigraphy: LOWESS Version 3: Best Fit to the Marine Sr-Isotope Curve for 0–509 Ma and Accompanying Look-up Table for Deriving Numerical Age. *The Journal of Geology*, *109*(2), 155–170. https://doi.org/10.1086/319243

Mccarthy, F., GOSTLIN, K., Mudie, P., & HOPKINS, J. (2003). *Terrestrial and marine palynomorphs as sea-level proxies: an example from quaternary sediments on the new jersey margin, U.S.A.* (pp. 119–129). https://doi.org/10.2110/pec.03.75.0119

McClay, Norton, M. G., Coney, P., & Davis, G. H. (1986). Collapse of the Caledonian orogen and the Old Red Sandstone. *Nature*, *323*(6084), 147–149.

Michelsen, O., Danielsen, M., Heilmann-Clausen, C., Jordt, H., Laursen, G. V., & Thomsen, E. (1995). Occurrence of major sequence stratigraphic boundaries in relation to basin development in Cenozoic deposits of the southeastern North Sea. *Steel, RJ et Al*, 415–427.

Michelsen, O., Thomsen, E., Danielsen, M., Heilmann-Clausen, C., Jordt, H., & Laursen, G. V. (1998). *Cenzoic sequence stratigraphy in the Easter North Sea*. https://sci-hub.ru/https://archives.datapages.com/data/sepm_sp/SP60/Cenzoic_Sequence_Stratigraphy_in_the_Easter_North_Sea.pdf

Mogensen, T. E., & Jensen, L. N. (1994). Cretaceous subsidence and inversion along the Tornquist Zone from Kattegat to the Egersund Basin. *First Break*, *12*(4). https://doi.org/10.3997/1365-2397.1994016

Mudie, P. J. (1982). Pollen distribution in recent marine sediments, eastern Canada. *Canadian Journal of Earth Sciences*, *19*(4), 729–747. https://doi.org/10.1139/e82-062

Muller, J. (1995). Palynology of Recent Orinoco delta and shelf sediments: Report of Orinco shelf Expedition. *Micropaleontology*, *5*(1), 1–32.

Nielsen, O. B., Rasmussen, E. S., & Thyberg, B. I. (2015). Distribution of clay minerals in the northern North Sea Basin during the Paleogene and Neogene: A result of source-area geology and sorting processes. *Journal of Sedimentary Research*, *85*(6), 562–581.

O'Brien, C. L., Robinson, S. A., Pancost, R. D., Sinninghe Damsté, J. S., Schouten, S., Lunt, D. J., Alsenz, H., Bornemann, A., Bottini, C., Brassell, S. C., Farnsworth, A., Forster, A., Huber, B. T., Inglis, G. N., Jenkyns, H. C., Linnert, C., Littler, K., Markwick, P., McAnena, A., & Wrobel, N. E. (2017). Cretaceous sea-surface temperature evolution: Constraints from TEX86 and planktonic foraminiferal oxygen isotopes. *Earth-Science Reviews*, *172*, 224–247. https://doi.org/10.1016/j.earscirev.2017.07.012

Poulsen, N. E. (1996). *Dinoflagellate Cysts from Marine Jurassic Deposits of Denmark and Poland*. https://pub.geus.dk/en/publications/dinoflagellate-cysts-from-marine-jurassic-deposits-of-denmark-and

Pross, J., & Brinkhuis, H. (2005). Organic-walled dinoflagellate cysts as paleoenvironmental indicators in the Paleogene; a synopsis of concepts. *Paläontologische Zeitschrift*, *79*, 53–59.

Quaijtaal, W., Donders, T. H., Persico, D., & Louwye, S. (2014). Characterising the middle Miocene Mi-events in the Eastern North Atlantic realm: A first high-resolution marine palynological record from the Porcupine Basin. *Palaeogeography, Palaeoclimatology, Palaeoecology*, *399*, 140–159.

Rasmussen, E., Dybkjaer, K., & Piasecki, S. (2006). Neogene fluvial and nearshore marine deposits of the Salten section, central Jylland, Denmark. *Bulletin of the Geological Society of Denmark*, *53*. https://doi.org/10.37570/bgsd-2006-53-02

Rasmussen, E. S. (1996). Sequence stratigraphie subdivision of the Oligocèneand Miocene succession in South Jutland. *Bulletin of the Geological Society of Denmark*, *43*, 143–155. https://doi.org/10.37570/bgsd-1996-43-14

Rasmussen, E. S. (2004a). Stratigraphy and depositional evolution of the uppermost Oligocene—Miocene succession in western Denmark. *Bulletin of the Geological Society of Denmark*, *51*, 89–109. https://doi.org/10.37570/bgsd-2004-51-07

Rasmussen, E. S. (2004b). The interplay between true eustatic sea-level changes, tectonics, and climatic changes: What is the dominating factor in sequence formation of the Upper Oligocene–Miocene succession in the eastern North Sea Basin, Denmark? *Global and Planetary Change*, *41*(1), 15–30.

Rasmussen, E. S. (2009). Neogene inversion of the central Graben and Ringkøbing-Fyn high, Denmark. *Tectonophysics*, *465*(1–4), 84–97.

Rasmussen, E. S. (2013). Cenozoic structures in the eastern North Sea Basin—A case for salt tectonics: Discussion. *Tectonophysics*, *601*, 226–233.

Rasmussen, E. S., Dybkjær, K., & Piasecki, S. (2010). Lithostratigraphy of the upper Oligocene–Miocene succession of Denmark. *GEUS Bulletin*, *22*, 1.

Rasmussen, E. S., Heilmann-Clausen, C., Waagstein, R., & Eidvin, T. (2008). The tertiary of Norden. *Episodes Journal of International Geoscience*, *31*(1), 66–72.

Rasmussen, E. S., Vejbæk, O. V., Bidstrup, T., Piasecki, S., & Dybkjær, K. (2005). Late Cenozoic depositional history of the Danish North Sea Basin: Implications for the petroleum systems in the Kraka, Halfdan, Siri and Nini fields. *Geological Society, London, Petroleum Geology Conference Series*, *6*(1), 1347–1358. https://doi.org/10.1144/0061347

Rasmussen, E. S., Dybkjær, K., Toft, J. C., Nielsen, O. B., Sheldon, E., & Mørk, F. (Submitted). Lithostratigraphy of the Neogene succession of the Danish North Sea. *GEUS Bulletin*.

Rees, G. (1980). Factors Affecting the Sedimentation Rate of Marine Fungal Spores. *Botanica Marina*, *23*(6), 375–386. https://doi.org/10.1515/bot-1980-230606

Roncaglia, L., & Kuijpers, A. (2006). Revision of the palynofacies model of Tyson (1993) based on recent high-latitude sediments from the North Atlantic. *Facies*, *52*(1), 19–39. https://doi.org/10.1007/s10347-005-0028-y

Rhys, G. H. (1974). 'A Proposed Standard Lithostratigraphic Nomenclature for the Southern North Sea and an Outline Structural Nomenclature for the Whole of the (UK) North Sea.

Rundberg, Y., & Eidvin. T., (2005). 'Controls on Depositional History and Architecture of the Oligocene-Miocene Succession, Northern North Sea Basin'. *Norwegian Petroleum Society Special Publications*, *12*, 207–39, Elsevier.

Schiøler, P. (2005). Dinoflagellate cysts and acritarchs from the Oligocene–Lower Miocene interval of the Alma-1X well, Danish North Sea. *Journal of Micropalaeontology*, *24*(1), 1–37.

Schiøler, P., Andsbjerg, J., Clausen, O. R., Dam, G., Dybkjær, K., Hamberg, L., Heilmann-Clausen, C., Johannessen, E. P., Kristensen, L. E., Prince, I., & Rasmussen, J. A. (2007). Lithostratigraphy of the Palaeogene – Lower Neogene succession of the Danish North Sea. *Geological Survey of Denmark and Greenland Bulletin*, *12*, 1–77. https://doi.org/10.34194/geusb.v12.5249

Schouten, S., Hopmans, E. C., Schefuß, E., & Sinninghe Damsté, J. S. (2002). Distributional variations in marine crenarchaeotal membrane lipids: A new tool for reconstructing ancient sea water temperatures? *Earth and Planetary Science Letters*, *204*(1–2), 265–274. https://doi.org/10.1016/S0012-821X(02)00979-2

Sheldon, E., Rasmussen, E. S., Dybkjær, K., Eidvin, T., Riis, F., & Weibel, R. (2018). Miocene oil-bearing diatom ooze from the North Sea. *GEUS Bulletin*, *41*, 29–32.

Sheldon, E., K. Dybkjær, Rasmussen, E. S., & Oksman, M. (Submitted). A detailed multidisciplinary biostratigraphic framework for the Lower to Middle Miocene of the Norwegian North Sea – the siliceous succession of the Valhall/Hod area. *GEUS Bulletin*.

Sinninghe Damsté, J. S., Ossebaar, J., Schouten, S., & Verschuren, D. (2012). Distribution of tetraether lipids in the 25-ka sedimentary record of Lake Challa: Extracting reliable TEX86 and MBT/CBT palaeotemperatures from an equatorial African lake. *Quaternary Science Reviews*, *50*, 43–54. https://doi.org/10.1016/j.quascirev.2012.07.001

Śliwińska, K. K. (2019). Early Oligocene dinocysts as a tool for palaeoenvironment reconstruction and stratigraphical framework–a case study from a North Sea well. *Journal of Micropalaeontology*, *38*(2), 143–176.

Śliwińska, Kasia K., Erik Thomsen, Stefan Schouten, Petra L. Schoon, & Claus Heilmann-Clausen. (2019). 'Climate- and Gateway-Driven Cooling of Late Eocene to Earliest Oligocene Sea Surface Temperatures in the North Sea Basin'. *Scientific Reports, 9*(1): 4458. doi: 10.1038/s41598-019-41013-7.

Śliwińska, K. K., Denk, T., Dybkjær, K., Fredborg, J. M., Lindström, S., Piasecki, S., & Rasmussen, E. S. (2024). Miocene vegetation and climate in the eastern North Sea Basin, onshore Denmark, compared to the present. *GEUS Bulletin*, *57,* 18. https://doi.org/10.34194/geusb.v57.8365

Śliwińska, K. K., Dybkjær, K., Schoon, P. L., Beyer, C., King, C., Schouten, S., & Nielsen, O. B. (2014). Paleoclimatic and paleoenvironmental records of the Oligocene–Miocene transition, central Jylland, Denmark. *Marine Geology*, *350*, 1–15.

Sluijs, A., Pross, J., & Brinkhuis, H. (2005). From greenhouse to icehouse; organic-walled dinoflagellate cysts as paleoenvironmental indicators in the Paleogene. *Earth-Science Reviews*, *68*(3–4), 281–315.

Sømme, T. O., Skogseid, J., Embry, P., & Løseth, H. (2019). Manifestation of tectonic and climatic perturbations in deep-time stratigraphy–an example from the Paleocene succession offshore western Norway. *Frontiers in Earth Science*, *7*, 303.

Sørensen, J. C., Gregersen, U., Breiner, M., & Michelsen, O. (1997). High-frequency sequence stratigraphy of Upper Cenozoic deposits in the central and southeastern North Sea areas. *Marine and Petroleum Geology*, *14*(2), 99–123.

Steinthorsdottir, M., Coxall, H. K., de Boer, A. M., Huber, M., Barbolini, N., Bradshaw, C. D., Burls, N. J., Feakins, S. J., Gasson, E., Henderiks, J., Holbourn, A. E., Kiel, S., Kohn, M. J., Knorr, G., Kürschner, W. M., Lear, C. H., Liebrand, D., Lunt, D. J., Mörs, T., & Strömberg, C. (2021). The Miocene: The Future of the Past. *Paleoceanography and Paleoclimatology*, *36*(4), e2020PA004037. https://doi.org/10.1029/2020PA004037

Sulsbrück, H., & Toft, J. (2018). *A new observation of a biosiliceous opal bearing sequence in the Miocene Lark Formation in the Danish North Sea. Abstract*. http://2dgf.dk/foreningen/33rd-nordic-geological-winter-meeting/ ngwm-2018-abstracts/3-sedimentary-rocks-and-processes/

Traverse, A. (1994) Sedimentation of Organic Particles. Cambridge University Press, Cambridge,1-544. https://doi.org/10.1017/CBO9780511524875

Tyson, R. V. (1995). *Sedimentary organic matter: Organic facies and palynofacies*. Springer Science & Business Media. https://sci-hub.ru/https://books.google.com/books?hl=pt-PT&lr=&id=Qp7uCAAAQBAJ&oi=fnd&pg=PR10&dq=Tyson+1995+organic+particles+distribution&ots=nMMuYXNOJe&sig=uAL-JKNEo89lBDiLn_Xd6Zk_Amc

Utescher, T., Mosbrugger, V., Ivanov, D., & Dilcher, D. L. (2009). Present-day climatic equivalents of European Cenozoic climates. *Earth and Planetary Science Letters*, *284*(3–4), 544–552.

Vieira, M., & David, J., (2020). 'Stratigraphic and Spatial Distribution of Palynomorphs in Deep-Water Turbidites: A Meta-Data Study from the UK Central North Sea Paleogene'. *Marine and Petroleum Geology,* 122: 104638.

Vejbæk, O. V., Bidstrup, T., Britze, P., Erlström, M., Rasmussen, E. S., & Sivhed, U. (2007). Chalk depth structure maps, central to eastern North Sea, Denmark. *GEUS Bulletin*, *13*, 9–12.

Westerhold, T., Marwan, N., Drury, A. J., Liebrand, D., Agnini, C., Anagnostou, E., Barnet, J. S. K., Bohaty, S. M., De Vleeschouwer, D., Florindo, F., Frederichs, T., Hodell, D. A., Holbourn, A. E., Kroon, D., Lauretano, V., Littler, K., Lourens, L. J., Lyle, M., Pälike, H., & Zachos, J. C. (2020). An astronomically dated record of Earth's climate and its predictability over the last 66 million years. *Science*, *369*(6509), 1383–1387. https://doi.org/10.1126/science.aba6853

Williams, G. L., Fensome, R. A., & Macrae, R. (2017).: The Lentin and Williams index of fossil dinoflagellates, American Association of Stratigraphic Palynologists Foundation (AASP), Contributions Series Number 48, Dallas, Texas, USA, 2017.

Zachos, J., Pagani, M., Sloan, L., Thomas, E., & Billups, K. (2001). Trends, Rhythms, and Aberrations in Global Climate 65 Ma to Present. *Science*, *292*(5517), 686–693. https://doi.org/10.1126/science.1059412

Zhang, Y. G., Pagani, M., & Wang, Z. (2016). Ring Index: A new strategy to evaluate the integrity of TEX $_{86}$ paleothermometry. *Paleoceanography*, *31*(2), 220–232. https://doi.org/10.1002/2015PA002848

Zhang, Y. G., Zhang, C. L., Liu, X.-L., Li, L., Hinrichs, K.-U., & Noakes, J. E. (2011). Methane Index: A tetraether archaeal lipid biomarker indicator for detecting the

instability of marine gas hydrates. *Earth and Planetary Science Letters*, *307*(3–4), 525–534. https://doi.org/10.1016/j.epsl.2011.05.031

Ziegler, P. A. (1990). *Geological atlas of western and central Europe* (Vol. 52). Shell Internationale Petroleum Maatschappij BV The Hague. https://sci-hub.ru/https://library.wur.nl/WebQuery/titel/559692

Zonneveld, K. A. F., Marret, F., Versteegh, G. J. M., Bogus, K., Bonnet, S., Bouimetarhan, I., Crouch, E., De Vernal, A., Elshanawany, R., Edwards, L., Esper, O., Forke, S., Grøsfjeld, K., Henry, M., Holzwarth, U., Kielt, J.-F., Kim, S.-Y., Ladouceur, S., Ledu, D., … Young, M. (2013). Atlas of modern dinoflagellate cyst distribution based on 2405 data points. *Review of Palaeobotany and Palynology*, *191*, 1–197. https://doi.org/10.1016/j.revpalbo.2012.08.003

Utrecht university. (2018). PALSYS.org. https://palsys.org/genus (consulted in August 2024, for every taxa in chapter 6 of Systematics and Taxonomy, see references for species authors therein).

William & Lentin (2017). DINOFLAJ3. http://dinoflaj.smu.ca/dinoflaj3/index.php/Main_Page (consulted in August 2024, for every taxa in chapter 6 of Systematics and Taxonomy, see references for species authors therein).

Appendices

10. Appendices

Appendix A: Raw countings

The values here presented are the countings of all palynomorph categories (non-saccate pollen, bisaccate pollen, spores, fungal spores, freshwater algae, acritarchs, dinocysts, undifferentiated palynomorphs, and thin-walled undifferentiated palynomorphs) of Sdr. Vium **(a)** and 12/11-12S **(b)**, were performed through the microscope. The program used for the raw values was Excel.

a) Sønder Vium

Sdr. Vium Proximal Samples GEUS	Non-Saccate pollen	Bissacate pollen	Spores	Fungal spores	Freshwater algaes	Acritarcs	Dinoflagellates	Undiferentiated PALY	Undf. PALY Thin walled	Total
Sdr Vium m. **43.08-43.12 m** Lab nr.16483 ARY, slide 6, S	145	11	0	0	0	3	189	2	3	353
Sdr Vium m. **51.38-51.42 m** Lab nr.16651 ARY, slide 9, OS+kom+s, F2	126	80	14	0	0	7	94	7	3	331
Sdr Vium m. **53.48-53.42 m** Lab nr.16658 ARY, slide 7, OS+kom+s, F1	182	143	3	9	0	1	27	4	4	373
Sdr Vium m. PRNR 74, **73.98-74.02 m** Lab nr.16826 ARY, slide 8, OS+kom+s, F2	176	56	6	2	1	10	75	2	8	336
Sdr Vium m.82 core 39, **87.98-88.02 m**, 3, YD 16.834, T	122	51	1	5	1	24	103	12	0	319
Sdr Vium m.87 core 44, **95.38-95.42 m**, 3, YD 16.839, T	157	60	4	2	1	20	72	5	2	323
Sdr Vium m.92 core 49, **112.63-112.67m**, 3, YD 16.844, T	112	10	0	2	8	21	140	9	2	304
Sdr Vium m.94 core 52, **119.03-119.07 m**, 3, YD 16.846, T	125	12	2	4	5	15	129	10	9	311
Sdr Vium m.104 core 61, **133.28-133.32m**, 5, YD. 16. 856,Fc	59	90	1	0	6	1	148	7	3	315
Sdr Vium m.113 core 70, **146.63-146.67 m**, 7, YD 16.916, S	156	51	7	1	2	5	67	6	23	318

b) 2/11-12S

2/11-12S Distal Samples Aker bp	Non-Saccate pollen	Bissacate pollen	Spores	Fungal spores	Freshwater algaes	Acritarcs	Dinoflagellates	Undiferentiated PALY	Undf. PALY Thin walled	Total
1611.54 m	40	16	2	1	0	6	253	3	10	331
1615.81 m	75	13	1	2	0	5	207	5	13	321
1620.42 m	74	16	2	1	3	12	212	5	7	332
1626.19 m	90	20	5	2	3	3	205	5	3	336
1631.51 m	72	41	0	0	0	5	211	2	6	337
1639.17 m	115	38	3	0	0	14	135	3	5	313
1644.41 m	140	29	1	0	0	12	122	1	10	315
1658.51 m	70	29	1	0	1	10	175	10	5	301
1662.72 m	115	28	0	2	4	2	155	10	4	320
1666.32 m	68	46	1	0	3	2	191	1	2	314
1670.74 m	126	68	2	0	0	3	109	1	5	314

Appendix B: Relative Abundances

The relative abundance (%) values here presented were obtained (see Material & Methods, subchapter 4.3) through the previous data (Appendix A) of palynomorph categories of Sdr. Vium **(a)** and 12/11-12S **(b)**. The program used to calculate the relative abundance (%) values was Excel.

a) Sønder Vium

Depth	D	NSP	BS	S	FU	FA	A	UP	TUP
Sdr Vium m. **43.08-43.12 m** Lab nr.16483 ARY, slide 6, S	53,54	41,08	3,12	0,00	0,00	0,00	0,85	0,57	0,85
Sdr Vium m. **51.38-51.42 m** Lab nr.16651 ARY, slide 9, OS+kom+s, F2	28,40	38,07	24,17	4,23	0,00	0,00	2,11	2,11	0,91
Sdr Vium m. **53.48-53.42 m** Lab nr.16658 ARY, slide 7, OS+kom+s, F1	7,24	48,79	38,34	0,80	2,41	0,00	0,27	1,07	1,07
Sdr Vium m. PRNR 74, **73.98-74.02 m** Lab nr.16826 ARY, slide 8, OS+k	22,32	52,38	16,67	1,79	0,60	0,30	2,98	0,60	2,38
Sdr Vium m.82 core 39, **87.98-88.02 m**, 3, YD 16.834, T	32,29	38,24	15,99	0,31	1,57	0,31	7,52	3,76	0,00
Sdr Vium m.87 core 44, **95.38-95.42 m**, 3, YD 16.839, T	22,29	48,61	18,58	1,24	0,62	0,31	6,19	1,55	0,62
Sdr Vium m.92 core 49, **112.63-112.67m**, 3, YD 16.844, T	46,05	36,84	3,29	0,00	0,66	2,63	6,91	2,96	0,66
Sdr Vium m.94 core 52, **119.03-119.07 m**, 3, YD 16.846, T	41,48	40,19	3,86	0,64	1,29	1,61	4,82	3,22	2,89
Sdr Vium m.104 core 61, **133.28-133.32m**, 5, YD. 16. 856,Fc	46,98	18,73	28,57	0,32	0,00	1,90	0,32	2,22	0,95
Sdr Vium m.113 core 70, **146.63-146.67 m**, 7, YD 16.916, S	21,07	49,06	16,04	2,20	0,31	0,63	1,57	1,89	7,23

b) 2/11-12S

Depth	D	NSP	BS	S	FU	FA	A	UP	TUP
1611.54 m	76,44	12,08	4,83	0,60	0,30	0,00	1,81	0,91	3,02
1615.81 m	64,49	23,36	4,05	0,31	0,62	0,00	1,56	1,56	4,05
1620.42 m	63,86	22,29	4,82	0,60	0,30	0,90	3,61	1,51	2,11
1626.19 m	61,01	26,79	5,95	1,49	0,60	0,89	0,89	1,49	0,89
1631.51 m	62,61	21,36	12,17	0,00	0,00	0,00	1,48	0,59	1,78
1639.17 m	43,13	36,74	12,14	0,96	0,00	0,00	4,47	0,96	1,60
1644.41 m	38,73	44,44	9,21	0,32	0,00	0,00	3,81	0,32	3,17
1658.51 m	58,14	23,26	9,63	0,33	0,00	0,33	3,32	3,32	1,66
1662.72 m	48,44	35,94	8,75	0,00	0,63	1,25	0,63	3,13	1,25
1666.32 m	60,83	21,66	14,65	0,32	0,00	0,96	0,64	0,32	0,64
1670.74 m	34,71	40,13	21,66	0,64	0,00	0,00	0,96	0,32	1,59

***NSP** (Non-saccate pollen), **BS** (Bisaccate pollen), **S** (Spores), **FU** (Fungal Spores), **FA** (Freshwater algae), **A** (Acritarchs), **D** (Dinocysts), **UP** (Undifferentiated Palynomorphs), and **TUP** (Thin-walled undifferentiated palynomorphs).

Appendix C: P/D Index

The values here presented are the calculations for the P/D (terrestrial /marine) index (see Material & Methods for the equation, subchapter 4.4) for the Sdr. Vium **(a)** and 12/11-12S **(b)**. The graphics presented are the values plotted. The program used to calculate the P/D index was Excel.

a) Sønder Vium

Depth	P/D index
43.08-43.12 m	43
51.38-51.42 m	60
53.48-53.42 m	88
73.98-74.02 m	71
87.98-88.02 m	56
95.38-95.42 m	69
112.63-112.67m	47
119.03-119.07 m	51
133.28-133.32m	31
146.63-146.67 m	71

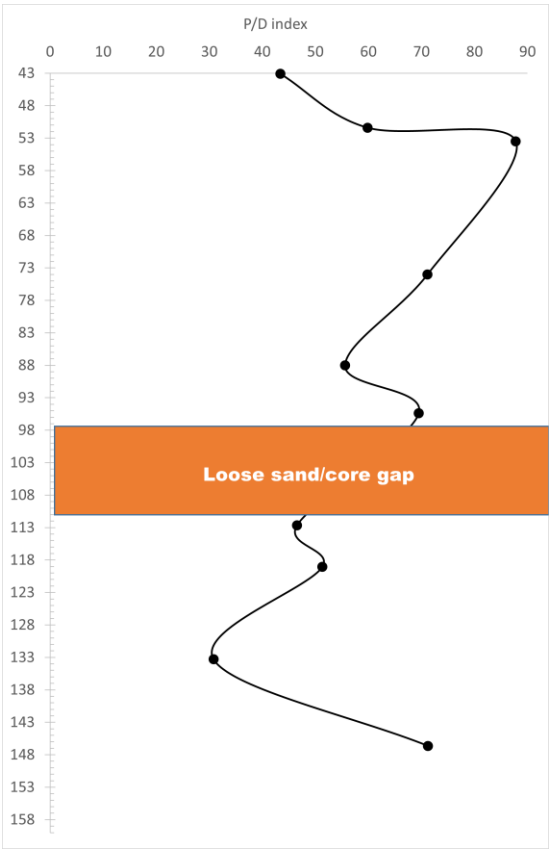

b) 2/11-12S

Depth	P/D index
1611.54 m	15
1615.81 m	27
1620.42 m	27
1626.19 m	33
1631.51 m	25
1639.17 m	47
1644.41 m	54
1658.51 m	29
1662.72 m	44
1666.32 m	27
1670.74 m	54

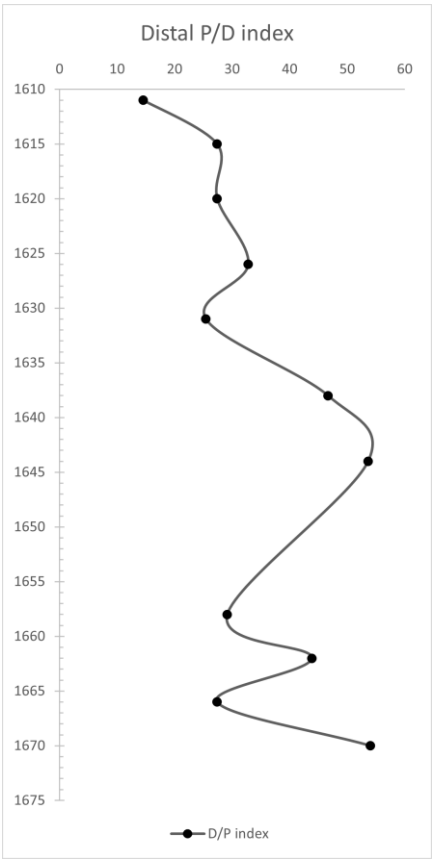

Appendix D: Raw counting dinocyst taxa

The values here presented are the countings of the Dinocyst taxa found in Sdr. Vium **(a)** and 12/11-12S **(b).**

a) Sønder Vium

Sdr. Vium Proximal Samples GEUS	"mini dinos" spp.	Apteodinium australiense	Apteodinium spiridoides	Apteodinium tectatum	Batiacasphaera spp.	Cerebrocysta poulsenii	Chiropteridium galea (Rework)	Cleistosphaeridium placacanthum	Cordosphaeridium minimum	Cordosphaeridium spp.	Cousteaudinium aubryae	Dapsilidinium pseudocolligerum	Dinopterygium cladoides	Distatodinium paradoxum	Distatodinium spp.	Exochosphaeridium insigne	Hystrichokolpoma rigaudiae	Hystrichosphaeropsis obscura	Impletosphaeridium insolitum	Labyrinthodinium truncatum modicum	Labyrinthodinium truncatum	Lingulodinium machaerophorum	Melitasphaeridium chonanophorum	Melitasphaeridium chonanophorum var. reducta	Melitasphaeridium spp.	Operculodinium centrocarpum	Operculodinium spp.	Palaeocystinium spp.	Pentadinium laticinctum	Polysphaeridium zoharyi	Reticulatosphaera actinocoronata	Spiniferites spp.	Sumatradinium hamulatum	Tectatodinium pellitum	Und. Dinos	Total
Sdr Vium m. **43.08-43.12 m** Lab nr.16483 ARY, slide 6, S	25	0	0	0	1	0	1	6	0	0	1	20	0	0	0	0	15	2	0	1	3	1	9	6	0	2	2	0	0	1	95	0	2	18	212
Sdr Vium m. **51.38-51.42 m** Lab nr.16651 ARY, slide 9, DS+kom	16	2	1	0	0	1	0	24	0	0	0	7	1	2	0	0	3	0	1	0	3	23	3	2	0	0	11	4	1	0	83	0	0	16	206
Sdr Vium m. **53.48-53.42 m** Lab nr.16658 ARY, slide 7, DS+kor	15	6	0	0	3	0	0	8	0	0	0	8	0	1	0	0	1	0	1	0	4	3	0	1	0	0	7	5	4	1	112	0	0	28	207
Sdr Vium m. PRNR.74, **73.38-74.02 m** Lab nr.16826 ARY, slid	6	2	6	17	0	0	0	55	0	1	1	11	0	1	0	0	0	0	0	4	0	6	1	0	0	0	9	6	1	0	55	0	0	17	204
Sdr Vium m.82 core 39, **87.98-88.02 m**, 3, YD 16.834, T	11	3	17	19	0	0	0	27	0	0	6	6	0	0	0	0	0	0	1	0	1	2	3	0	0	3	8	1	0	0	58	0	0	29	205
Sdr Vium m.87 core 44, **95.38-95.42 m**, 3, YD 16.839, T	12	4	1	37	0	0	0	31	0	0	0	9	0	0	0	0	0	0	0	6	0	0	2	3	1	1	0	8	0	2	66	0	0	19	209
Sdr Vium m.92 core 49, **112.63-112.67m**, 3, YD 16.844, T	10	16	0	2	0	0	0	27	2	0	1	8	0	1	0	0	3	9	0	0	6	9	1	1	0	0	15	0	0	0	58	0	0	35	205
Sdr Vium m.94 core 52, **119.03-119.07 m**, 3, YD 16.846, T	35	1	0	8	0	0	1	30	1	0	0	3	0	1	0	0	0	0	0	11	0	0	7	0	0	0	10	2	0	1	66	1	0	22	200
Sdr Vium m.104 core 61, **133.28-133.32m**, 5, YD 16. 856,Fo	9	9	0	0	1	0	0	49	0	0	0	17	0	1	0	0	4	0	0	14	0	0	13	1	0	0	21	9	0	0	85	0	0	27	260
Sdr Vium m.113 core 70, **146.63-146.67 m**, 7, YD 16.916, S	37	2	0	0	4	0	0	35	0	0	0	10	0	3	0	0	2	0	0	9	0	0	8	1	0	0	5	9	0	1	58	0	0	27	215

b) 2/11-12S

2/11-12S Distal Samples Aker bp	"mini dinos"	Apteodinium australiense	Apteodinium spiridoides	Apteodinium tectatum	Batiacasphaera spp.	Cerebrocysta poulsenii	Cleistosphaeridium placanthum	Cordosphaeridium cantharellus	Cousteaudinium aubryae	Dapsilidinium pseudocolligerum	Distatodinium paradoxum	Heteraulacacysta campanula	Hystrichokolpoma rigaudiae	Hystrichosphaeropsis obscura	Impagidinium paradoxum	Impagidinium spp.	Impletosphaeridium insolitum	Leptineocysta globosa	Lingulodinium machaerophorum	Melitasphaeridium chonanophorum	Melitasphaeridium chonanophorum var. reducta	Nematosphaeropsis spp.	Operculodinium centrocarpum	Operculodinium spp.	Palaeocystinium spp.	Pentadinium laticinctum	Reticulatosphaera actinocoronata	Spiniferites spp.	Und. Dinos	Total
1611.54 m	42	1	0	0	2	0	15	0	2	1	1	2	2	0	0	0	0	0	12	1	0	1	1	10	5	0	1	85	24	208
1615.81 m	35	0	0	1	3	1	14	0	1	8	0	3	0	1	1	0	8	0	4	3	0	0	0	4	6	3	0	0	17	212
1620.42 m	34	1	0	0	0	0	14	0	0	8	0	0	0	0	3	0	7	0	12	0	1	9	2	9	3	0	2	92	19	216
1626.19 m	17	0	2	7	0	0	25	0	1	9	0	0	1	0	4	0	2	0	4	3	0	10	5	8	0	0	0	86	16	200
1631.51 m	26	2	1	4	1	0	18	0	3	9	0	0	0	0	1	0	2	0	6	2	0	7	12	5	2	0	0	89	20	210
1639.17 m	47	0	5	0	2	0	16	0	2	3	1	1	0	0	4	3	13	0	6	1	0	8	11	12	4	0	0	42	19	200
1644.41 m	41	0	0	0	0	0	4	0	0	2	2	7	1	0	0	2	50	4	11	1	0	5	4	5	23	3	0	52	8	225
1658.51 m	35	6	0	1	0	0	11	0	0	2	1	2	1	0	0	2	22	0	10	0	0	17	15	15	3	0	3	60	11	217
1662.72 m	23	5	0	0	2	0	9	1	0	3	0	1	0	0	2	1	26	3	11	0	0	4	17	14	2	0	0	68	12	204
1666.32 m	20	3	0	0	0	0	16	0	0	1	0	2	0	0	6	4	20	1	11	1	0	0	16	23	2	0	1	60	16	203
1670.74 m	38	2	0	0	1	0	13	0	0	5	0	0	0	0	3	0	39	3	11	0	0	3	15	17	2	1	0	43	6	202

Appendix E: Relative abundances dinocyst taxa

The relative abundance values (%) here presented were obtained from previous data (Appendix D) of the dinocyst taxa found in Sdr. Vium **(a)** and 12/11-12S **(b).** The same equation from Material & Methods subchapter 4.3 was used for the dinocyst taxa relative abundance.

a) Sønder Vium

Sdr. Vium Proximal Samples GEUS	"mini dinos" spp.	Apteodinium australiense	Apteodinium spiridoides	Apteodinium tectatum	Batiacasphaera spp.	Cerebrocysta poulsenii	Chiropteridium galea (Rework)	Cleistosphaeridium placacanthum	Cordosphaeridium minimum	Cordosphaeridium spp.	Cousteaudinium aubryae	Dapsilidinium pseudocolligerum	Dinopterygium cladoides	Distatodinium paradoxum	Distatodinium spp.	Exochosphaeridium insigne	Hystrichokolpoma rigaudiae	Hystrichosphaeropsis obscura	Impletosphaeridium insolitum	Labyrinthodinium truncatum modicum	Labyrinthodinium truncatum	Lingulodinium machaerophorum	Melitasphaeridium choanophorum	Melitasphaeridium choanophorum var. reducta	Melitasphaeridium spp.	Operculodinium centrocarpum	Operculodinium spp.	Palaeocystinium spp.	Pentadinium laticinctum	Polysphaeridium zoharyi	Reticulatosphaera actinocoronata	Spiniferites spp.	Sumatradinium hamulatum	Tectatodinium pellitum	Und. Dinos
Sdr Vium m. **43.08-43.12 m** Lab.nr.16483 ARY, slide 6, S	12	0	0	0	0	0	0	3	0	0	0	9	0	0	0	0	7	1	0	0	4	3	0	0	1	1	0	0	0	0	45	0	1	8
Sdr Vium m. **51.38-51.42 m** Lab.nr.16651 ARY, slide 9, OS+M.com	8	1	0	0	0	0	0	12	0	0	0	3	0	0	1	0	1	0	0	1	1	11	1	0	0	0	0	0	2	0	40	0	0	8
Sdr Vium m. **53.48-53.42 m** Lab.nr.16658 ARY, slide 7, OS+Kok	7	3	0	0	1	0	0	4	0	0	0	4	0	0	1	0	1	0	0	1	1	1	0	0	0	0	0	0	2	0	54	0	0	14
Sdr Vium m. PRMR 74, **73.98-74.02 m**, Lab.nr.16826 ARY, slide	3	1	3	8	0	0	0	27	0	0	3	5	0	0	0	0	2	0	0	2	0	3	0	0	0	0	0	0	2	0	27	0	0	8
Sdr Vium m.82 core 39, **87.98-88.02 m**, 3, YD 16.834, T	5	1	8	9	0	0	0	13	0	0	3	3	0	0	0	0	0	0	0	0	0	1	0	0	0	1	0	0	4	1	28	0	0	14
Sdr Vium m.87 core 44, **95.38-95.42 m**, 3, YD 16.839, T	6	2	0	18	0	0	0	15	0	0	4	0	0	0	0	0	0	0	0	0	1	1	0	0	0	0	0	0	7	0	32	0	0	9
Sdr Vium m.92 core 49, **112.63-112.67m**, 3, YD 16.844, T	5	8	0	1	0	0	0	13	1	0	0	4	0	0	0	1	4	0	3	0	0	4	0	0	0	0	0	0	7	0	28	0	0	17
Sdr Vium m.94 core 52, **119.03-119.07 m**, 3, YD 16.846, T	18	1	0	4	0	0	1	15	1	0	0	2	0	1	0	0	0	0	6	0	0	4	0	0	0	0	0	0	5	1	0	0	1	11
Sdr Vium m.104 core 61, **133.28-133.32m**, 5, YD 16. 856,Fc	3	3	0	0	0	0	0	19	0	0	0	7	0	0	0	0	2	0	5	0	0	5	0	0	0	0	0	0	8	3	0	0	0	10
Sdr Vium m.113 core 70, **146.63-146.67 m**, 7, YD 16.316, S	17	1	0	0	2	0	0	16	0	0	0	5	0	0	1	0	1	0	4	0	0	4	0	0	0	0	0	0	2	4	0	0	0	13

b) 2/11-12S

2/11-12S Distal Samples Aker	"mini dinos"	Apteodinium australiense	Apteodinium spiridoides	Apteodinium tectatum	Batiacasphaera spp.	Cerebrocysta poulsenii	Cleistosphaeridium placacanthum	Cordosphaeridium cantharellus	Cousteaudinium aubryae	Dapsilidinium pseudocolligerum	Distatodinium paradoxum	Heteraulacacysta campanula	Hystrichokolpoma rigaudiae	Hystrichosphaeropsis obscura	Impagidinium paradoxum	Impagidinium spp.	Impletosphaeridium insolitum	Leptineocysta globosa	Lingulodinium machaerophorum	Melitasphaeridium choanophorum	Melitasphaeridium choanophorum var. reducta	Nematosphaeropsis spp.	Operculodinium centrocarpum	Operculodinium spp.	Palaeocystinium spp.	Pentadinium laticinctum	Reticulatosphaera actinocoronata	Spiniferites spp.	Und. Dinos
1611.54 m	20	0	0	0	1	0	7	0	1	0	0	1	0	0	0	0	0	0	6	0	0	0	0	5	2	0	0	0	41	12
1615.81 m	17	0	0	0	0	0	0	0	0	4	0	0	1	0	0	0	4	0	2	1	0	0	2	3	1	0	0	1	47	8
1620.42 m	16	0	0	0	0	0	7	0	0	4	0	0	0	0	1	0	3	0	6	0	0	0	4	1	4	1	0	1	43	9
1626.19 m	9	0	1	4	0	0	0	13	0	1	5	0	0	1	0	0	0	0	2	0	0	5	3	4	0	0	0	0	43	8
1631.51 m	12	1	0	2	0	0	0	9	0	1	4	0	0	0	0	0	1	0	3	1	0	3	6	2	1	0	0	0	42	10
1639.17 m	24	0	3	0	0	0	0	8	0	1	2	1	1	0	2	2	7	0	3	1	0	4	6	6	2	0	0	0	21	10
1644.41 m	18	0	0	0	0	0	2	0	0	1	1	3	0	0	0	1	22	2	5	0	0	2	2	2	10	1	0	0	23	4
1658.51 m	16	3	0	0	0	0	5	0	0	1	0	1	0	0	1	0	10	0	5	0	0	8	7	7	1	0	1	0	28	5
1662.72 m	11	2	0	0	0	1	0	4	0	0	0	0	0	1	0	0	13	1	5	0	0	2	8	7	1	0	0	0	33	6
1666.32 m	10	1	0	0	0	0	8	0	0	0	0	1	0	3	2	10	0	5	0	0	0	0	8	11	1	0	0	0	30	8
1670.74 m	19	1	0	0	0	0	6	0	0	0	0	2	0	0	1	0	19	1	5	0	0	1	7	8	1	0	0	0	21	3

Appendix F: GDGTs mass values

The organic geochemistry values from the 2/11-12S well here presented were obtained from mass spectrometry **(a)** at Utrecht University (by Dra. Francien Peterse) and calculated **(b)** and plotted by Excel program **(c)**. Equations are presented in chapter 4 (Methods).

a) Calculated values

				GDGT-0	GDGT-1	GDGT-2	GDGT-3	Cren	Cren'
Sample depth	sample depth bottom		LCMS ID	Area 1302	Area 1300	Area 1298	Area 1296	Area 1292	Area 1292'
1672,00	1672,07	Prove 1	LC24090035	4,62E+05	7,86E+04	3,58E+04		3,48E+05	
1664,63	1664,69	Prove 3	LC24090046	5,24E+06	8,02E+05	4,09E+05	1,93E+05	5,66E+06	2,23E+05
1653,72	1653,80	Prove 6	LC24090047	3,45E+06	5,38E+05	3,80E+05	1,56E+05	4,25E+06	2,55E+05
1636,30	1636,37	Prove 10	LC24090048	9,36E+06	2,13E+06	1,50E+06	7,58E+05	1,08E+07	6,98E+05
1601,54	1601,63	Prove22	LC24090049	2,15E+07	3,91E+06	2,48E+06	1,23E+06	2,73E+07	1,30E+06
1509,56	1509,66	Prove 48	LC24090050	1,55E+07	2,02E+06	9,95E+05	3,16E+05	1,48E+07	5,48E+05
1491,61	1491,74	Prove 53	LC24090051	1,69E+07	2,24E+06	9,88E+05	2,79E+05	1,59E+07	5,31E+05

				brGDGT-IIIa	brGDGT-IIIa'	brGDGT-IIIb	brGDGT-IIIb'	brGDGT-IIIc	brGDGT-IIIc'	brGDGT-IIa	brGDGT-IIa'	brGDGT-IIb
Sample depth	sample depth bottom		LCMS ID	Area 1050	area 1050'	area 1048	area 1048'	area 1046	area 1046'	Area 1036	area 1036'	area 1034
1672,00	1672,07	Prove 1	LC24090035									
1664,63	1664,69	Prove 3	LC24090046									
1653,72	1653,80	Prove 6	LC24090047									
1636,30	1636,37	Prove 10	LC24090048									
1601,54	1601,63	Prove22	LC24090049							1,98E+05	7,21E+04	6,05E+04
1509,56	1509,66	Prove 48	LC24090050							1,03E+05	4,75E+04	
1491,61	1491,74	Prove 53	LC24090051							1,15E+05	1,11E+05	7,74E+04

				brGDGT-IIb	brGDGT-IIb'	brGDGT-IIc	brGDGT-IIc'	brGDGT-Ia	brGDGT-Ib	brGDGT-Ic
Sample depth	sample depth bottom		LCMS ID	area 1034	area 1034'	area 1032	area 1032'	Area 1022	Area 1020	Area 1018
1672,00	1672,07	Prove 1	LC24090035							
1664,63	1664,69	Prove 3	LC24090046					1,17E+05		
1653,72	1653,80	Prove 6	LC24090047					4,25E+05		
1636,30	1636,37	Prove 10	LC24090048					9,58E+05		
1601,54	1601,63	Prove22	LC24090049	6,05E+04	5,89E+04			9,78E+05	9,05E+04	4,73E+04
1509,56	1509,66	Prove 48	LC24090050					4,80E+05	4,85E+04	
1491,61	1491,74	Prove 53	LC24090051	7,74E+04	1,43E+05			3,82E+05	7,84E+04	

b) Values obtained from the equations

Sample depth	sample depth bottom		LCMS ID	TEX86	SST (TEX86H)	TEX86H	BIT	MI	GDGT2/3	%GDGT-0
1672,00	1672,07	Prove 1	LC24090035	0,31	4,10	-0,50	0,00	0,247	#DIV/0!	57,05
1664,63	1664,69	Prove 3	LC24090046	0,51	18,43	-0,29	0,02	0,19	2,12	48,07
1653,72	1653,80	Prove 6	LC24090047	0,60	23,19	-0,23	0,09	0,19	2,44	44,77
1636,30	1636,37	Prove 10	LC24090048	0,58	22,48	-0,24	0,08	0,28	1,98	46,46
1601,54	1601,63	Prove22	LC24090049	0,56	21,45	-0,25	0,04	0,21	2,01	43,98
1509,56	1509,66	Prove 48	LC24090050	0,48	16,76	-0,32	0,04	0,18	3,15	51,15
1491,61	1491,74	Prove 53	LC24090051	0,45	14,57	-0,35	0,03	0,18	3,55	51,62

Sample depth	sample depth bottom		LCMS ID	RI	RITEX	ΔRI	fCren':Cren' + Cren
1672,00	1672,07	Prove 1	LC24090035	1,67	1,67	0,01	0,0
1664,63	1664,69	Prove 3	LC24090046	2,05	2,05	0,00	0,0
1653,72	1653,80	Prove 6	LC24090047	2,19	2,31	0,12	0,1
1636,30	1636,37	Prove 10	LC24090048	2,11	2,26	0,15	0,1
1601,54	1601,63	Prove22	LC24090049	2,20	2,20	0,00	0,0
1509,56	1509,66	Prove 48	LC24090050	1,94	1,98	0,04	0,0
1491,61	1491,74	Prove 53	LC24090051	1,92	1,91	-0,01	0,0

Appendix G: GDGTs Structures

Structures of (a) isoprenoid and (branched) glycerol dialkyl glycerol tetraethers. Associated values of M+H+ ions are given for each lipid. **Source**: Śliwińska et al. (2019).

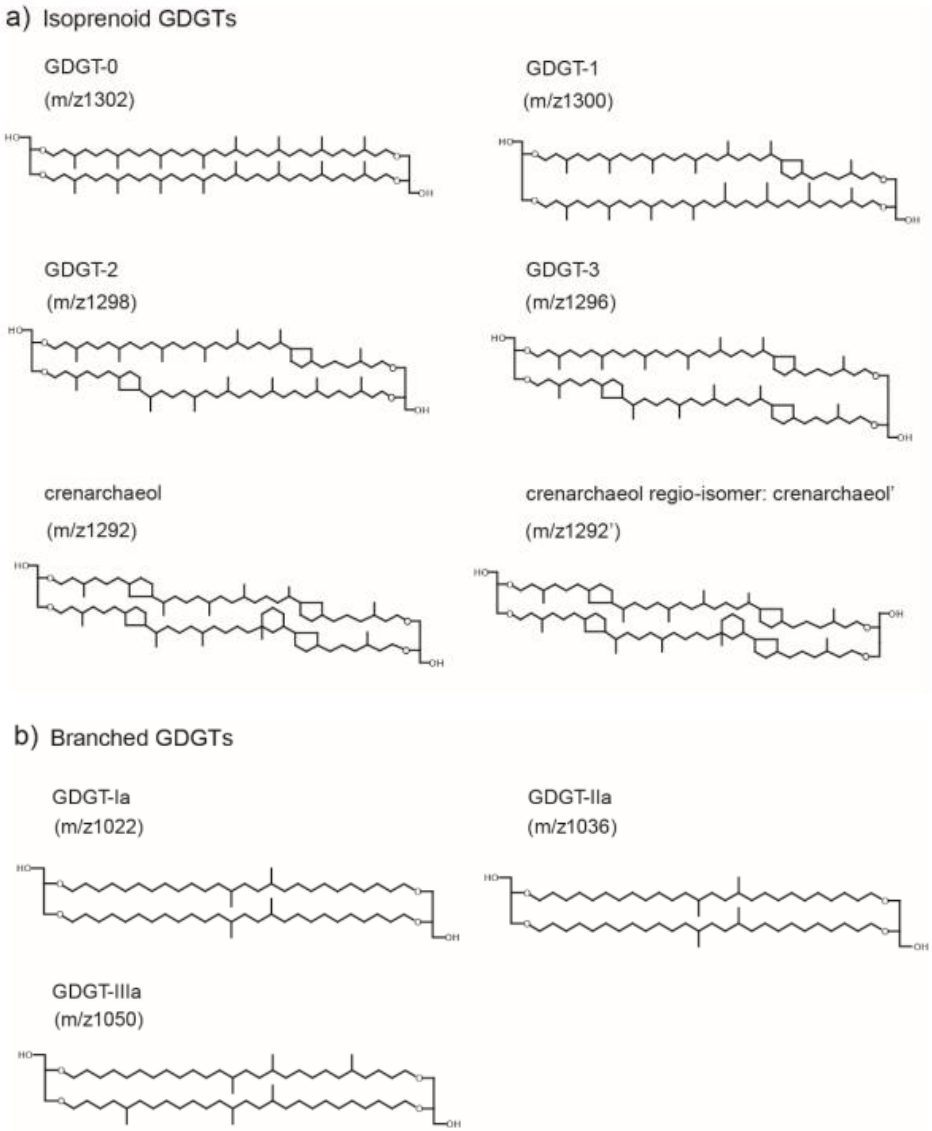

Appendix H: Correlation figure

Figure of the correlation between Sønder Vium and the 2/11-12S wells, through the dinocyst zonation defined by Dybkjær and Piasecki (2010). **Source:** adaptation from Kellner et al. (submitted). Since the figure is of big dimension, is presented alone in the next page.

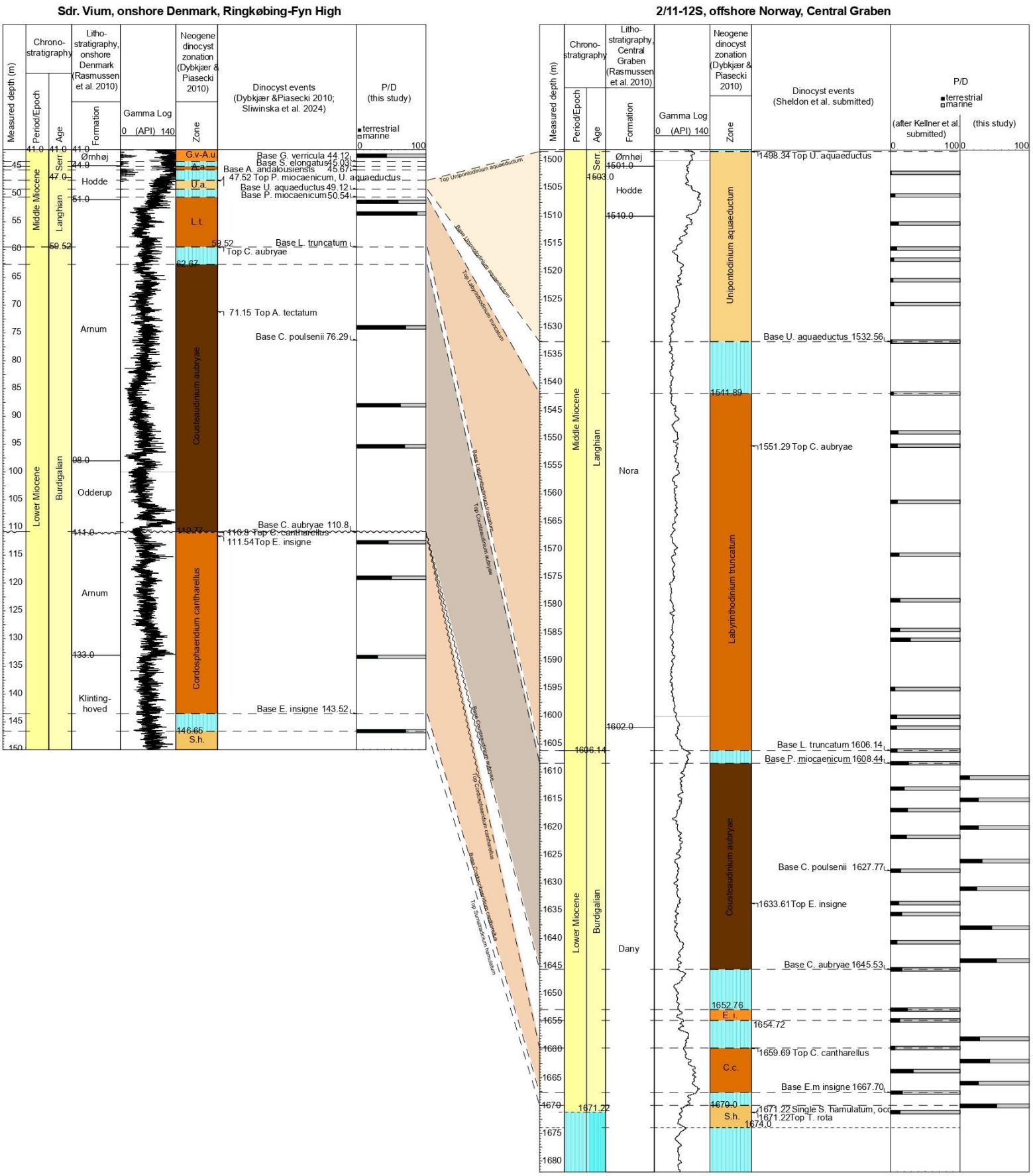
Sdr. Vium, onshore Denmark, Ringkøbing-Fyn High
2/11-12S, offshore Norway, Central Graben
Measured depth (m)
Chrono-stratigraphy
Period/Epoch
Age
Litho-stratigraphy, onshore Denmark (Rasmussen et al. 2010)
Formation
Gamma Log
0 (API) 140
Neogene dinocyst zonation (Dybkjær & Piasecki 2010)
Zone
Dinocyst events (Dybkjær &Piasecki 2010; Sliwinska et al. 2024)
P/D (this study)
terrestrial
marine
0 100
Middle Miocene
Lower Miocene
Serr.
Langhian
Burdigalian
Ørnhøj
Hodde
Arnum
Odderup
Klinting-hoved
G.v-A.u
A.a.
U.a.
L.t.
Cousteaudinium aubryae
Cordosphaeridium cantharellus
S.h.
Base G. verricula 44.12
Base S. elongatus 45.03
Base A. andalousiensis 45.67
47.52 Top P. miocaenicum, U. aquaeductus
Base U. aquaeductus 49.12
Base P. miocaenicum 50.54
Base L. truncatum
Top C. aubryae
71.15 Top A. tectatum
Base C. poulsenii 76.29
Base C. aubryae 110.8
110.8 Top C. cantharellus
111.54 Top E. insigne
Base E. insigne 143.52
Top Unipontodinium aquaeductum
Base Unipontodinium aquaeductum
Top Labyrinthodinium truncatum
Base Labyrinthodinium truncatum
Top Cousteaudinium aubryae
Base Cousteaudinium aubryae
Top Cordosphaeridium cantharellus
Base Cordosphaeridium cantharellus
Top Sumatradinium hamulatum
Nora
Dany
Unipontodinium aquaeductum
Labyrinthodinium truncatum
C.c.
E. i.
1498.34 Top U. aquaeductus
Base U. aquaeductus 1532.56
1551.29 Top C. aubryae
Base L. truncatum 1606.14
Base P. miocaenicum 1608.44
Base C. poulsenii 1627.77
1633.61 Top E. insigne
Base C. aubryae 1645.53
1659.69 Top C. cantharellus
Base E.m insigne 1667.70
1671.22 Single S. hamulatum, occ
1671.22 Top T. rota